UNIVERSITY OF CALIFORNIA,
IRVINE

Analysis of integrated hard and soft sensors for process control and monitoring in Water Resource Recovery Facilities

DISSERTATION

submitted in partial satisfaction of the requirements
for the degree of

DOCTOR OF PHILOSOPHY

in Civil and Environmental Engineering

by

Francesca Cecconi

Dissertation Committee:
Professor Diego Rosso, Chair
Professor Sunny Jiang
Professor Adeyemi S. Adeleye

2020

DEDICATION

This dissertation is dedicated to my beloved parents, Grazia and Daniele and to my sister Bianca who have supported this long journey of mine overseas. A special thought to my husband Sam who has always been by my side.

TABLE OF CONTENTS

LIST OF FIGURES

LIST OF TABLES

ACKNOWLEDGMENTS

First and foremost I would like to extend my deepest appreciation to my advisor, Professor Diego Rosso, for giving me the opportunity to accomplish my Ph.D. degree under his guidance. His invaluable supervision, continuous support, and insightful advice throughout my PhD program has helped me realize my academic goals and develop an independent and critical thinking.

I would also like to extend my gratitude to my committee members, Professor Sunny Jiang and Professor Adeyemi S. Adeleye for their constructive comments and advice in my qualifying exam, as well as during my PhD studies.

I would like to thank Dr. Reza Sobhani, engineer from Orange County Sanitation District, for his continuous support and valuable advise along all my Ph.D. project.

I also appreciate the assistance and knowledge of Yuichi Ito, from HORIBA Ltd, for his continuous support and technical assistance thru ought my project.

Many thanks to my colleagues and friends from the EPL and Uc Irvine who made my Ph.D. years an incredible experience and have helped my extend my knowledge in different disciplines.

Furthermore, I would like to acknowledge who made this dissertation possible through their financial and technical support: DOE CERC-WET project, HORIBA Advanced Techno, Co., Ltd. and Orange County Sanitation District (OCSD). I would like to acknowledge Margil Jimenez and all the operators from OCSD for their kindness and support.

Finally, I am extremely grateful to my parents, Daniele and Grazia and my sister Bianca for their constant love and support, even with nine hours of time difference. Also, I thank my husband Sam for his constant encouragement and incredible patience in our life together.

VITA

Francesca Cecconi

EDUCATION

Doctor of Philosophy in Civil and Environmental Engineering **2020**
University of California, Irvine *Irvine, California*

Master of Science in Environmental Engineering **2016**
University of Florence *Florence, Italy*

Bachelor of Science in Environmental Engineering **2014**
University of Florence *Florence, Italy*

RESEARCH EXPERIENCE

Graduate Research Assistant **2017–2020**
University of California, Irvine *Irvine, California*

INTERNSHIPS

Engineering Trainee **2016–2017**
TU Delft *Delft, Netherlands*

Research Intern **2014–2015**
Publiacqua Sanitation Agency *Florence, Italy*

REFEREED JOURNAL PUBLICATIONS

F. Cecconi, S. Reifsnyder, R. Sobhani, A. Cisquella-Serra, M, Madou, D. Rosso, Functional behavior and microscopic analysis of ammonium sensors subject to fouling in activated sludge processes — **Jun 2020**
Environmental Science: Water Research and Technology

S. Reifsnyder, M. Garrido-Baserba, F. Cecconi, L. Wong, P. Ackman, N. Melitas, D. Rosso, Relationship between manual air valve positioning, water quality and energy usage in activated sludge processes — **Jan 2020**
Water Research

F. Cecconi, M. Garrido-Baserba, R. Eschborn, J. Damerel, D. Rosso, Oxygen transfer investigations in an aerobic granular sludge reactor — **Dec 2019**
Environmental Science: Water Research and Technology

F. Cecconi, S. Reifsnyder, Y. Ito, M. Jimenez, R. Sobhani, D. Rosso, ISE-ammonium sensors in WRRFs: Field assessment of their influencing factors — **Jan 2019**
Environmental Science: Water Research and Technology

REFEREED CONFERENCE PUBLICATIONS

Morphology And Composition Analysis Of Ammonium Sensor Fouling In WRRFs — **May 2021**
IWA World Water Congress and Exhibition

Soft sensor application to improve ammonium sensor robustness in WRRFs — **Oct 2020**
WEFTEC

Soft-sensor application for fault detection of ammonium sensors in WRRFs — **Sep 2020**
IWA Nutrient Removal and Recovery

Aerobic granular sludge and activated sludge: aeration efficiency using off-gas testing — **Oct 2019**
WEFTEC

Oxygen Transfer Efficiency Study On Aerobic Granular Sludge: Pilot Studies In North America — **Jun 2019**
IWA Leading Edge Conference

Field evaluation of ISE-ammonium sensors and their influencing factors in WRRFs **Oct 2018**
WEFTEC

Suitability of High/Low range ISE-ammonium sensors for monitoring and control in WRRFs **Jun 2018**
IWA EcoSTP

ABSTRACT OF THE DISSERTATION

Analysis of integrated hard and soft sensors for process control and monitoring in Water Resource Recovery Facilities

By

Francesca Cecconi

Doctor of Philosophy in Civil and Environmental Engineering

University of California, Irvine, 2020

Professor Diego Rosso, Chair

Online continuous monitoring of water quality variables is a crucial aspect to ensure the correct performance in Water Resource Recovery Facilities. In the last few decades, with the advent of water reclamation and the use of new technologies to lower the energy consumption of processes, real-time measurements have gained a larger role in both process monitoring and control. In order to obtain on-line data, sensors and analyzers are essential, which technology in time have been improved to obtain reliable high-frequency measurements, and to optimize maintenance and costs of operation. Despite the improvements and the development of new technologies for measuring different water quality, sensors are often expensive and usually present problems of fouling, poor calibration, and lack of reliability. A common perception is that sensors represent the bottleneck for implementing online process control of wastewater treatment, especially in consideration of the harsh environment they are deployed and the number of water professionals sufficiently confident to rely entirely on them. In this dissertation we focused on ammonium sensors, typically based on Ion-Selective-Electrode technology, which are often found to incur into faulty behavior compared to other water quality sensors, but they have a large potential application for different monitoring and control systems. In this study we analyzed the field limitations of ISE-NH_4^+ sensors installed in different sections of the activated sludge tank at a full-scale treatment plant. Among the

different field influencing factors, a special focus was given to the development of fouling on the sensor's membrane, both in terms of composition of the film layer and effect on the functional behavior of the sensor when subject to fouling. The results show that the sensors presented a reduced accuracy when working in the lower ammonium range, due to the larger interference of cations like K^+ and Na^+, which exposes a limit to the possible deployment of these sensors for effluent monitoring. The fouling development was found to be increasing as a negative exponential against time, with a high content of Iron in the inert fraction. The sensor was affected by the fouling development, showing a negative drift in time, therefore leading to an underestimation of the ammonium reading. In consideration of the demonstrated low reliability of such sensors, especially in effluent installations and concurrently the high request for the use of ammonium sensors for effluent measurement, this study aimed at improving the sensor's accuracy and reliability for low range installations. A machine learning methodology, based on the use of Artificial Neural Networks and Principal Component Analysis, was employed to develop a fault detection chart to promptly detect the occurrence drifts, biases and in general sensor faults. In detail, the fault detection methodology shows promising results, requiring only few hours to detect an incorrect calibration procedure and one day to detect a fouling drift of the sensor.

Chapter 1

Introduction

Challenges with water supply are increasing all over the world due to rising demand, drought, depletion and pollution of groundwater and the recurrent issue of depending on one single source of supply (Wade Miller, 2006, Hering et al., 2013). As a consequence, existing water supply must evolve, creating new sources of high-quality water by focusing on water reclamation, recycling, and reuse (Okun, 1996, Hochstrat et al., 2010, Leverenz et al., 2011). Water resources recovery facilities (WRRFs), whose role is to collect, treat and convert the pollutants of municipal wastewaters, have been facing increased regulations on water quality discharge as more strict limits are imposed with the rise of water reclamation and use of wastewater. The energy required to operate the various processes for wastewater treatment is substantial, especially with the advent of water reclamation and the use tertiary treatments (Rygaard et al., 2011; WEF, 2009; Longo et al., 2016). Secondary treatment is commonly arranged into activated sludge tanks (AS) and requires aerobic conditions for the rapid and complete degradation of contaminants. The oxic conditions are achieved through an air supply system, typically composed of subsurface diffusers, for the air distribution in the tank, and blowers to pressurize the air. Due to the high power demand required to operate the blowers of the air supply system, diffused aeration is the most energy intensive process in

WRRFs, representing 45-75% of the energy use (Olsson, 2015; Reardon, 1995; Rosso et al., 2008). Therefore, in light of the operating costs of secondary and tertiary treatments, many have focused both on deploying new technologies characterized by lower energy consumption and on developing control systems to minimize the energy consumption of conventional technologies. Many control strategies have been developed over to optimize the air delivery of diffused aeration systems (Holenda et al 2008). Control strategies based on dissolved oxygen (DO) set points (Ekman et al., 2006) and ammonia-based aeration control (ABAC) (Rieger et al., 2014, 2012; Uprety et al., 2016) have found large applications in order to achieve improved effluent quality and minimize the energy use of the aeration system.

1.1 Real-time measurements

In order to ensure both quality consistency for water reuse and energy minimization strategies, real-time measurements have become a compelling requirement. Moreover, with increasing pressure to recycle and reuse water in certain areas of the world, closely monitoring the effluent water quality has become the standard treatment strategy (Metcalf Eddy, 2007). Wastewater characteristics have an important spatial and time variability, therefore automatic on-line monitoring of several parameters to determine the quality of the wastewater is evidently required (Bourgeois et al., 2001). In order to obtain on-line data for monitoring and control in WRRFs, sensors are essential (Jeppsson et al., 2002) and in time they have been improved to obtain reliable real-time measurements, optimizing maintenance and costs of operation (Lynggaard-Jensen, 1999). New technologies and computers together with rising problems related to water quality made water quality monitoring increase exponentially during the last decades.

1.2 Importance of real-time ammonia measurement: monitoring, aeration control, disinfection control

Among the different quality constituents, online ammonium quantification has raised attention because of the diverse possible applications, both for monitoring and control. The most common implementation concerns the biological ammonia removal process. Depending on the biological process, the instrumentation can be applied in aerated tanks or in anoxic conditions and in different positions along the same process. Therefore, the mixed liquor composition can vary significantly in terms of solids content, organic matter, and biomass, and as a result the instrumentation requires different maintenance. The different applications for continuous ammonium reading are listed below. The instrumentation can be installed in the effluent of the primary clarifier to monitor the nutrient load in the secondary treatment. Also, it can be installed at the beginning and/or at the end of the aeration step in secondary treatment processes, especially for the implementation of ammonium-based aeration control for the optimization of air delivery and energy use (Rieger et al 2012a, Rieger et al 2014). In addition, the ammonium content of the secondary clarifier effluent can be continuously measured for monitoring or can be used to control the chlorine dosage of the following disinfection step in order to estimate the monochloroamines formation or to balance the ratio between chlorine and ammonium (Shuck 1973). Real-time ammonium measurement can be achieved with diverse instrumentations: an analyzer or an ISE sensor. Analyzers are based on colorimetry or on gas sensitive probe and are installed *ex situ*. Colorimetric-based analyzers conduct analysis on samples of mixed liquor collected periodically and automatically. The sample volume is pumped through an ultrafiltration unit, and then chemicals are added in a small reactor. The reaction generates a colored component which is correlated with the ammonium concentration and is measured by an optical cell. Gas sensitive electrodes require an *ex-situ* installation with a pumping system, and in some cases a filtration step is also required. The measurement is based on the complete transformation of ammonium

ions (NH_4^+) to ammonia gas (NH_3) by increasing the pH up to 11. The gas is then directly measured without chemical reactions because the electrode membrane is selectively permeable to the ammonia gas. Finally, Ion-Selective-Electrodes (ISEs) are *in-situ* sensors directly immerged in the environment. These sensors are widespread, low-cost, and are suitable for nutrient measurements in their ionic species, e.g. ammonium, nitrate, chlorine, pH, potassium, sodium, etc. (Bonastre et al 2005, Kaelin et al 2008, Ingildsen et al 2002, Winkler et al 2004). ISE-NH_4^+ sensors provide a faster response compared to the other ammonium methods and do not consume analytes (Rieger et al 2002). Such sensors directly measure the ammonium content without a chemical reaction. Furthermore, due to the ion selective membrane of the ISE sensors, the ultrafiltration unit required for analyzers and gas sensitive electrodes can be eliminated, thus avoiding the frequent clogging issues caused by the solids in the mixed liquor (Devisscher et al., 2002, Ingildsen et al 2003).

1.3 Typical issues with online sensors

Despite the improvements and the development of new technologies for measuring different water qualities, sensors are often expensive, and they also still cause problems. Harremoes et al. (1993) showed that any sensor usually presents problems of fouling, bad calibration and lack of reliability. A common perception is that sensors represent the bottleneck for implementing online process control of wastewater treatment plants (Harremoës et al., 1993), especially in consideration of the harsh environment they are deployed. In recent years, large improvements have been done on the performance and the reliability of sensors, but there are still not many water professionals that feel sufficiently confident to entirely rely on them. Also, the existing facilities are frequently not equipped for automated control systems or do not take advantage of the on-line information (Campisano et al., 2013; Jeppsson et al., 2002). These issues are typical for any type of on-line sensor used in the WRRFs

due to severe environmental conditions, anomalies in sensors, inadequate maintenance or other external factors. Still nowadays good maintenance methodologies remain a challenge, especially when handling new and more unstable technologies. Another issue resides in managing high quantity of data without losing their quality.

Real-time measurements instrumentation can be subject to various issues such as noise, bias, drift, outliers, etc. (Thomann et al 2002, Alferes et al., 2013), which determine a lack of reliability of the signal. Sensors can show partial failures such as bias, drift or precision degradation as shown in Figure 1.1 (Yoo et al 2007). This results into a decrease in accuracy and reliability of the instrument, which can cause an erroneous control action and incorrect perception of the performance of the process being monitored. Sensors can also be subject to different type of errors, including catastrophic failure and power outages (Schraa et al 2006). Sensors in complete or partial failing deliver erroneous information both for monitoring and control application, which can be detrimental to data-driven decision schemes. Due to sensor malfunction or communication problems (electrical failures) data may not be available for certain periods of time, which makes it difficult to extract and interpret information from data. Therefore, sensors are often checked and recalibrated periodically to detect and correct failures.

In wastewater application, sensors are also often corrupted due to the presence of air bubbles, significant electrical noise, or they may incur to complete failure due to sludge fouling, since they operate in very harsh environments (Olsson and Newell, 1999; Bourgeois et al, 2003). Fouling is an issue associated to all the instrumentation that is deployed in water/wastewater environment, which causes a loss in sensitivity, reproducibility and frequent re-calibration requirements (Regan et al, 2009; Bourgeois et al, 2001, Olsson and Newell, 1999). Also, fouling determines a reduction in the sensor performance, it decreases the operating lifetime of the sensor and it smoothens the sensor reading, introducing a degree of error in the collected data (Regan et al 2009). This is because fouling can create an artificial environment around

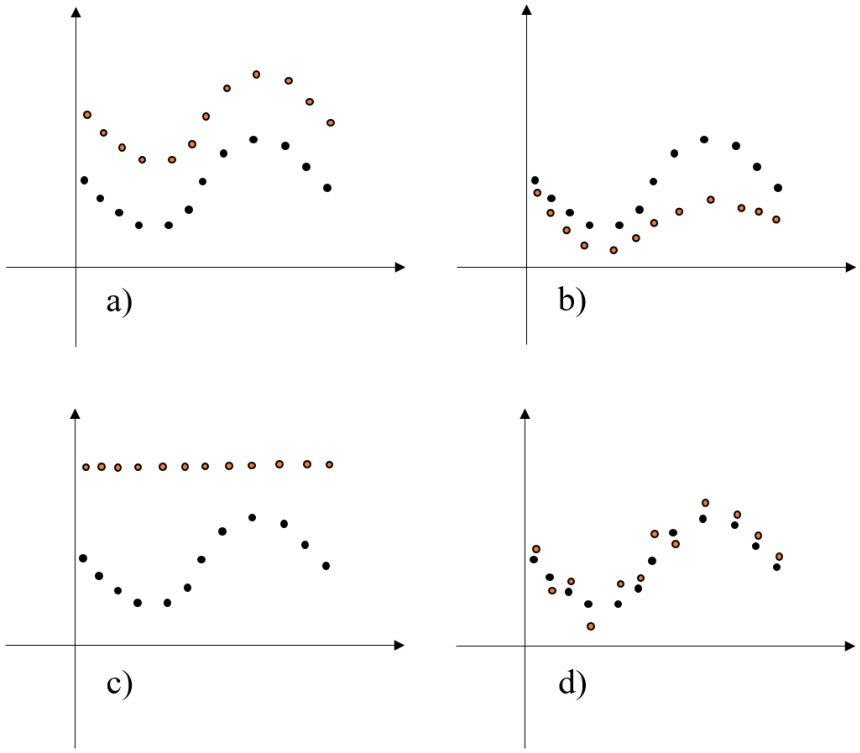

Figure 1.1: Four types of sensor faults, (a) bias, (b) drifting, (c) complete failure, (d) precision degradation.

the sensing surface of the sensor and hence, the measured data will not be truly representative of the location sampled (Whelan et al, 2006). In wastewater application, sensors can be subject to different degree of fouling, depending on the wastewater composition, in terms of suspended solids, organic compounds and biomass composition (Amy 2008, Wu et al, 2008; Le-Clech et al, 2006; Jarusutthirak et al, 2002).

1.4 Software-based sensors in wastewater application

Commercially available control systems rely on real-time instrumentation, in detail for ammonium control systems, either *in-situ* ion selective electrodes or ammonium *ex-situ* analysers are required. However, instrumentation can be costly to operate and depending on the technology can require frequent maintenance by skilled staff (Kaelin et al., 2008). In fact, in

small or remotely controlled WRRFs, ammonium control systems can be inconvenient because the installation and maintenance costs may not be covered by the energy cost savings. As an alternative to hardware-based ammonium control systems, soft-sensors can offer an interesting solution to avoid using expensive yet error-prone instruments. Soft-sensors are inferential models where the variable of interest, often hard to measure for technology limitations or high investments costs, is estimated using one or multiple cheaper and/or more robust sensors (Kadlec et al., 2009, Haimi et al., 2013, Liu et al., 2016, Thurlimann et al 2018). They are often used for fault diagnosis as well as control applications (Aguado and Rosen 2008, Baggiani and Libelli, 2009). These models can be based on empirical black-box relationships or on mechanistic concepts. In the first case, such soft-sensors can be affected by issues in practice due to their lack of transparency, lack of general validity and/or their (re-)calibration and fine-tuning requirements (Durrenmatt Gujer, 2012). Therefore, hybrid models that incorporate mechanistic concepts with empirical large datasets are preferable. In wastewater application, examples of soft-sensors based on mechanistic understanding can be found with the use of conductivity for ammonia (e.g. Joss et al., 2009, Bongards 2001) or pH/ORP for control of biological denitrification (e.g. Peng et al., 2002). Zanetti et al., 2012 showed a summary of the different soft-sensors used for the control of wastewater treatment.

1.5 Artificial Neural Networks

There are different methodologies for data mining, which can be based on the development of linear or non-linear relationships. If the system which needs to be described is rather complex, it is preferable to rely on non-linear projections (Despagne and Massart 1998). Among the different machine learning techniques, Artificial Neural Networks have raised attention also in the wastewater treatment world, especially for prediction in complex settings and pattern recognition (Cote et al., 1995, Fu et al., 1995, Despagne and Massart 1998, Choi et al., 2001,

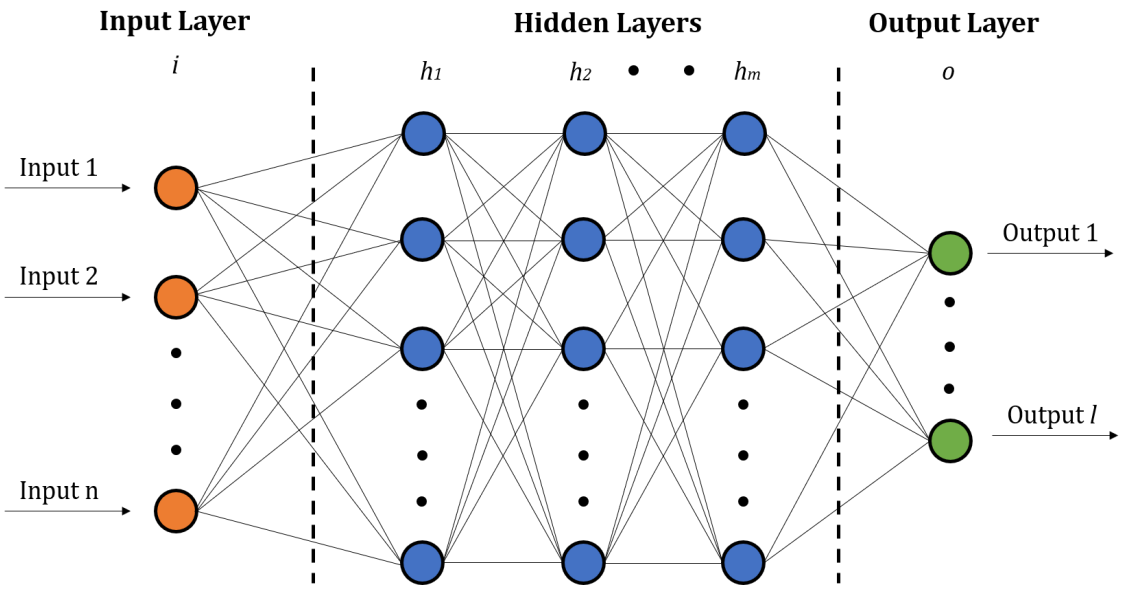

Figure 1.2: Artificial neural Network general scheme.

Chen et al., 2003, Hamed et al., 2004, Mjalli et al., 2007, de Canete et al., 2016). Neural networks are a set of algorithms that process information in a similar way the human brain works, by which the name originates (Hamed et al., 2004). The network is composed of a large number of highly interconnected processing elements (neurons) working in parallel to solve the problem (see Figure 1.2). Every neuron can have multiple inputs but has only one output. To every neuron is associated a coefficient or weight that determines the extent to which the input of the neuron is transmitted to its output. The network is composed of a first layer, called input layer, constituted by the independent variables and an output layer, constituted by the dependent variables. One or more layers are located between them, called hidden layers, which operate like features detector.

1.6 Research Motivation and Approaches

In recent years, the water/wastewater treatment field has seen a large rise, where engineers have developed new technologies, diverse treatment processes and control systems to improve

the removal of a large number of contaminants while also incentivizing energy consumption abatement. For the successfully implementation of more complex and sophisticated technologies, a larger variety of water quality constituents must be monitored frequently and accurately. However, field and large-scale application of new technologies can find restraints also because of the often unreliability of field instrumentation and sensors given the harsh field installation in wastewater. Although there have been many studies focusing on improving control systems and diverse treatment processes in lab-scale reactors or simulators, not enough researches have been considering the direct implication of sensors failures on control processes, which field factors can influence sensors behavior and at which extent. There have been a few studies analyzing sensors failures and possible methodology to both promptly detect the instrumentation fault and address it by appropriate maintenance procedures. Some studies have focused on the detection of sensors failures, usually based on Principal Component Analysis, however these studies have often focused on large faults, i.e. complete sensor failures, loss of signal, abnormal measurement ranges, etc.. which can frequently be recognized also visually, just by looking at the historic data (Alferes and Vanrollenghem, 2013; Baggiani and Libelli, 2009; Schraa et al 2006; Rosen et al 2003; Olsson et al 2003; Tao et al 2013). Other studies have analyzed the implication of sensor and process failures on control systems and/or the improvement obtained using fault detection methodology to promptly discover and isolate erratic sensors. However, they would often rely on simulation environments to test out the control systems and simulated sensors signal disruption, which can often be unrealistic of the actual behavior of an erratic sensor (Fuente et al, 2012; Cheng et al 2005). In some cases, real sensors failures where analyzed and detected using SBR lab or pilot-scale reactors, which is a very confined and controlled environment, not representative of the complex full-scale conditions (Villez et al, 2008; Schneider et al, 2019). Only a few studies have analyzed sensors behaviors in full scale reactors and have applied different fault detection methods on real sensor data, without the use of simulators. However, the results show how very few fault detection methods can be successfully implemented and

often require additional sensors duplicates as reference and a large number of grab sample lab analysis information that increases the load of work of operators (Samuelsson et al 2019; Papias et al 2018). Therefore, herein, a methodology framework is proposed for assessing the reliability of online sensors in field application. First, the study is centered around ammonium sensors, given their large potential application and significance. Three ammonium sensors were installed in full scale reactors, in the aeration tank of Orange County Sanitation District. Two sensors were installed in parallel in the same tank, in order to use one of the sensors as a reference and the other as a test for different operating conditions in order to better study the sensor's behavior. The third sensor was installed in the effluent of the activated sludge process in order to focus also on how the sensor's accuracy and reliability changes depending on the installation position and measuring range. Given the complex nature of wastewater, in terms of composition and variability, numerous experiments were performed, and different operating conditions and maintenance procedures were tested to thoroughly investigate the sensor behavior in field application. Once the ammonium sensors performance had been deeply analyzed and the main flaws were identified and quantified, the second part of the project was centered around improving the sensors reliability, integrating the support of machine learning techniques. Further online sensors were installed in the same aeration tank, specifically pH, ORP, DO and TSS. These additional sensors are typically found in treatment plants and are used to monitor the process behavior and/or control the aeration phase. The datasets from all the sensors, including the ammonium sensors, were utilized to develop a Decision Support System (DSS), to identify sensors faults, specifically ammonium sensors, and promptly generate an alarm to indicate the necessity of a sensors maintenance or adjustment. The DSS implemented was based on the use of Artificial Neural Networks, Principal Components Analysis and different control charts, in order to detect typical ammonium sensors partial failures, which otherwise would be impossible to visually individuate in the raw dataset. Thanks to the use of different sensors, all installed in the same location and descriptive of the same biological process, it is possible to isolate faulty

sensors by looking at the cross-correlation of the different datasets.

1.7 Research Hypothesis and Structure of the Dissertation

The research hypothesis is presented, together with the null hypothesis it attempts to deny.

Research hypothesis: H1

Real-time instrumentation applied in Water Resource Recovery Facilities (WRRFs) can result into a robust and reliable dataset, both for monitoring and control application. In addition, if we build an interconnected network between different sensors, using machine learning techniques, the robustness can further improve by predicting and fault detecting the variables of interest utilizing the information from other water variables. The quantification of robustness and reliability of a sensor can be expressed in terms of accuracy during the entire lifetime of the instrumentation, which refers to the difference between a measured value and a reference. When working with sensors, reference methods are typically performed in a laboratory, under controlled settings. The measurements obtained with the reference method provide a smaller margin of error and can thus better approximate the real value.

The soft-sensor prediction based on multi-variate correlations is more accurate of the actual measurements of the sensor themselves, therefore the summation of the errors of the individual sensors, in time, is higher than the summation of the errors of the network predictions, in time:

$\forall\ e_s^i(\text{t}) \in \{[NH_4^+]$,[pH],[DO],[TSS],[ORP],[Temperature]$\}$

$$\sum_{i=1}^{n} e_s^i(t) > \sum_{i=1}^{n} e_p^i(t)\ \ for\ i \in \{1, ..., n\} \tag{1.1}$$

Where n is the number of water variables considered in the network,

e_s^i(t) is the error between the i-th water variable measured by sensors and lab measurements, in time;

e_p^i(t) is the error between the i-th water variable prediction obtained with the soft-sensor and lab measurements, in time.

Null Hypothesis: H0

Online instrumentation cannot be reliable in wastewater application because of the impossibility to timely detect sensors' faults, even when sensors are considered in an interconnected network.

Testing procedure:

The research hypothesis H1 will be tested by analyzing the sensors reliability and accuracy in field conditions, focusing on ammonium sensors. In detail, ammonium, DO, pH, ORP, temperature and TSS sensors will be installed in the full-scale aeration reactors of the facility of Orange County Sanitation District. The data collected from the sensors will be used to train an Artificial Neural Network (ANN). The network topology will be tuned in order to minimize the error function between predictions and real data, such as the mean squared error (MSE). Finally, the network will be tested during different sensors and/or process faults in order to access the capacity and the timing of the model to recognize a fault, and if it can provide good predictions to be used in replacement of faulty signals.

In Chapter 2, a yearlong field evaluation of ISE-ammonium sensors is described, studying the sensor performance under different operating conditions during daily, weekly, and seasonal variations. Three ISE-ammonium sensors were installed in the aeration tank of the activated sludge process of Orange County Sanitation District. Various factors, influencing the sensor in field application, are presented critically, such as fouling, interfering ions, disturbance from aeration bubbles, and different maintenance and operations. The study highlights how the background ion content of the mixed liquor influences the performance for the low range application. We recorded a 40% error over the full measurement range due to K^+ and Na^+ concentrations below 18 and 225 mg l^{-1}, respectively. This 40% error is comparable in magnitude to the sensor precision, for the high range application, whereas for the low range application the percent error exceeds the sensor precision by 1-log, showing how critical is the application of this technology for low range measurements. Finally, we tracked sensor fouling over time in operation, and observed both reversible and irreversible fouling, and their effects on the sensor operation and maintenance schedule.

Chapter 3 of the dissertation presents a comprehensive analysis of the fouling development in activated sludge process with a case study on ammonium sensors and Ion-Selective Electrodes technology. The response time of the electrodes is found to be the most impacted by fouling. By analyzing step-change experiments with a diffusion model, after one week of fouling the response time is demonstrated to increase exponentially with time. The performance of the sensor is also affected in terms of measurement accuracy, showing a negative drift of the fouled sensor (-0.11 mg NH_4^+ $l^{-1}d^{-1}$). Scanning electron microscope analysis and energy dispersive x-ray spectroscopy elemental mapping were performed over new and used sensor membranes to study the irreversible fouling composition and morphology. Fouling appears as thick coating with different agglomerates and crevasses, which reveal damages on the PTFE protective layer of the membrane. Fe, P, Ca, Mn, S, K and Cl were the main elements detected, in decreasing order. The high content of Fe in the fouling layer originates from the addition of ferric salts to the primary treatment of the plant, which becomes a major

contributor to the inorganic fouling of the sensor. The study also quantifies the increase in Total Suspended Solids (TSS), Volatile Suspended Solids (VSS), and total Fe in the reversible fouling layer over time as described by a saturation model. However, the relative composition remains stable: 84% of VSS/TSS and 20% of Fe/iSS, on average.

In Chapter 4, the study focuses on the fault detection of ammonium sensors, especially for effluent monitoring, given their potentiality in Ammonium-Based Aeration Control (ABAC) but the historical lack of reliability. An Artificial Neural Network model was built to predict the ammonium content in the effluent by utilizing the information from other five sensor installed in the activated sludge tank: NH_4^+; pH; ORP; DO; TSS. The residual between the model prediction and the effluent ammonium sensor signal was utilized for a fault detection mechanism, based on Principal Component Analysis monitoring charts. Differing from other research, the present study utilizes sensor faults collected from one year of historic data of the actual sensor setup instead of artificially generate process anomalies using deterministic models. The most common issues identified from the historic data using the proposed fault detection methodology were treatment process anomalies, calibration biases, and fouling drifts. Treatment process anomalies, calibration bias fault, and a fouling drift, were the most common issues identified from the historic data and promptly individuated by the proposed fault detection methodology. Once a fault is detected, the model prediction can be actively used in place of the sensor to control those processes that rely on the said sensor, without affecting the treatment process by utilizing faulty datasets.

Chapter 2

ISE-ammonium Sensors in WRRFs: Field Assessment of Their Influencing Factors

A version of this chapter is published in the journal Environmental Science: Water Research Technology, 2019, 5(4), 737-746.

2.1 Abstract

Real-time quantification of the ammonium content in water resource recovery facilities (WRRFs) has raised attention in recent years for both monitoring and process control. Ion-selective-electrodes are a viable solution for online ammonium measurements with increasing number of installations worldwide. This paper describes a year-long field evaluation of ISE-ammonium sensors and discusses the sensor performance under different operating conditions during diurnal, and seasonal variations. Three ISE-ammonium sensors were installed

in the aeration tank of an activated sludge process. Specifically, one probe was installed at the end of the aeration tank, to test the sensor in low range conditions ($\leq$ 1 mg N-NH_4^+ L^{-1}). Several factors that influenced the sensor in field applications are presented critically, such as fouling, interfering ions, disturbance from aeration bubbles, and various maintenance and operating procedures. The study highlights how the background ion content of the mixed liquor affects the performance of the low range application. We recorded a 40% error in NH_4^+-N concentration over the low range measurement ($\leq$ 1 mg L^{-1}) due to K^+ and Na^+ content (18 and 225 mg L^{-1}) on average respectively. This 40% error exceeds the sensor precision by 1-log. Therefore, for low range installation, the background interference due to other cations represents the main bottleneck in the current state of this technology. On the other hand, for the high range application, the ion interference led to an error comparable in magnitude to the sensor precision of 5%. Sensor fouling was tracked over the time in operation: both reversible and irreversible fouling was observed, and it differed according to the application and, therefore, to the wastewater composition. Different operation and maintenance procedures were addressed, and the study points out how overzealous maintenance or improper procedure can be counterproductive.

2.2 Introduction

In recent years, water resources recovery facilities (WRRFs) have been facing increased regulations on water quality discharge as more strict limits are imposed. To meet the required quality standards, more frequent comparison measurements, like continuous real-time measurements, have become an appealing option. Moreover, with increasing pressure to recycle and reuse water in certain areas of the world, closely monitoring the effluent water quality has become the standard treatment strategy (Metcalf & Eddy, 2007). Among the different quality constituents, online ammonium quantification has raised attention because of the

diverse possible applications, both for monitoring and control. The most common implementation concerns the biological ammonia removal process. Depending on the biological process, the instrumentation can be applied in aerated tanks or in anoxic conditions and in different positions along the same process. Therefore, the mixed liquor composition can vary significantly in terms of solids content, organic matter, and biomass, and as a result the instrumentation requires different maintenance. The different applications for continuous ammonium reading are listed below. The instrumentation can be installed in the effluent of the primary clarifier to monitor the nutrient load in the secondary treatment. Also, it can be installed at the beginning and/or at the end of the aeration step in secondary treatment processes, especially for the implementation of ammonium-based aeration control (Rieger et al, 2012a, Rieger et al, 2014) for the optimization of air delivery and energy use. In addition, the ammonium content of the secondary clarifier effluent can be continuously measured for monitoring or can be used to control the chlorine dosage of the following disinfection step in order to estimate the monochloroamines formation or to balance the ratio between chlorine and ammonium (Schuk et al, 1973). Real-time ammonium measurement can be achieved with diverse instrumentations: an analyser or an ISE sensor. Analysers are based on colorimetry or on gas sensitive probe and are installed ex situ. Colorimetric-based analysers conduct analysis on samples of mixed liquor collected periodically and automatically. The sample volume is pumped through an ultrafiltration unit, and then chemicals are added in a small reactor. The reaction generates a coloured component which is correlated with the ammonium concentration and is measured by an optical cell. Gas sensitive electrodes require an ex-situ installation with a pumping system, and in some cases a filtration step is also required. The measurement is based on the complete transformation of ammonium ions (NH_4^+) to ammonia gas (NH_3) by increasing the pH up to 11. The gas is then directly measured without chemical reactions because the electrode membrane is selectively permeable to the ammonia gas. Finally, Ion-Selective-Electrodes (ISEs) are in-situ sensors directly immerged in the environment. These sensors are widespread, low-cost, and are suitable for

nutrient measurements in their ionic species, *e.g.* ammonium, nitrate, chlorine, pH, potassium, sodium, etc. (Winkler et al, 2004, Bonastre et al, 2005, Kaelin et al, 2008, Ingildsen et al, 2002). ISE-NH_4^+ sensors provide a faster response compared to the other ammonium methods and do not consume analytes (Rieger et al, 2002). Such sensors directly measure the ammonium content without a chemical reaction. Furthermore, due to the ion selective membrane of the ISE sensors, the ultrafiltration unit required for analysers and gas sensitive electrodes can be eliminated, thus avoiding the frequent clogging issues caused by the solids in the mixed liquor (Ingildsen et al, 2003; Devisscher et al., 2002).

2.2.1 ISE technology description

Ion-Selective-Electrodes measure the potential difference between two electrodes: a reference electrode and an ion-electrode (Fig. 2.1). The ion-electrode is equipped with an ion-selective membrane to which specific ions can bind to reversibly (Cammann, 1979). The reversible ion-exchange process causes a change in the electrical potential at the interface between the membrane and the liquid analysed. The variations in electrical potential are a function of the logarithm of the ionic activity, and in accordance with Nernst equation:

$$E = E_0 + \frac{RT}{zF} ln(Q) \tag{2.1}$$

where E = measured voltage $[V]$, E_0 = reference constant $[V]$, R = universal gas constant $[JK^{-1}mol^{-1}]$, T = temperature $[K]$, z = charge of the ion [-], F = Faraday constant $[Cmol^{-1}]$, Q = reaction quotient of the cell reaction [-].

A major limit of the ISE technology in wastewater treatment applications is the disturbance caused by other ions with similar binding behaviour toward the ion-electrode. Therefore, the presence of other ions can be detected as ammonium by the sensor. Interference by other

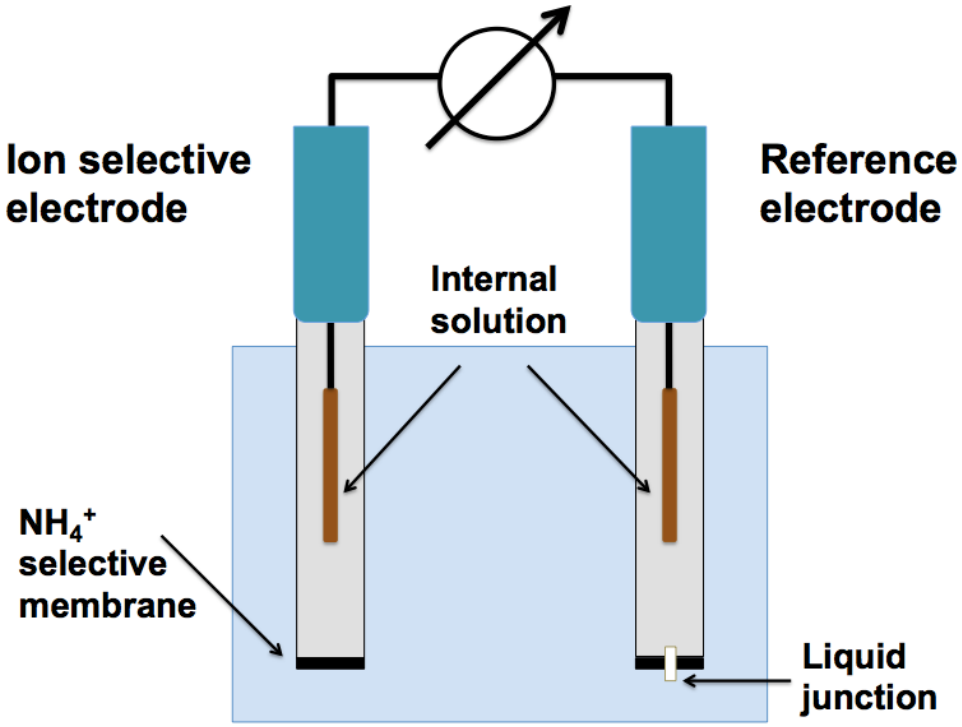

Figure 2.1: Graphic scheme of the physical operation of the ISE-NH_4^+ sensor.

ions can be quantified with the cross-sensitivity ratio:

$$[NH_4^+] = \frac{[M^+]}{CSR} \tag{2.2}$$

where $[NH_4^+]$ = ammonium concentration $[mgL^{-1}]$, $[M^+]$ = interference cation concentration $[mgL^{-1}]$, CSR = cross-sensitivity ratio [-].

In the case of the ISE-NH_4^+ electrode, monovalent cations like potassium and sodium are the major challenge for the ammonium measurement, with a cross-sensitivity ratio of 1:(15–30) and 1:(1000-1300), respectively, over the ammonium electrode. This implies that a potassium concentration of 20 mg L^{-1} establishes the same potential difference of approximate 1 mg L^{-1} of ammonium. Sodium interference applies analogously. Because the potassium disturbance is the major issue for ammonium measurement, ISE-NH_4^+ sensors have recently been supplied with a potassium-electrode for automatic real-time compensation of the potassium disturbance.

A primary concern with online monitoring concerns the signals' consistency over time, as they can be subject to various issues such as noise, bias, drift, outliers, etc. (Thomann et al, 2002). Previous studies have approached the topic surrounding the measurement uncertainty of online probes in general (Rieger et al, 2005; Thomann et al, 2008) and ISE applications more specifically (Rieger et al, 2002). However, further investigation is required to identify the factors influencing the reliability of the ISE-NH_4^+ sensors, to test their effect on the technology, to evaluate the stability of the sensor's performance in time, and to quantify the accuracy of the sensor in different field conditions and ammonium ranges. The goal of this paper is to present the results of a year-long field study in a full-scale WRRF. This study aims to evaluate the fouling development with different wastewater composition, to quantify the inaccuracy of the sensor reading due to the cation interference under different field applications, to evaluate the disturbance of aeration bubbles, and to analyse how different maintenance and operation procedures affect the performance of the sensor over time.

2.3 Materials and Methods

Three ISE-ammonium sensors (Horiba model HC-200NH) were installed in the aeration zone of a WRRF's secondary tank. The plant is comprised of two parallel biological processes and the overall secondary effluent is fed to a subsequent advanced tertiary process for water reclamation. In this plant there are two parallel biological processes, one of which is an activated sludge process operating in the Ludzack-Ettinger configuration with an annual average SRT of 5 days. The influent to the activated sludge process presents the following average water quality characteristics: 251 mg COD L^{-1}, 55 mg TSS L^{-1}, 25 mg N-NH_4^+ L^{-1} and pH 7.8. The aeration tank is divided in five aerated zones, with an initial anoxic zone mixed with coarse-bubble diffusers and the rest aerated with 7in fine-pore disc diffusers. There exist full baffles between stages 2 and 3, and between 3 and the rest of the tank. Two

sensors were installed in the center of the first aerated zone (Fig. 2.2).

Figure 2.2: Photograph of the installation of two ammonium probes at the beginning of the aeration tank (high range conditions).

Another probe was subsequently installed in the same tank in the centre of the last aeration zone where the ammonium content in wastewater falls within the low range (≤ 1 mg L^{-1} for extended periods of time). This third sensor is characterized by the same technology, but is set with a higher precision which is required when measuring low range ammonium (precision of 0.2 mg L^{-1} for high range measurement and 0.02 mg L^{-1} for low range measurement). In our case study, the potassium cross-sensitivity ratio was 1:22 and the sodium ratio was 1:1000. The probes are supplied with a potassium ion-selective electrode, which measures the potassium content and allows interference compensation from the potassium in wastewater. Furthermore, an auto-cleaning system was installed. This auto-cleaning device is designed to use ultrasounds to delay the growth of the fouling layer. The sensors provided signals with a 2-minute frequency which were collected with a data logger (Graphtec Mod. GL240).

2.3.1 Low range measurement considerations

ISE technology has shown unstable behavior when applied for long periods in low range concentrations (< 1 mg L^{-1} of ammonium for ISE-NH_4^+ sensor). The issue originates from the strong osmotic pressure that is established between the internal solution of the ion-electrode (high ionic concentration) and the sample (low ionic concentration), which leads to irreversible water absorption into the electrode and inevitable deterioration (Fig. 2.3). Therefore, ion-electrodes are characterized by a shorter lifetime when applied to low range conditions.

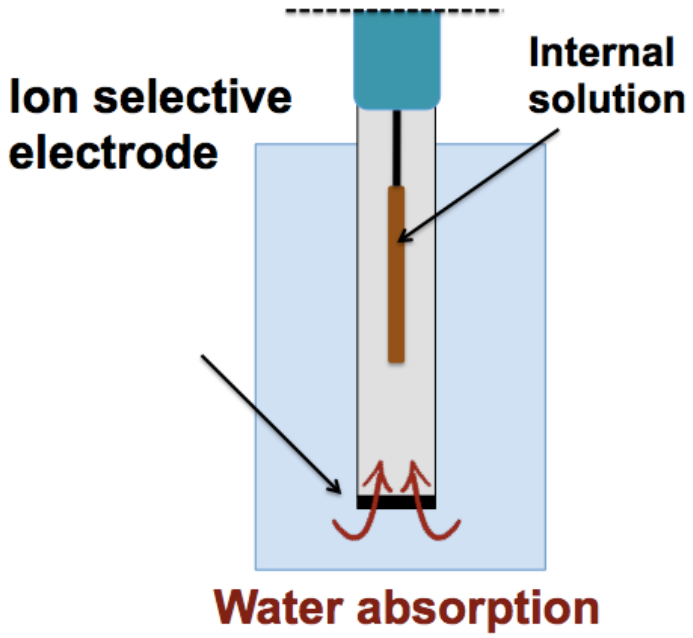

Figure 2.3: Graphic explanation of the water absorption phenomenon, triggered by the ammonium low range conditions.

2.3.2 Technology validation procedure

For the technology validation, a standard of procedure was developed to compare the sensor measurements against grab sample analyses. A weekly sample of wastewater of 2L was collected from the tank, next to the sensor installation, and maintained well mixed with a stirrer in a cylindric container. The ISE sensor was pulled out from the tank and immersed

in the 2L container, and the measured value was recorded while a grab sample of 50 mL from the cylindric container was simultaneously taken for lab analysis. After collection, the grab-sample was immediately filtered at 0.45 μm (Simsii, Inc, hydrophobic PVDF syringe filter). The ammonium concentration was measured using the salicylate method (AmVer TNT, Hach according to the APHA Standard Method 4500-NH3), with a precision of ± 0.05 mg L^{-1}. The cation content (primarily sodium and potassium) was measured using ion chromatography (940 Professional IC Vario, Metrohm USA), with a precision of 0.3 mg L^{-1} for potassium and 5 mg L^{-1} for sodium.

2.3.3 Sensor preparation

After the installation of the probe, a two-point calibration using standard solutions was performed. The ammonium and potassium electrodes were simultaneously calibrated using two standard solutions with the following ammonium and potassium content: 1 mg N-NH_4^+ L^{-1} and 5 mg K^+ L^{-1} for the first solution, and 10 mg N-NH_4^+ L^{-1} and 50 mg K^+ L^{-1} for the second solution. Both standard solutions were also composed of 0.1 mol L^{-1} of Lithium Acetate Dihydrate, which contributes to the ionic strength of the solution and therefore to the voltage measurement by the sensor. The standard solutions were provided by the vendor and they determined a calibration range of ammonium and potassium (1 to 10 mg L^{-1} for ammonium and 5 to 50 mg L^{-1} for potassium) similar to the corresponding wastewater content. The calibration slope represents the correlation between the potential difference measured by the voltmeter and the logarithm of ammonium concentration. Afterwards, another calibration procedure called sample adjustment was performed. The sensor is immersed in the wastewater and the reading is compared to the lab analysis of a grab-sample of wastewater collected next to the sensor. With this procedure the calibration curve is adjusted to environmental conditions, thus removing the background from disturbance ions. The sample adjustment was performed every two-three months, depending on the drifting rate of the sensor, in order to perform the procedure when the difference between sensor's reading and lab analysis was

20% (or 2 mg L^{-1}) at the peak. For the low range installation, no sample adjustment was performed because of the difficulty to perform an accurate procedure in the low working range.

2.3.4 Sensor cleaning procedure

The probes were continuously exposed to ultrasonic cleaning with 70 KHz of frequency. The ultrasonic effect allows for a delay in the fouling development. The manual cleaning event was conducted by using a cloth dampened with water. The manual cleaning procedure was consistently performed by wiping the front element of the sensor twice. Chemical cleaning, using a solution of NaOCl 0.08M, was performed every 2 months to remove the persistent fouling.

2.4 Results and Discussion

The various factors influencing the sensor performance were studied and are described below. We divided our report into the following sections: fouling; interfering ions; disturbance from aeration bubbles; maintenance and human error.

2.4.1 Fouling

The probe signal was evaluated at high and low range of ammonia concentration. In addition, different cleaning at different frequency was conducted in order to study the sensor signals under different degrees of fouling. The fouling development was studied for six months in order to consider the lifetime of the electrodes. In this period of time the temperature of the wastewater was 28±2°C and no changing in process operation or in the wastewater composition was identified, which otherwise could have altered the fouling study. Figure 2.4 shows the effects of the cleaning procedure on the high range application in different fouling

conditions and at different times of operation. It can be seen that two types of fouling are formed: reversible fouling, building up as a thick layer and dependent on the frequency of cleaning, and irreversible fouling, developing in the long-term operation, which can be removed only with a chemical cleaning procedure.

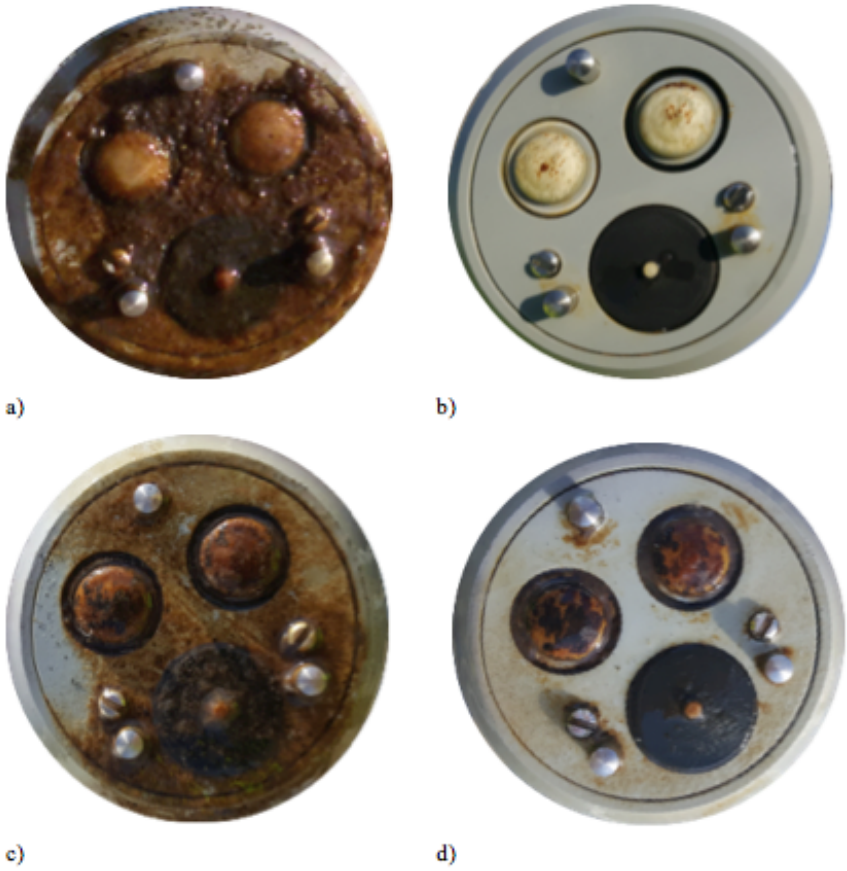

Figure 2.4: Pictures of different fouling conditions of the sensors installed in high range application. a) One month of operation after one month from installation (i.e., new sensor). b) Outcome of the cleaning procedure of sensor in (a). c) One month of operation after six months from installation. d) Outcome of the cleaning procedure of sensor in (c) .

Figure 2.5 displays the probe installed in low range application in different fouling conditions. The low range sensor was cleaned with the same methodology and frequency of the high range application. In both pictures, no thick fouling layer is denoted but a similar irreversible fouling is identified after three months from installation. The irreversible fouling is a function of the time of operation of the electrode itself and it represents a major component of the aging of the electrodes, both at high and low range application.

Figure 2.5: Pictures of different fouling conditions of the probe installed in low range application. a) One month of fouling in the first month since installation. b) One month of fouling after three months from installation.

2.4.2 Interfering ions

After the installation of the instrument, a 2-point calibration is required with standard solutions. This step is followed by sample adjustment with wastewater, during which the calibration curve is corrected by comparing the sensor measurement against an accurate reference. This procedure is conducted to remove the background signal of other ionic species, such as sodium. However, the sample adjustment may still not be able to fully remove the background interference due to the variations in ionic composition (such as sodium) at a daily, weekly, and seasonal timescale. Therefore, a study on the inaccuracy of the potassium sensor and on the dynamic variations in background ionic species was conducted in order to quantify their influence on the ammonium readings. The potassium electrode accuracy was tested by comparing the probe measurements against the ion chromatography of the grab samples (Table 2.1). High and low range application were studied separately. Their respective potassium electrode presented a similar accuracy, as expected, since the technology of the electrodes is identical. For high range applications, the error over the ammonium measurement (due to the inaccuracy of the potassium measurement) is 0.2 ± 0.2 mg L^{-1} of $N\text{-}NH_4^+$, comparable to the precision of the sensor itself (0.2 mg $N\text{-}NH_4^+$ L^{-1}) and therefore negligible. On the other hand, for low range applications the ammonium error is 0.1 ± 0.1 mg L^{-1} of $N\text{-}NH_4^+$, which is one order of magnitude higher than the precision of

the sensor (0.02 mg N-NH_4^+ L^{-1}) and therefore must be taken into consideration. Also, on the same grab samples, lab analyses of the ammonium measurement were compared to the sensors reading, showing the following ammonium error: 0.30 ± 1.61 mg L^{-1} of N-NH_4^+ for the high range and 0.31 ± 0.62 mg L^{-1} of N-NH_4^+ for the low range sensor. It can be noticed that the measured ammonium error range is higher than the estimated error range due to the potassium interference, since other factors simultaneously are affecting the performance (i.e., other cations and drifting behaviour).

Table 2.1: Summary of the accuracy analysis for both ranges. The potassium measurement of the sensor is compared to ion chromatography results on grab-samples. The ammonium measurement of the sensor is compared to lab analysis on grab samples. The average error on the ammonium measurement (due to potassium measurement inaccuracy) and the 95% confidence interval error range are calculated, assuming a cross-sensitivity ratio of 1:22 between ammonium and potassium.

Potassium interference	**High range application**		**Low range application**	
field study	Concentration (mg L^{-1})	Pct. (%)	Concentration (mg L^{-1})	Pct. (%)
Number of samples	21	-	20	-
K^+ average content	18.1	-	17.7	-
Average K^+ error	+4.3	+24%	+2.9	+14%
68% Confidence interval of K^+ error on t-student (1 σ)	± 4.4	24%	± 2.4	17%
Average NH_4^+ error	+0.30	+7%	+0.31	+31%
68% Confidence interval of NH_4^+ error on t-student (1 σ)	± 1.61	± 37%	± 0.62	± 63%
Interference NH_4^+/K^+ ratio [$mgNH_4^+$/ mg K^+]	1:22	-	1:22	-
Estimated average error on NH_4^+ due to K^+	+0.2	-	+0.1	-
Error range on NH_4^+ due to K^+ (68% CI)	0-0.4	-	0-0.2	-
Precision of the sensor	0.2	-	0.02	-

Figure 2.6 reports the fluctuation of sodium and potassium on a daily basis in the secondary effluent of this facility. It can be seen that the ranges of sodium and potassium over a week are 180-270 mg Na^+ L^{-1} and 12-29 mg K^+ L^{-1}, respectively.

In order to study the uncorrected signal interference originating from the sodium fluctuations

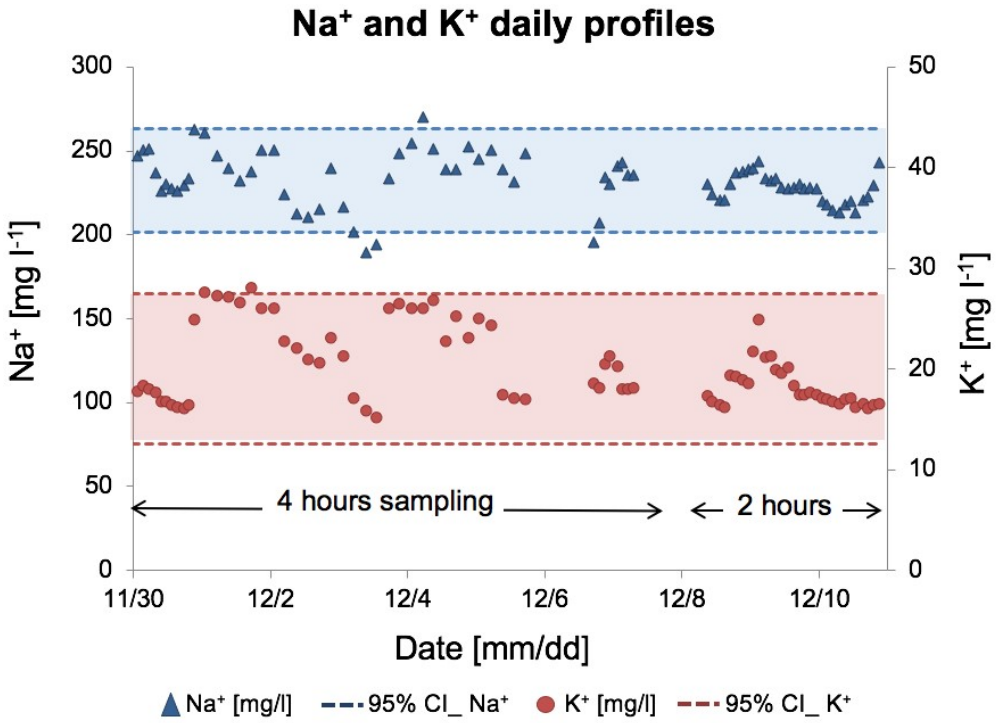

Figure 2.6: Sodium (triangles) and potassium (dots) content in wastewater over a 5.5d period. The samples were collected every four hours at first (days 1.0-4.4) and every two hours subsequently (days 4.0-5.5). The cation concentrations were measured with ion chromatography. The dashed lines represent the 95% confidence intervals of the sodium and potassium ranges.

in the aeration tank, the sensor was evaluated at different sodium concentrations. Different experiments on the field and in the lab were conducted to cover the sodium range observed in the field (Table 2.2). Overall, the sodium increase led to an increase overestimation of the ammonium content, as expected. The maximum error calculated from the lab experiments was consistently approximating 0.5 mg N-NH_4^+ L^{-1}, within the ammonium range tested (from 1 to 10 mg N-NH_4^+ L^{-1}), which can be negligible for high range applications (in relative terms, corresponding to 5-6% error), while it represents a more evident issue when working in low range applications (40% of maximum error). The field experiments, conversely, did not exhibit consistent results due to the uncontrolled environmental conditions.

The effect at low range overlaps with the expected shorter life span of the ISE at this range, which is hypothesized to originate from the osmotic gradient that is established between the

Table 2.2: Evaluation of the sodium influence over the ammonium measurement, obtained performing different experiments at laboratory and field scales. The lab experiments were performed using twelve standards with four different sodium contents (150, 200, 250, and 300 mg L^{-1}), fixed content of potassium (20 mg L^{-1}) and three different concentrations of ammonium (10, 5, and 1 mg L^{-1}). The standards were tested three times each with the sensor. A similar experiment was conducted in the field with three different samples of process water with equal ammonium (4.8 mg L^{-1}) and potassium (19.7 mg L^{-1}) content but diverse sodium content (257, 307, and 360 mg L^{-1}).

Sodium interference in lab				**Field study**	
Sodium content $[mgL^{-1}]$	NH_4^+ reading $[mgL^{-1}]$ $(10mgL^{-1})$	NH_4^+ reading $[mgL^{-1}]$ $(5mgL^{-1})$	NH_4^+ reading $[mgL^{-1}]$ $(1mgL^{-1})$	Sodium content $[mgL^{-1}]$	NH_4^+ probe $[mgL^{-1}]$ $(4.8mgL^{-1})$
150	9.8	5.1	1.3	257	4.8
200	9.8	5.3	1.5	307	4.9
250	10.3	5.3	1.3	360	4.8
300	10.5	5.1	1.4	-	-
Maximum error (ppm)	**0.5**	**0.3**	**0.4**	**Maximum error (ppm)**	**0.1**
Maximum error (%)	**5.0%**	**6.0%**	**40%**	**Maximum error (%)**	**2.0%**

internal solution of the ion-electrode (i.e., with elevated ionic concentration) and the sample (*i.e.*, with low ionic concentration).

2.4.3 Disturbance from aeration bubbles

Another potential disturbance we evaluated was the effect of aeration bubbles. The bubbles present in the mixed liquor impact the sensor membrane. The potential disturbance of the bubble impact on the membrane was evaluated with a lab experiment, using a tubular diffuser installed in a Plexiglas tank 4x2x1.5 ft (or 1.22x0.61x0.46 m) in size. Figure 2.7 shows the setup of the experiment and provides the visual effect of the operation of the diffuser. The probe was positioned over the diffuser in order to get a vertical impact of the bubbles. The conditions tested on the sensor were more invasive than in a large-scale aeration tank, since the limited depth of the lab tank restricts the horizontal spreading of the

bubble plume and determines a higher frequency of collision with the electrodes' membrane. The experiment was performed with four different flow rates: 0 (mixing conditions without aeration), 20, 30, and 40 SCFH (or 0, 0.57, 0.85 and 1.13 $Nm^3\ h^{-1}$). The bubble impact on the electrodes did not show substantial interference: ±1% of ammonium variation and ±2% of potassium variation (9±0.1 mg L^{-1} of $N\text{-}NH_4^+$ and 150±3 mg L^{-1} of K^+), which is within the precision range of the sensor itself.

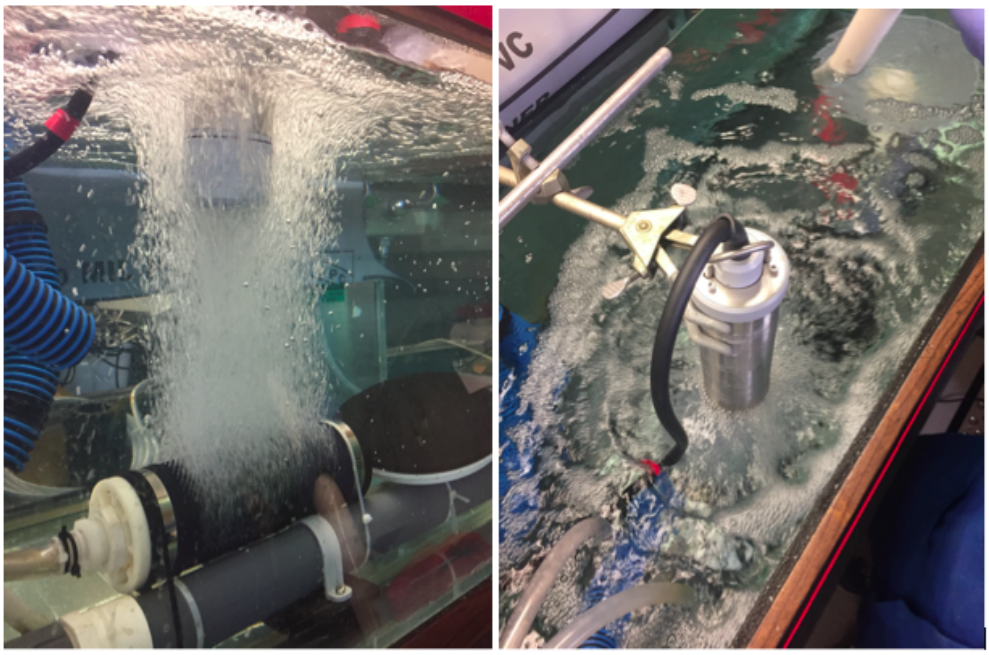

Figure 2.7: Photographs of the experimental setup to assess the aeration impact. The view from the side (left) shows the placement of the probe over the tubular diffuser. The view from the top (right) shows the surface due to bubble rise.

2.4.4 Maintenance and Human Error

Various maintenance operations were addressed to study their influence on the sensor signal. Ammonium analysis on grab samples was performed before and after each periodic cleaning event to compare it with the probe signal. Figure 2.8 reports the difference in percentage between the signal from the high range sensor and the reference analysis on a weekly basis. The bottom chart provides information on the time schedule of the different maintenance events. It is clear that cleaning procedures do not always result in lower error because other

factors may also influence the signal: for example, incorrect calibration or sample adjustment. A reduced error range can be seen since a new reference method was adopted (orange line in Fig. 2.8). Prior to the employment of this method, the comparison was done by leaving the probe inside the aeration tank and collecting the sample in proximity of the sensor for laboratory analysis. However, the aeration tank is not perfectly mixed and homogeneous, and the grab-sample might not be collected at the exact depth and position of where the sensor is immersed. Therefore, the grab sample composition might not be identical to the wastewater measured by the sensor, leading to a misrepresented comparison between reference and sensor. This phenomenon highlights the importance of following a consistent procedure when evaluating a sensor using a comparison with grab sample analysis. The standard deviation of the signal error, calculated since the new reference method was implemented, is 1.7 mg L^{-1}, which corresponds to a coefficient of variation of 30%. Considering the large variation of the error obtained by the weekly comparison (described by the standard deviation), a more thorough evaluation of the sensor accuracy was performed: a high-frequency comparison campaign for the high and the low range application (Fig. 2.9). The samples were collected on an hourly basis for two and four days, respectively.

The average error and the standard deviation were calculated from both of the high-frequency grab sampling campaigns: average error of 0.8 mg L^{-1} and standard deviation of 0.5 mg L^{-1} for the high range and an average error of 0.1 mg L^{-1} and standard deviation of 0.5 mg L^{-1} for the low range application. The standard deviation for the two applications is comparable. However, the standard deviation calculated from the weekly comparison is three times higher (1.7 mg L^{-1}) than the one obtained with the high-frequency sampling campaign. This observation shows how the different maintenance operations and fouling conditions can significantly influence the reading of the probe, thus increasing the difficulty of judging the performance of the probe over the long term. Furthermore, the high-frequency sampling campaign was analysed by plotting the data from low to high range, as shown in Fig. 2.10. In this plot the relative error in percentage is illustrated using three regions with

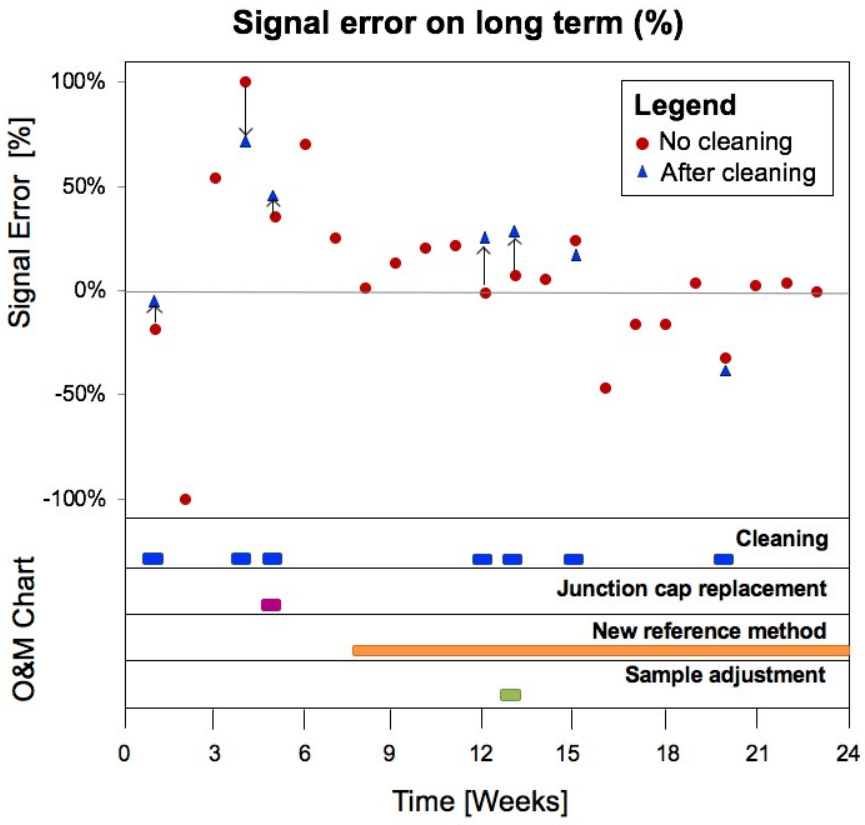

Figure 2.8: Ammonium signal error in percentage over time (difference between probe and grab sample ammonium measurements). The comparison between probe and grab sample was conducted once a week. When cleaning maintenance was performed, the error was calculated also after cleaning. The dots represent the error obtained with fouled probe and the triangles after the probe was cleaned. The bottom part of the graph reports the operations and maintenance (OM) conducted on the probe in time.

different shading: ±50% in red, ±30% in green and ±15% in blue. The data points are coloured consistently with their corresponding error region. It can be seen that the lower the ammonium range, the higher the relative error percentages. This phenomenon is due to the relatively greater absolute error at lower ranges.

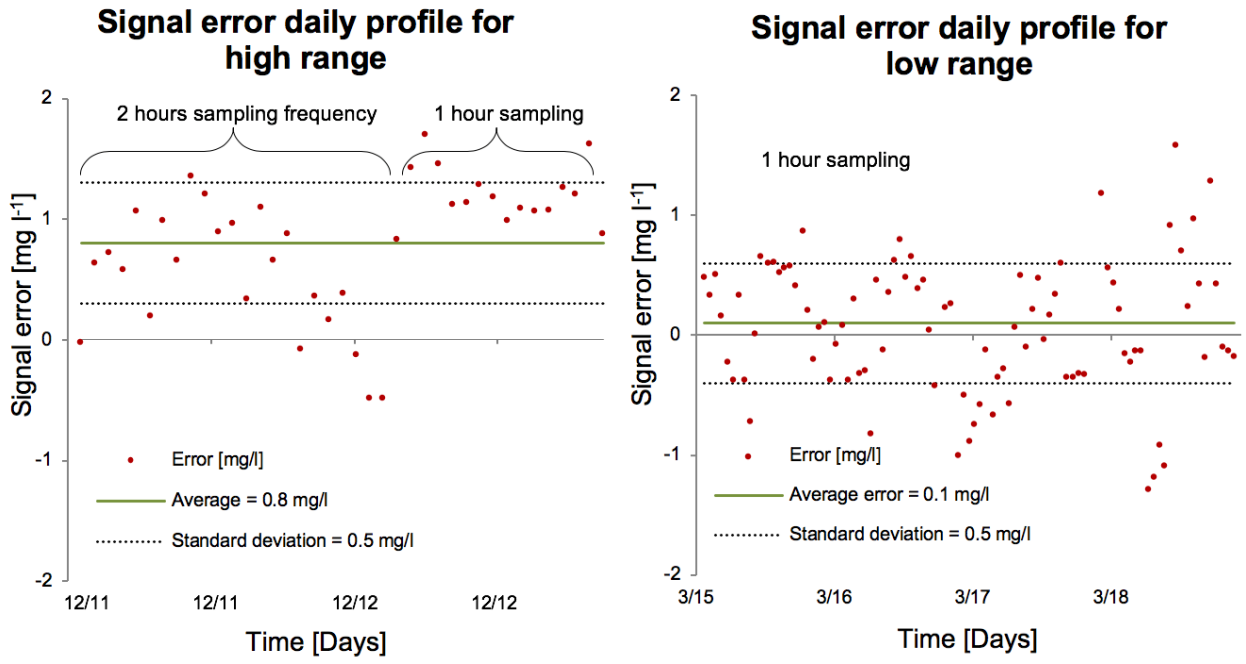

(a) (b)

Figure 2.9: Signal error over time (difference in ammonium between probe and grab sample). The solid lines show the average error and the dashed lines the standard deviation. (left) The samples were collected every two hours at first and every hour subsequently for the high range campaign. (right) For the low range campaign the samples were collected every hour.

Sample adjustment is another critical maintenance operation due to its potential to create signal disruption. Figure 2.11 shows that the incorrect sample adjustment led to a bias of the signal, including an enhancement of the peaks and therefore a general overestimation of the ammonium content. Consequently, it is important to follow a robust procedure when performing a sample adjustment (using the technology validation methodology explained in Materials and Methods). Also, limiting the number of sample adjustments to the minimum required can help avoid human-induced bias in the signal. Hence, the cation content in wastewater was also studied on a weekly basis to address the frequency required for a sample adjustment procedure on a long-term scale.

Figure 2.12 reports the trend of sodium and potassium over time. The monthly fluctuation of the interfering cations is relatively restrained comparable to the weekly range (Fig. 2.6). Therefore, for this case study, an excessively frequent renewal of the sample adjustment

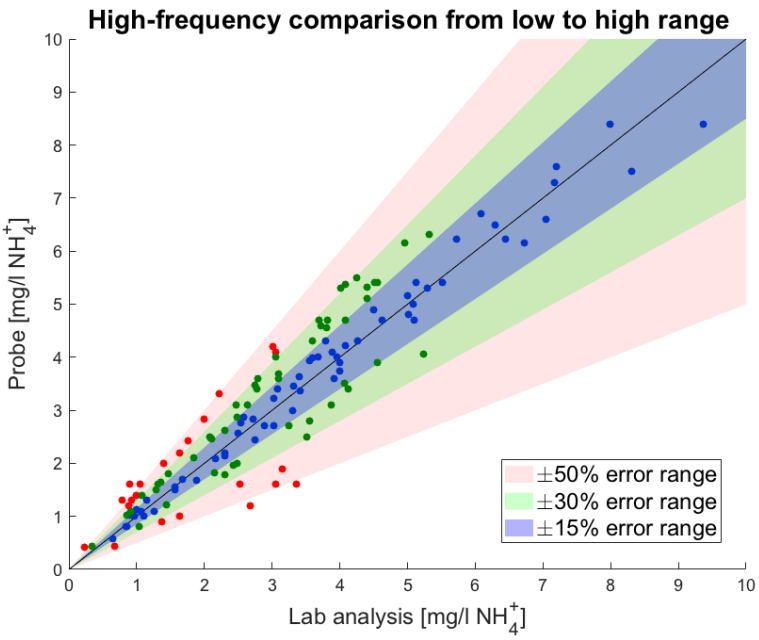

Figure 2.10: High-frequency comparison of the probe signal with lab analysis as function of the ammonium concentration, from low to high range. The red, green and blue regions represent the ±50%, ±30%, and ±15% of error range, respectively. The data points are reported in different colours (red, green and blue) corresponding to the error region they belong to.

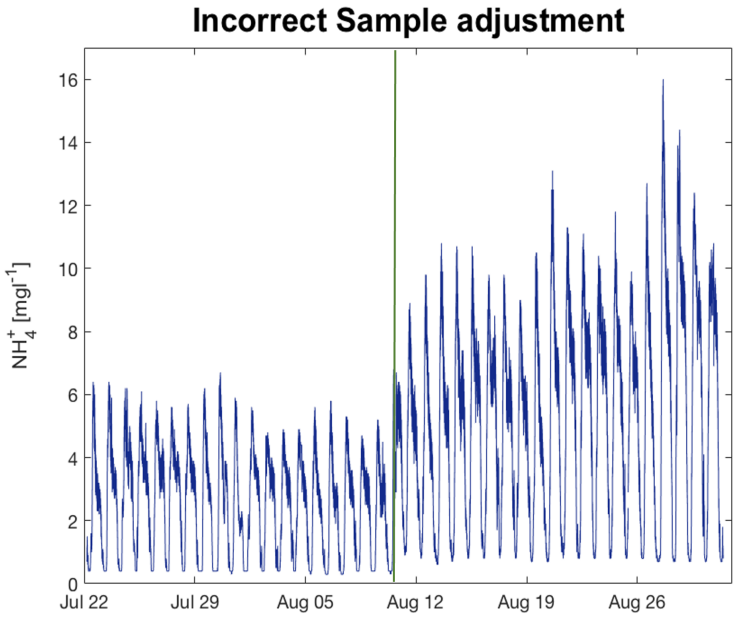

Figure 2.11: Effect of an incorrect sample adjustment on the ammonium signal vs. time. The vertical line highlights the sample adjustment event.

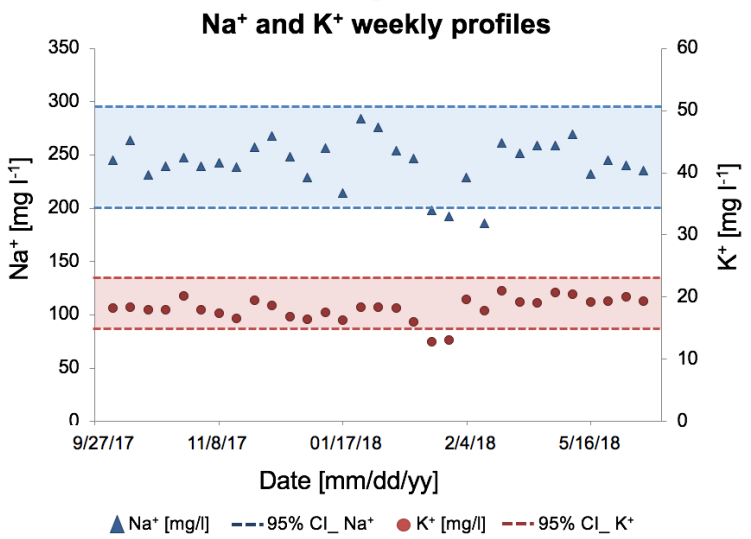

Figure 2.12: Sodium (triangles) and potassium (dots) trend in time. The dashed lines represent the 95% confidence interval of the sodium and potassium range.

was not advisable. However, in WRRFs that are connected to a combined sewer system or that are subject to periodic industrial discharges, higher ionic fluctuations may manifest. Hence, more frequent sample adjustment may be necessary in order to control the signal error. Furthermore, since the high-frequency comparison showed more consistent results (*i.e.*, smaller standard deviation), it could be advisable to perform a multi-point sample adjustment instead of a single-point procedure. Multiple comparisons should be planned for different times of the day, taking into account the periodic variations of the background interference. This procedure would increase the consistency of the sensor signal since it has been demonstrated how the sample adjustment can significantly affect the sensor reading if not performed properly.

2.5 Summary and Conclusions

Two types of fouling are formed on the selective membrane of the sensor: reversible fouling and irreversible fouling. The first is dependent on the cleaning frequency of the sensor, on

the composition of the wastewater characteristics, and on the sensor location along the tank. This type of fouling can be easily removed by gently wiping the surface with a damp cloth. The sensor application in high range condition presents a faster and enhanced reversible fouling formation. In low range applications, reversible fouling appears less pronounced and requires more time to develop. Therefore, the cleaning frequency of low-range sensor applications could be reduced. Also, the fouling development is related not only to the ammonium concentration and wastewater composition but also to the bacterial activity and stage of the bioprocess treatment, which is maximum in low range. The irreversible fouling, on the other hand, is comparable for both high and low range applications and is one of the main contributors to the ageing of the electrodes. This behaviour could be explained if the irreversible fouling were mainly composed of inorganic compounds (scaling), since their content in wastewater is usually not affected by secondary treatment. The sodium and the potassium interference (due to the inaccuracy of the electrode) indicate similar results. For high range applications, the disturbance is comparable to the precision required by the sensor and represents a small relative error over the measurement (5%). For a low range application, the resulting ion interference is one order of magnitude higher than the precision of the sensor, denoting a significant relative error over the measurement (40%). Therefore, for low range installation, precision and the accuracy of the sensor are not comparable, representing a bottleneck in the current state of this technology. The sensor readings were sensitive to the sample adjustment procedure. It is important to understand that while a correct sample adjustment can compensate for the background ionic interference, an improper procedure may induce a bias in the signal and/or result in amplification/narrowing of the signal peaks. These issues can be prevented by limiting the number of sample adjustments to those strictly required over the lifetime of the sensor. Also, future research should evaluate the number of samples and of sampling points necessary for optimal sample adjustment.

Chapter 3

Functional behavior and microscopic analysis of ammonium sensors subject to fouling in activated sludge processes

A version of this chapter is published in the journal Environmental Science: Water Research Technology, 2020, DOI: 10.1039/D0EW00359J.

3.1 Abstract

Fouling is an issue associated with all sensor instrumentation deployed in wastewater that causes a loss in sensitivity and reproducibility of the sensor elements, thus requiring frequent re-calibration. This paper presents a comprehensive analysis of the fouling development in activated sludge process with a case study on ammonium sensors and Ion-Selective Electrodes

technology. The response time of the electrodes is found to be the most impacted by fouling. By analyzing step-change experiments with a diffusion model, after one week of fouling the response time is demonstrated to increase exponentially with time. The performance of the sensor is also affected in terms of measurement accuracy, showing a negative drift of the fouled sensor (-0.11 mg NH_4^+ $l^{-1}d^{-1}$). Scanning electron microscope analysis and energy dispersive x-ray spectroscopy elemental mapping were performed over new and used sensor membranes to study the irreversible fouling composition and morphology. Fouling appears as thick coating with different agglomerates and crevasses, which reveal damages on the PTFE protective layer of the membrane. Fe, P, Ca, Mn, S, K and Cl were the main elements detected, in decreasing order. The high content of Fe in the fouling layer originates from the addition of ferric salts to the primary treatment of the plant, which becomes a major contributor to the inorganic fouling of the sensor. The study also quantifies the increase in Total Suspended Solids (TSS), Volatile Suspended Solids (VSS), and total Fe in the reversible fouling layer over time as described by a saturation model. However, the relative composition remains stable: 84% of VSS/TSS and 20% of Fe/iSS, on average.

3.2 Introduction

In recent years, many water resources recovery facilities (WRRFs) focusing on water reclamation have faced stricter limits for nutrients discharge (Oneby et al, 2010; Gerrity et al, 2013). Continuous online measurements are fundamental to deploy new and improved control strategies, which would otherwise not be possible with a low sampling frequency rate. In addition, the increasing trend towards water reuse has led to the high frequency monitoring of effluent quality to guarantee the safety of reclaimed water (Metcalf and Eddy, 2007). Among the different water quality constituents, recent focus has been given towards online ammonium quantification for both monitoring and control purposes. The ability to obtain

continuous ammonium measurements has allowed the implementation of ammonium-based aeration control to optimize the air delivery of the aeration system with consequent reductions in energy use (Rieger et al, 2012a; Rieger et al, 2014; Regmi et al, 2014). Recently, ion-selective electrode (ISE) sensors have largely being deployed for online ammonium measurement due to their fast response, low initial capital investment and absence of analytes consumption and filtration unit requirements. In detail, ammonium ion-selective electrodes are constituted by a polymeric membrane, often PVC $(C_2H_3Cl)n$ plus plasticizer, that contains a specific ionophore for the target analyte. However, the polymeric membrane can easily be damaged by exposure to harsh environments and is characterized by low durability. Usually, the membrane is also coated with a layer of PTFE $(C_2F_4)n$, which provides a hydrophobic surface, as a result of the low surface energy and surface roughness of the material, that reduces and delays the adhesion of bacteria on the membrane (Lewis and Buck, 1979; Zhang et al, 2008; Xue et al, 2010).

3.2.1 Fouling of sensors

Fouling is an issue associated with all sensor instrumentation that is deployed in water/wastewater environment, which causes a loss in sensitivity, reproducibility and necessitates frequent recalibration requirements (Adu-Manu et al, 2017; Ghernaout et al, 2018). In addition, fouling decreases the operating lifetime of the sensor and introduces a degree of error in the collected data (Adu-Manu et al, 2017; Schneider et al, 2019). This is because as fouling develops, an artificial environment around the sensing surface is established, therefore the measured data will not be truly representative of the location sampled (Fettweis et al, 2019).

3.2.2 Analogy with membrane filtration fouling

A limited amount of studies has examined the fouling coating composition and the quantitative impact of fouling on sensors performance. On the other hand, fouling development on filtration membranes (both microfiltration and ultrafiltration) and its effect on the fil-

tration performance has been a widely investigated topic (Yang et al, 2019; Yu et al, 2016; Aslam et al, 2017; Guo et al, 2012). Given the similarity in the membrane composition (polymers), and the analogy in the application (long-term operation in wastewater), literature studies regarding the fouling of filtration membranes can provide a useful comparative reference when approaching the fouling of ISE sensors. Among the factors influencing the fouling development on filtration membranes, the iron content in wastewater was shown to increase the fouling rate due to the rapid formation of colloidal iron oxides (Wang et al, 2010). Coagulants such as ferric chloride and aluminum sulfate are commonly used in water and wastewater treatment for chemical precipitation, including phosphorous removal, and/or for odor control purposes (Rebosura et al, 2018; Racar et al, 2017; Wan et al, 2016; Madhavi et al, 2017; Li et al, 2017; Caravelli et al, 2010; Rosso and Al-Omari, 2019). Iron dosage in wastewater can lead to severe filtration membrane fouling due to the formation of both amorphous ferric oxyhydroxide particles and gelatinous aggregates containing Fe(III), which bind to polysaccharide materials, and are responsible especially for irreversible membrane fouling. In consideration of the scarcity of literature on sensor fouling in wastewater treatment, the goal of this paper is to provide a detailed analysis of the fouling development with a case study on ammonium sensors. To achieve this goal, we studied two parallel ISE-NH_4^+ sensors, installed in the aeration tank of an activated sludge process. The effect of fouling on the sensor performance was investigated by analyzing sensor response time, signal drifting and operating lifetime of the electrodes. Moreover, the fouling morphology and composition was examined using scanning electron microscopy (SEM) and energy dispersive x-ray spectroscopy (EDX), respectively.

3.3 Materials and Methods

A set of two ISE-ammonium sensors (Horiba model HC-200NH) were installed in the aeration zone of a WRRF's secondary tank. The facility is located in the Southwestern United States, characterized by an arid to semi-arid climate. The secondary treatment of the plant includes an activated sludge process operating in the Ludzack-Ettinger configuration, divided into six zones in series, with an annual average SRT of 5 days and Mixed Liquor Suspended Solids (MLSS) of 2700 mg L^{-1}. The process is operated in step-feed mode, with a 60/40 split between the first and third zones, which are operated under anoxic conditions. The temperature of the wastewater in the aeration tank ranges from 25°C to 30°C, between the winter and summer season, respectively. The aeration tank is divided in six zones, separated by baffles, aerated with 7in EPDM fine-pore disc diffusers. The first zone presents a Neethling anaerobic selector zone mixed with coarse-bubble diffusers (discussed in Rosso, 2019) and the third zone is anoxic mixed with a mechanical mixer.A rack composed of ten ammonium ion-selective-electrodes was built and immersed in the activated sludge tank, next to the sensors previously mentioned (See Fig. 3.1). The rack was used to study the reversible fouling development and composition on the electrodes' surface over time.

3.3.1 ISE membrane technology

Among the different types of ion-selective electrodes (glass membranes, crystalline membranes and ionophore based membranes (often PVC plus plasticizer)) ionophore based membranes are the most widespread type in wastewater applications, since they allow to target a wide range of both cations and anions (Buck and Linder, 1994; Gross et al, 2008). Ion exchange membranes are made of a polymeric membrane (often PVC plus plasticizer) that contains a specific ion-exchange agent (ionophore) for the target analyte. Typical applications include the measurement of ions such as ammonium, potassium, chloride and nitrate.

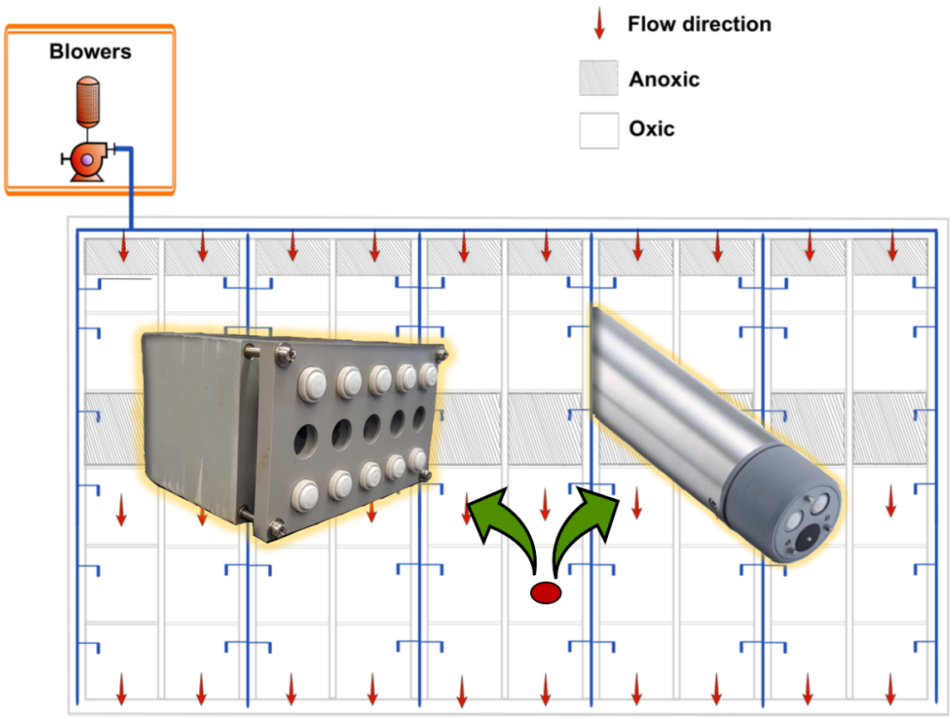

Figure 3.1: Aeration tank configuration and location where the ammonium sensors and electrodes rack were installed.

However, the polymeric membrane can easily be damaged by exposure to harsh environments and are characterized by low durability. In particular, when considering ISE-ammonium sensors, the selective membrane is composed of a polymer such as polyvinylchloride (PVC), a plasticizer (like dioctyl phthalate – DOP), and a neutral ion carrier or ionophore, typically valinomycin for potassium and enniatin or nonactin for ammonium sensors (Yim et al, 1993; Hauser, 2016; Suzuki et al, 2000). Usually, the membrane is also coated with a layer of PTFE $(C_2F_4)_n$, which provides a hydrophobic surface that reduces the adhesion of bacteria on the membrane. The plasticizer operates as a solvent and is bonded by solvation forces within the PVC, creating a homogenous medium where the solvent is evenly distributed. The ion-selectivity derives from the ionophores, which are the critical component of the membrane. Ionophores are molecules that bind to the targeted ions at the membrane-sample interface, establishing an electrical potential difference.

3.3.2 Step-change experiments

The step-change experiment can be divided into different phases. The delay time is the time interval between the instant when the on-line sensor/analyzing equipment is subjected to an abrupt change in the solution content and the instant when the readings pass (and remain beyond) 10% of the difference between the initial and final value of the abrupt change (APHA, 1998). The rise time is the difference between the response time and the delay time when the abrupt change in the solution content is positive. The fall time is the difference between the response time and the delay time when the abrupt change in solution is negative. The dynamic response of the sensor to the step-change experiments leads to an exponential time-relationship, which was evaluated with a mass balance model, based on the Fick's diffusion law (ISO 15839, 2203; Morf and Linder, 1975):

$$J = -D\frac{\delta c}{\delta x} \tag{3.1}$$

where J is the mass transfer rate per unit of surface (mol m^{-2} s^{-1}), D is the molecular diffusion coefficient (m^2 s^{-1}), and c is the concentration of ammonium (mol m^{-3}). The equation can be further developed applying the two-film theory of Lewis and Whitman (1924):

$$\frac{dc}{dt} = k[c_{sat} - c(t)] \tag{3.2}$$

The ordinary differential equation is analytically solved as follows:

$$c(t) = c_{sat} - (c_{sat} - c(t)) \cdot e^{-kt} \tag{3.3}$$

where k is the volumetric mass transfer coefficient (time^{-1}) and c_0 and c_{sat} are the initial and final ammonium concentration, respectively.

The response time of the ammonium sensor was measured by performing step-change experiments according to the ISO 1583926 as described in Rieger et al. (2003). Specifically, the step-change experiments were performed switching between two standard solutions of 10 mg L^{-1} and 25 mg L^{-1} of ammonium. First, the sensor was subject to an abrupt change from the lower solution to the higher. Following the stabilization at the higher concentration, the sensor was switched back to the lower concentration solution. Similarly to Morf et al 1975 and Frankær et al 2019, the exponential diffusion model was formulated to calculate the volumetric mass transfer coefficient, k, for both the rise and fall times of the step-change experiment.

3.3.3 Iron Measurements

Ferric chloride is continuously added in the primary clarifier of the treatment plant to ensure a concentration of 24 mg L^{-1} for odor control. Therefore, total iron measurements were performed on both grab samples of wastewater and for the fouling accumulated on the ISE membranes, in order to investigate the contribution of iron on the fouling development. The iron content analysis was performed both on the fouling accumulated over the sensor and over the rack electrodes, using the same procedure. Total iron measurements were performed using the 1,10 phenanthroline method (Iron, Total, FerroVer Method 8008, Hach) for both grab samples of wastewater and for the fouling accumulated on the ISE membranes. Total iron analysis was performed in triplicates on each fouling sample collected. The reversible fouling accumulated on the sensor membranes surface was collected in falcon tubes using a spatula. The same procedure was performed for the membranes of the electrodes on the rack by collecting each time the fouling accumulated on three electrodes in order to obtain a sufficient amount of fouling to analyze in a single sample. For every fouling sample

retrieved, triplicate samples of 50 mL of wastewater were collected in falcon tubes and stored in a cooling container. Within 2 hours from the collection of the fouling samples, total and volatile suspended solids analyses were performed for both fouling and wastewater samples according to the Standard Methods (APHA, 2005). The residual ashes were collected in a beaker with 50 mL of DI water, pH was adjusted at 2 using a 68% HNO3 solution, and the sample was maintained in mixed condition using a magnetic stirrer for 1h to crush the ashes and obtain a homogeneous suspension. Total iron analysis was performed on the suspension at pH within the range 3 to 5, adjusting the pH using nitric acid and 5.0 N sodium hydroxide solution.

3.3.4 SEM-EDS

The membrane surfaces of the ammonium electrodes were analyzed in pristine conditions and after six months of activity in the aeration tank. The electrodes were first cleaned manually with DI water in order to remove the superficial, reversible fouling, and were consequently air dried. Next, a FEI MAGELLAN 400 XHR scanning electron microscope was used to obtain SEM images of the membranes, to visualize the effect of irreversible fouling at a micron scale and compare the changes in membrane morphology with time. Previously to the topographic examination of the membranes in the SEM a 4 nm layer of Iridium was sputtered over the surface of the membranes. Sputtering a conductive layer of Iridium on the membranes inhibits charging, reduces the thermal damage, and improves the secondary electron signal required for topographic examination in the SEM. Additionally, complementary EDX elemental mapping of different areas of the membranes were obtained in new and used membranes to identify the main fouling elements. The Aztec software suite (Oxford Instruments, Abingdon, UK) was used for the qualitative and quantitative analysis where Iridium was chosen as deconvolution element to improve quantification accuracy.

3.4 Results and Discussion

The sensor performance was evaluated under different degrees of fouling development, depending on the cleaning frequency adopted. The fouling accumulation on the sensor surface was studied for 6 months in order to account for the changes with time in operation. In this period of time the temperature of the wastewater was 282°C, with no significant changes in process operation or in wastewater composition, which could otherwise have altered the fouling study. Figure 3.2 shows the ammonium profile over time along with images of the sensor before and after the cleaning event. In Fig. 3.2, starting from the leftmost image, the sensor after one month of fouling presents a dense layer of fouling, which was easily cleaned with water (center photograph). At last (photograph on the right), after 6 months of activity, the sensor was cleaned again with water, but the electrodes' membrane shows a brown/red coating, which could only be removed with a chemical cleaning (6% NaOCl).As previously mentioned, two types of fouling were recognized: reversible fouling, building up as a thick layer and dependent on the cleaning frequency; and irreversible fouling, developing over long-term operations, which cannot be removed via normal cleaning procedures.

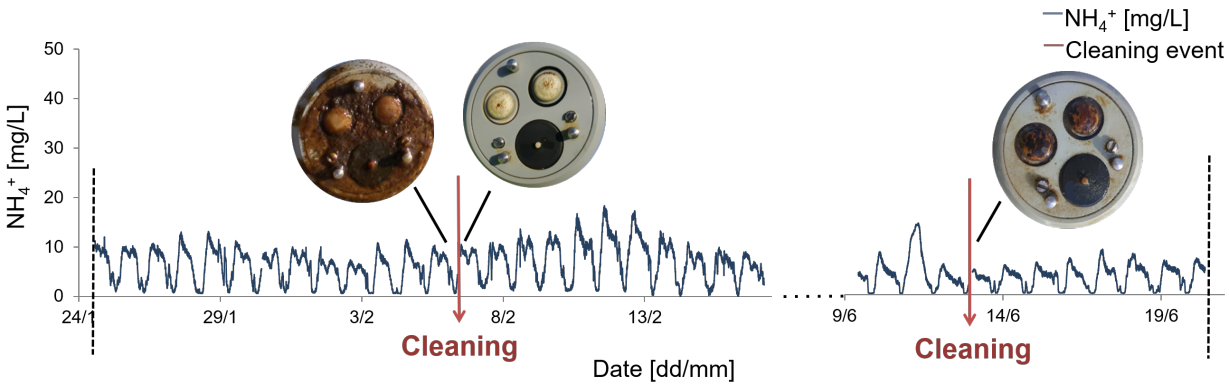

Figure 3.2: Pictures of different fouling conditions of the sensor installed. Starting from the left side, the first picture shows the sensor with one month of fouling developed, then the sensor right after the cleaning event. The last picture on the right shows the effect of a cleaning event, after six months of operation.

3.4.1 Response time

Figure 3.3 shows a graphical explanation of the transport phenomena of ammonium from the bulk of the solution to the electrode's membrane interface under cleaned and fouled conditions. The transport process of a clean ISE membrane can be represented by its equivalent electrical circuit (Fig. 3.3.a). In detail, the impedance spectrum, which describes the electrochemical behavior of the sensor, is composed of four circuit elements: R_B (bulk resistance), C_{dl} (double layer capacitance), R_{ct} (charge transfer resistance), and W_E (Warburg impedance) (Mikhelson et al, 2006; Anderson and Buhlmann, 2016; Armstrong et al, 1983). The fouling development adds an additional diffusional resistance layer which characteristics could be further analyzed by impedance spectroscopy (Fig. 3.3.b) (Radu et al, 2010). Therefore, depending on the level of fouling, the sensor's response to concentration fluctuations in the bulk solution is expected to show a delay.

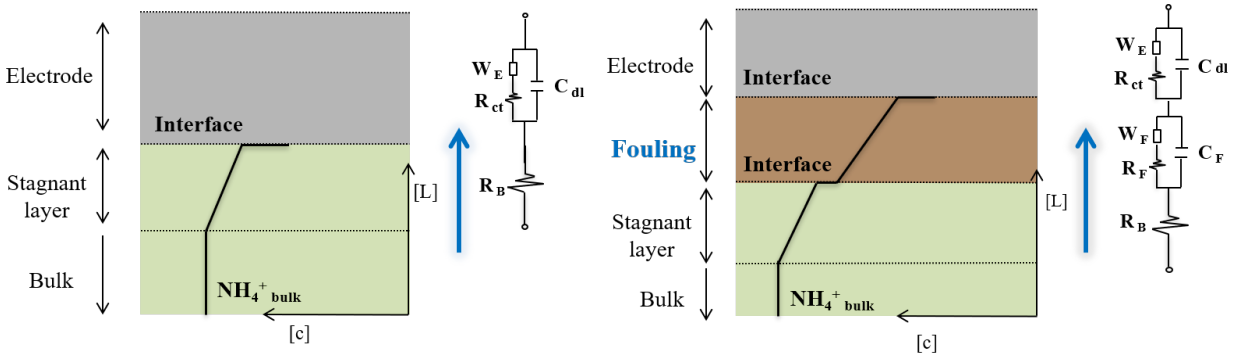

a) b)

Figure 3.3: Illustration of the transport phenomena of the ammonium ions from the bulk of the wastewater to the sensor's membrane interface in cleaned (a) and in fouled conditions (b). (a) The overall transport process of ammonium in a cleaned membrane can be described by four equivalent circuit elements: R_B (bulk resistance), C_{dl} (double layer capacitance), R_{ct} (charge transfer resistance), and W_E (Warburg impedance). (b) In the presence of fouling the transport process presents an additional diffusional resistance in series between the stagnant layer and the electrode, described by a Warburg impedance W_F in series with a fouling layer resistance, R_F.

To demonstrate the effect of fouling on sensor performance, the response time of the sen-

sor was measured at different fouling conditions by performing step-change experiments. Figure 3.4.a shows the example of a step-change experiments performed under cleaned conditions. An example of the step-change experiment conducted on a fouled membrane can be seen in Fig. 3.4.b. The results are reported in mV and the sensor's signal was recorded every 5 seconds. The diffusion model was fitted to the signal for every experiment during the rise and fall time at different fouling conditions and presents, on average, a coefficient of determination R^2 of 0.95. For each test conducted, the volumetric mass transfer coefficient (k) was calculated both for the rise and the fall times (see Table 3.1). The mass transfer coefficients calculated for each fouling condition (averaging between the rise and the fall time) are reported in Fig. 3.4.c as function of the time of fouling development.

Table 3.1: Results of the step-change experiments, in terms of the volumetric mass transfer coefficient, k, both for the rise and fall time.

Time in operation [Weeks]	**0**	**1**	**2**	**4**	**7**	**9**	**12**
$\mathbf{k}_{rise}$ [$\mathbf{s}^{-1}$]	0.090	0.095	0.070	0.028	0.024	0.007	0.008
$\mathbf{k}_{fall}$ [$\mathbf{s}^{-1}$]	0.098	0.100	0.090	0.043	0.023	0.005	0.003
($\mathbf{t}_{rise}$ - $\mathbf{t}_{fall}$) [s]	-0.9	-0.5	-3.2	-12.4	-3.8	+57.1	+208.3
($\mathbf{t}_{rise}$ - $\mathbf{t}_{fall}$)/$\mathbf{t}_{rise}$	-3.3	-1.1	-4.0	-1.1	-3.3	+7.2	+18.7
$\mathbf{R}^2$ **of the model**	0.95	0.96	0.85	0.99	0.98	0.97	0.98

After a lag-time of approximately one week, where no evident effect on response time was noticed, the volumetric mass transfer coefficient showed an exponential decrease with the time of fouling. Thus, under these specific process conditions, a cleaning frequency of more than once per week was not required. The exponential decay model, reported in Fig. 3.4.c, presents a coefficient of determination R^2 of 0.97. Therefore, it highlights how the fouling development in time on the sensor membrane results in the exponential increase of the response time of the sensor. This impact on the sensor responsiveness can indeed pose a limit on its capacity to follow the dynamics of the ammonium content in the wastewater. The experiments performed after protracted periods of fouling (3 or 4 months), show small dif-

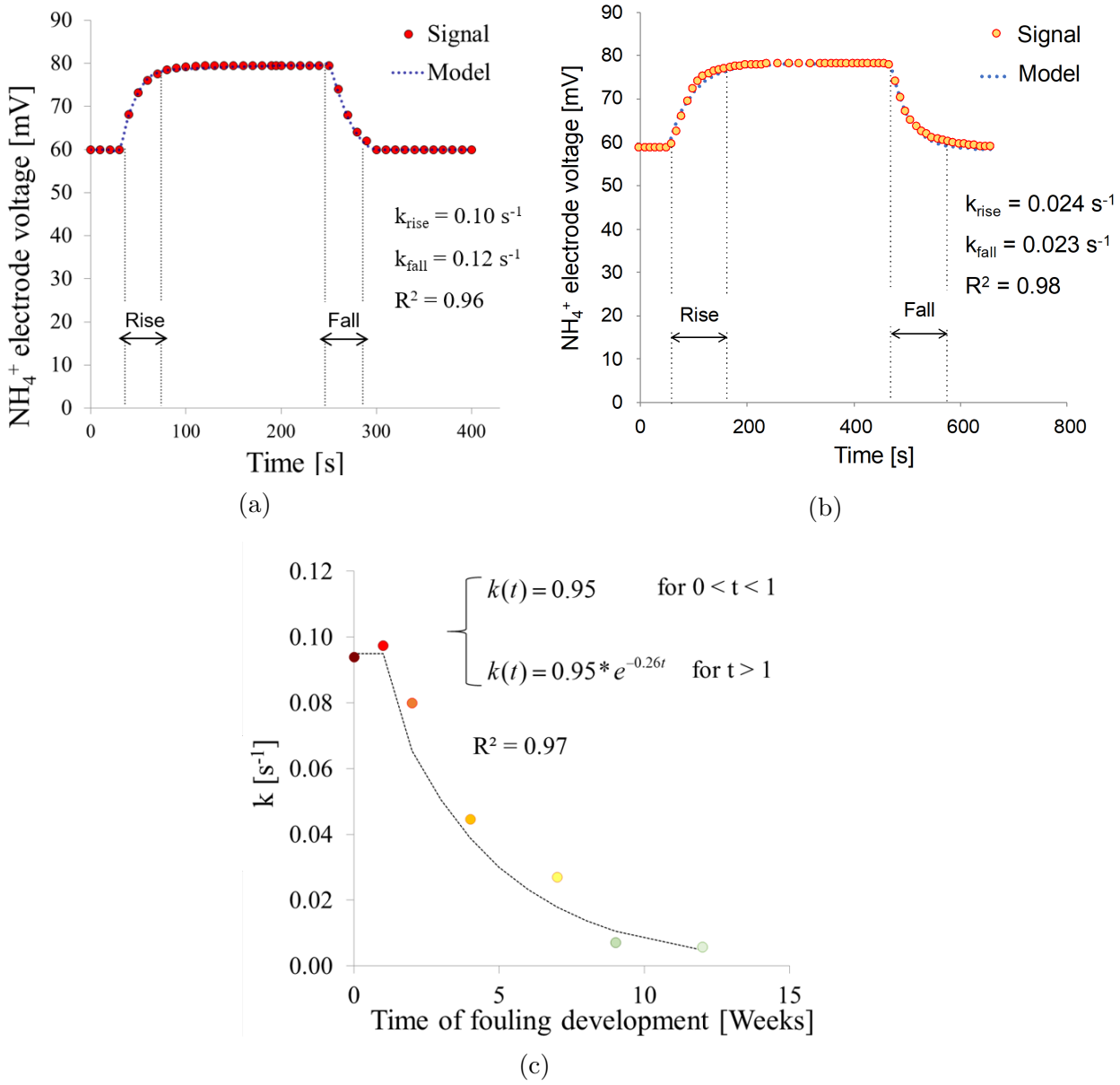

Figure 3.4: a) Comparison between the sensor signal during a step-change experiment (in red) and the diffusion model (in blue), for cleaned conditions. b) Comparison between the sensor signal during a step-change experiment (in orange) and the diffusion model (in blue), for fouled conditions.c) Volumetric mass transfer coefficient, k, as a function of the time of fouling development. The average measured volumetric mass transfer coefficient between rise and fall time is reported for each experiment conducted (circles). The black dashed line represents the exponential model. Model equation and coefficient of determination, R^2, are reported in the graph.

ferences in response time between before and after cleaning. Thus, as the sensor's electrodes gradually begin to approach the end of their operating lifetime, the irreversible fouling becomes the main contributor in increasing the response time of the sensor, regardless of the cleaning frequency. Therefore, for short-term operating periods (2 to 4 weeks), the reversible fouling is the main factor influencing the sensor performance, whereas, for the long-term operating periods (3 to 5 months), the irreversible fouling is the main contributor behind the increase in sensor response time. Due to the challenges associated with the prevention of the irreversible fouling development, the response time of the sensor is inevitably expected to increase during the lifetime of the electrodes, which therefore can be considered one of the main factors associated with the "aging" of the electrodes.

Furthermore, the step-change experiments can be studied by comparing the difference of the sensor behavior between rise and fall phase. At medium-short fouling time (2-4 weeks), the volumetric mass transfer coefficient is comparable between rise and fall time for the different experiments conducted, presenting no relevant hysteresis (see Table 3.1). The small difference between rise and fall time could be explained by the accuracy of the experiment. Differences between rise and fall time become significant only at fouling periods of 9 and 12 weeks, with an increase in fall time over rise time of 7.2% and 18.7% (57s and 208s), respectively. The electrodes at 12 weeks of fouling had been operating in wastewater the longest time, around 5 months in total, showing a consistent irreversible fouling formation. The hysteresis phenomenon observed at longer fouling time, displaying a higher fall time, could therefore be related to the irreversible fouling formation and to other aging factors of the electrode (*e.g.* bacterial degradation, membrane damage, structural changes of the membrane).

3.4.2 Drift behavior

If not periodically recalibrated, every sensor is subjected to drift phenomena in the long term, even if regularly cleaned (Ohmura et al, 2018; Papias et al, 2018). Drift, expressed as

a loss of sensitivity, occurs even when well maintained, and is typically caused by physical changes in the sensor and/or by environmental contamination. Therefore, the drift behavior of a well-maintained ammonium sensor during its whole lifetime was analyzed by comparing the reading of the sensor with lab analysis on grab-samples. During the study, the sensor was manually cleaned twice a week, no other maintenance and operation procedures were conducted, and no changing in process operation or in the wastewater composition was recorded. On average, the comparison with lab analysis was conducted every 3 days, collecting 5 samples over a 3 hours span. Figure 3.5 shows the comparison between the lab measurement and the sensor reading during 4 months of operation. The dataset is divided into months, from the first month after the calibration of the sensor (red triangles) till the fourth month (blue diamonds). The intercept and slope of the first month was normalized to 0 and 1, respectively. The data of the other months (from 2 to 4) were normalized relatively to the first month dataset.

From Fig. 3.5 it is evident that the sensor incurs drift over time with a negative trend of -0.01 mg NH_4^+ l^{-1} d^{-1}, which leads to an inexorable underestimation of the ammonium content in wastewater. Despite that reversible fouling development is prevented by adopting a consistent cleaning procedure, the ammonium sensor still requires a recalibration every 3 months, which corresponds to a loss of accuracy of $\sim 1 mgl^{-1}$ of ammonium. Subsequently, the performance of the ammonium sensor, in terms of signal accuracy, was evaluated under fouling development. The differences between the signals of two parallel ammonium sensors were analyzed over time. One sensor was not cleaned for 20 days while the other sensor, installed in the same tank right next to the other sensor, was cleaned twice a week in order to prevent the fouling build-up. The same experiment was conducted three times for 20 days each. Figure 3.6 shows in blue the difference between the two sensors (expressed as cleaned sensor signal minus the fouled sensor signal) at a 2-minute frequency. The top right insert shows the comparison of the drift trend of the cleaned sensor previously measured (in orange) with the drift trend measured with the current fouling experiment (in blue).

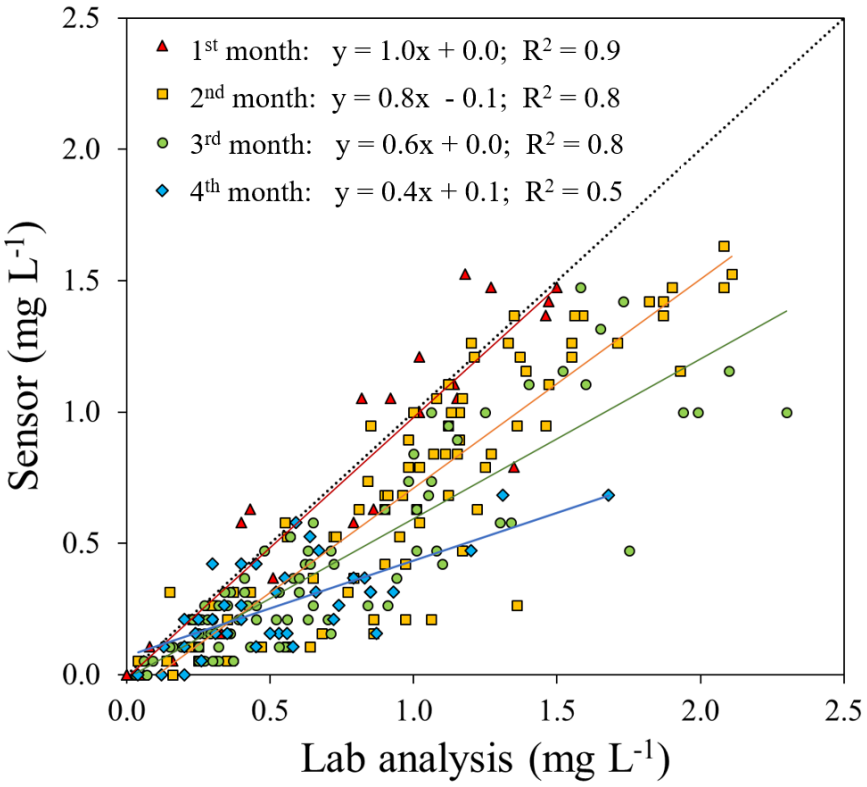

Figure 3.5: Comparison between sensor reading and lab analysis for 4 months of operation of the sensor. The dataset is divided into months, from the first month after the calibration of the sensor (red triangles) till the fourth month (blue diamonds). The linear trends of each month are shown, which equation and coefficient of determination, R^2, are reported in the graph.

The fouling leads to an underestimation of the ammonium reading, which degrades in time with a monotonically decreasing trend. The drift, calculated from the three experiments, presents a slope of -0.11 $\pm$ 0.03 mg NH_4^+ $l^{-1}d^{-1}$. The slope of the linear trend of the fouled sensor is one order of magnitude higher (-0.11 mg NH_4^+ $l^{-1}d^{-1}$) than the drift of the cleaned sensor (-0.01 mg NH_4^+ $l^{-1}d^{-1}$), showing that a fouled sensor drifts much faster than a cleaned one. These results highlight the importance of adopting a consistent maintenance procedure, since it was demonstrated that fouling also affects the absolute accuracy of the sensor reading, independently on the response time of it. The position of the sensor installation along the aeration tank can also influence the sensor fouling since the wastewater composition changes

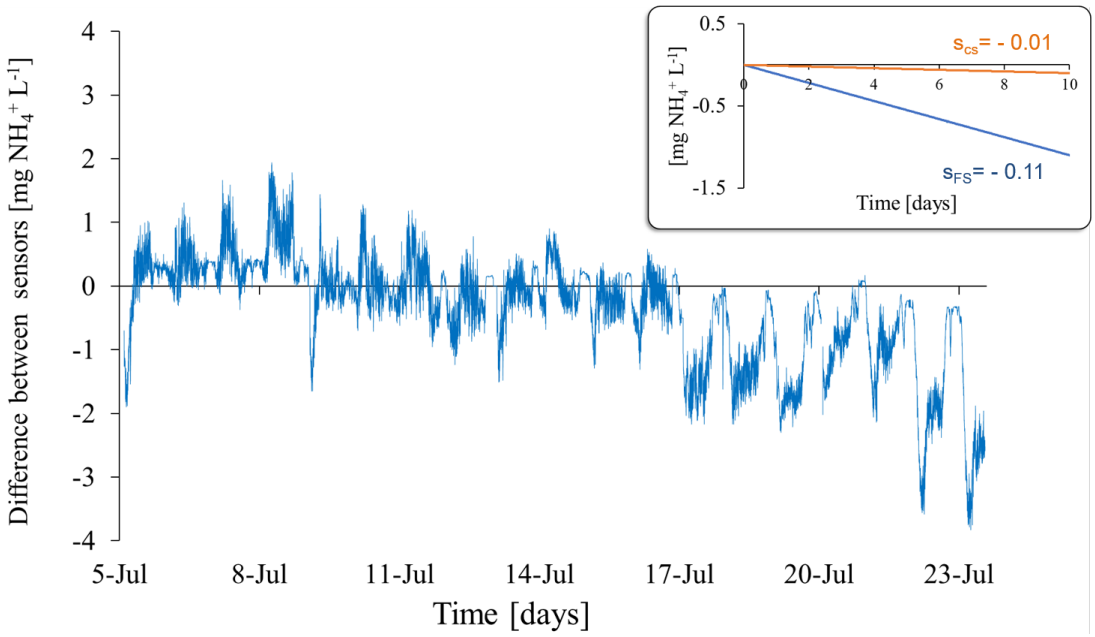

Figure 3.6: Difference between the cleaned and the fouled sensor signal, reported in blue with a 2-minute frequency. s_{CS} = drift slope of the cleaned sensor in time (orange). s_{FS} = drift slope of fouled sensor in time (blue).

along the process. Therefore, it can be expected a faster fouling development for an influent installation, and therefore a larger drift slope if the sensor is left unmaintained compared to the same type of sensor installed in the effluent.

3.4.3 Iron analysis

Analysis of the iron content, due to the addition of ferric salts in the primary treatment at the facility, was conducted on the reversible fouling layer. The iron composition of the fouling layer was investigated over time. Fouling was collected from the electrode membranes of both the two sensors and from the rack immersed in the wastewater, containing 10 electrodes (See Fig. 3.1). A summary of the fouling and wastewater composition over time, in terms of total iron, VSS, and TSS is reported in the Table. 3.2.

After a preliminary examination, it was observed that the iron present in both wastewater and fouling was mainly in the form of Fe(III) and was absorbed to the solids' surface since

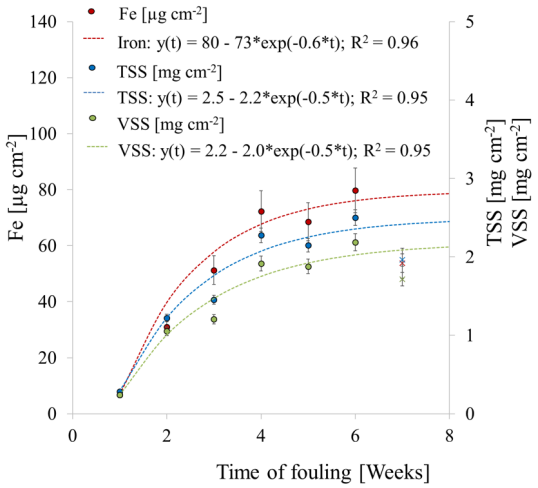

(a)

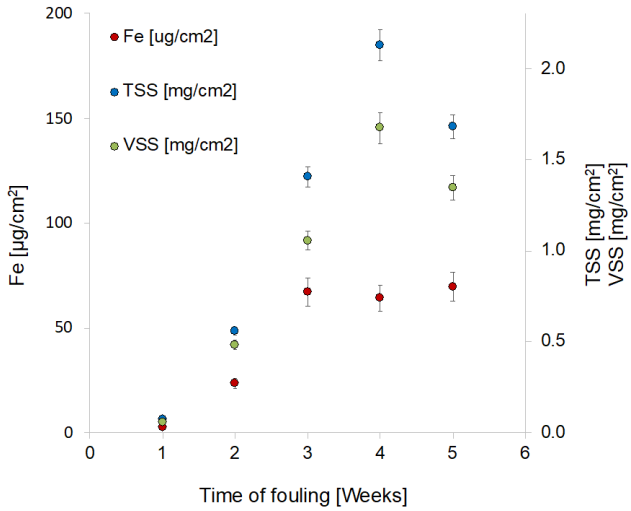

(b)

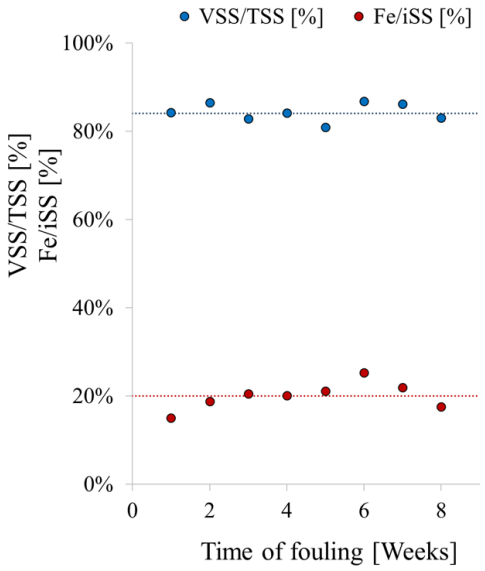

(c)

Figure 3.7: a) Trend of TSS, VSS and iron of the fouling layer, per unit of area, over time on the rack. b)Trend of TSS, VSS and iron of the fouling layer, per unit of area, over time on the sensor. In blue are reported the TSS, in green the VSS and in red the iron content of fouling. The dashed lines represent the exponential model, with relative equation and coefficient of determination. The X markers show a foaming event of the treatment plant, and therefore are considered outliers. c) Trend of VSS/TSS (blue) and Fe/iSS (red) over the time of fouling, the dashed lines report the average value.

Table 3.2: Fouling and wastewater composition over time, in terms of total iron, VSS and TSS.

Time in operation [Weeks]	**1**	**2**	**3**	**4**	**5**	**6**	**7**	**8**
Total Fe sensor [μg Fe/cm^2]	2.7	23.6	67.0	64.3	69.6	-	-	-
TSS sensor [mg TSS/cm^2]	0.1	0.5	1.4	2.1	1.7	-	-	-
VSS sensor [mg VSS/cm^2]	0.1	0.4	1.0	1.7	1.3	-	-	-
Fe/TSS sensor [%]	3.8	4.2	4.8	3.0	4.1	-	-	-
Total Fe rack [μg Fe/cm^2]	6.8	31.0	51.2	72.3	68.6	79.7	53.7	102.0
TSS rack [mg TSS/cm^2]	0.3	1.2	1.4	2.3	2.1	2.5	1.9	2.3
VSS rack [mg VSS/cm^2]	0.2	1.0	1.2	1.9	1.8	2.2	1.7	1.9
Fe/TSS rack [%]	2.4	2.5	3.5	3.2	5.9	3.2	2.7	3.0
Total Fe wastewater [mg Fe/L]	29	-	70	40	40	89	45	73
TSS wastewater [g TSS/L]	2.9	2.0	2.0	3.4	3.5	5.4	5.2	8.1
VSS wastewater [g VSS/L]	2.3	1.6	1.6	2.7	2.7	4.7	4.5	7.3
Fe/TSS wastewater [%]	4.9	6.2	16.1	5.5	5.6	11.9	6.4	10.2

no trace of iron was detected on filtered samples. This result is in accordance with the findings of Kazadi Mbamba et al (2019) and Wang and Waite (2010), regarding the iron speciation in wastewater. Figure 3.7.a shows the trend of TSS, VSS and total iron collected from the surface of the rack's electrodes during the period of fouling development. The data was analyzed with a saturation model, for TSS, VSS and iron accumulation, showing a R^2 of 0.95, on average. In time, solids accumulate on the surface of the electrode, creating a thick layer of fouling. After one month, the growth of fouling decreases eventually reaching a balance between fouling accumulation and detachment, due to the shear stress provoked by the aeration bubbles and the wastewater flow. At seven weeks of fouling a foaming event of the treatment plant had influenced the fouling composition, which was then treated as an outlier. Due to the excess of foam, the rack was covered in bubbles, which had dispersed the fouling layer that had developed previously. The same increasing trend of fouling build-

up was noticed also on the analysis performed on the fouling samples collected from the sensor's surface (see Fig. 3.7.b), which shows a similar behavior with the results obtained for the rack's electrodes experiments. Figure 3.7.c presents the ratio of VSS/TSS and Fe/iSS of the fouling composition over the time of fouling development, comprising fouling samples collected from both the rack's electrodes and the sensor's surface. Even if the accumulation of iron and solids on the surface increases over time, the relative composition is relatively stable: 84% of VSS/TSS and 20% of Fe/iSS, on average.

Furthermore, after the 6 months in operation, the electrode membranes were cleaned with water and were detached from the electrodes. TSS, VSS, and iron analyses were conducted on the membranes of four electrodes, using the same methodology adopted for the reversible fouling analysis. On average, the membrane was composed of 48$\pm$10 μg of Fe, which represents the 2% of the total membrane composition and 17% of the inorganic compounds content. The accumulation of iron salts was then observed both on the reversible fouling layer and attached to the membrane, in the irreversible fouling. Finally, the addition of FeCl as coagulant in the primary clarifier is a very common practice and the composition analysis for this study points out that the presence of high concentration of iron in the wastewater largely influences the inorganic fouling development. It can be inferred that other plants that utilize the same coagulants application could find similar issues with the development of inorganic fouling.

3.4.4 Scanning Electron Microscopy

Scanning Electron Microscopy was used to characterize the morphology and composition of the irreversible fouling, which plays an important role on the aging of the electrodes as well as on the performance of the sensor itself. Fig. 3.8 shows surface sections of new and used electrodes' membranes analyzed with SEM. The used membranes were collected after six months of operation of the sensor in wastewater, at the end of the lifetime of the electrode.

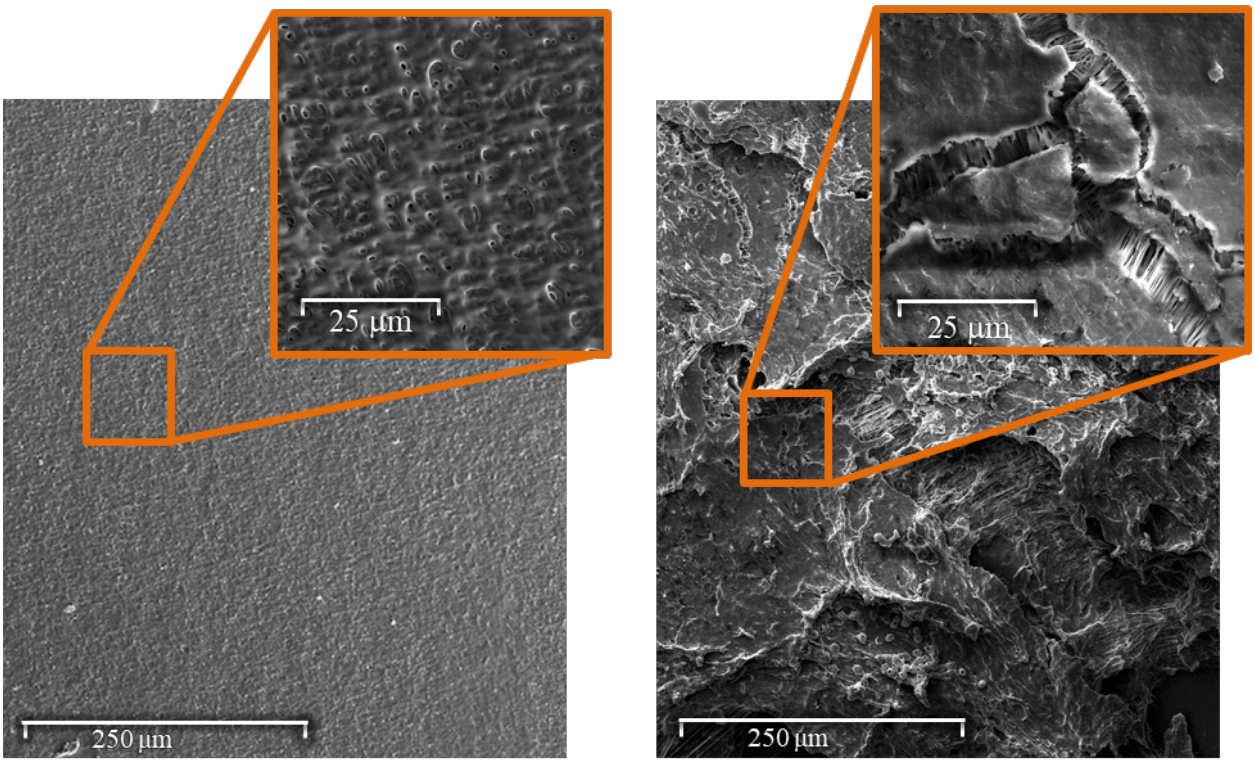

a) b)

Figure 3.8: SEM images of the cleaned membrane (left) and fouled (right).

The clean membrane shows a homogeneous surface and the porous structure of the membrane is clearly visible in the magnified image (Fig. 3.8.a). The used membrane (Fig. 3.8.b) instead shows a rough surface, with different type of agglomerates, crevasses and the pores of the original membrane are not visible anymore, completely covered by the coating of the fouling which appears dense and non-porous. The fouling SEM pictures of the sensor membranes show similarities mainly with organic fouling of filtration membranes (Jiang et al, 2018), since evidence of specific precipitate structures and scaling are scarce, and no microbial colonies can be observed. Different areas of the fouled membranes' surface were analyzed at different levels of magnification to recognize different agglomerates and details (See Fig. 3.9 and Fig. 3.10). Analogously to the observed SEM pictures of fouling on microfiltration membranes, the fouling on the sensor develops as a cake or gel layer, composed of bacteria clusters and

biopolymers, which is indicator of biofouling formation (An et al, 2009; Al-Halbouni et al, 2008; Wang et al, 2008).

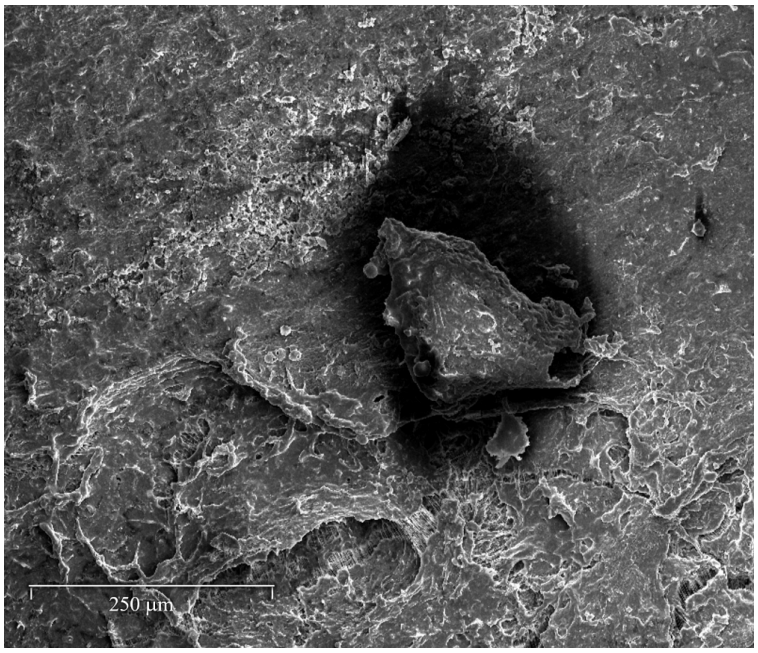

Figure 3.9: SEM images of the fouled membrane at 250 magnification.

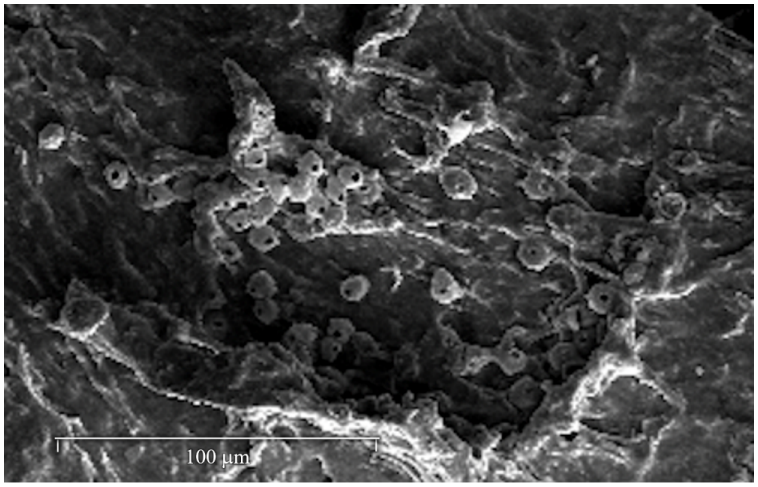

Figure 3.10: SEM detail image of the "doughnut-shaped" holdfasts on the fouled membrane.

Figure 3.10 shows the presence of spherical structures approximately 10μm in diameter, with a hollow center deposited on the surface of the fouling. The accumulation is too big to be associated to individual microorganisms, but more likely to biofilm structures. Such deposits could be related to so called "doughnut-like shaped holdfasts", which are agglomerates of

biological origin together with inorganics like silicates, iron oxides or calcium carbonate (Guo et al, 2011; Cao et al, 2016; Santos et al, 2018).

The cracks and crevasses in the fouling, highlighted in Fig. 3.8.b, are numerous, dense and get extended for large portions of the fouled surface. Such cracks, which are fibrous in nature, denote a typical behavior of polymers under stress, and originate from the stretching and damaging of the PTFE protection layer. Also, the crevasses show a clear similarity to other SEM pictures of stretched PTFE membranes obtained under stress reported in literature, which are characterized by the same type of fiber-like stretch typical of polymers (Liu et al, 2015; Zhang et al, 2017). The same type of sample preparation to perform SEM and EDX analysis, as described in the Materials and Methods, was employed on both the fouled and the new membranes. The PTFE cracks were never detected in new membranes, which instead always showed a homogenous surface (see Figure 3.11), and therefore it can inferred that the PTFE protective layer damages originated during the six months of activity of the sensor in wastewater, and not from the handling of the sensor membranes during the SEM experimental procedures.

EDX elemental analysis was applied to the clean and fouled membranes for each of the previous sections analyzed with SEM. Quantitative analysis in EDX is only used as an estimation due to the error of quantification of light elements such as oxygen, nitrogen and carbon but is useful for polymer materials that have unique elemental signatures such as the fluorine of PTFE. Furthermore, the atomic percent distribution obtained helps to estimate the relative proportion of some contaminants like salts and metal oxides. A summary of the quantitative analysis of the elements for each of the sections mapped with EDX technique on the new and used membranes and the statistical error are reported in Table 3.3. By comparing the difference in composition between new and used membrane, it is possible to identify the changes in composition due to fouling.

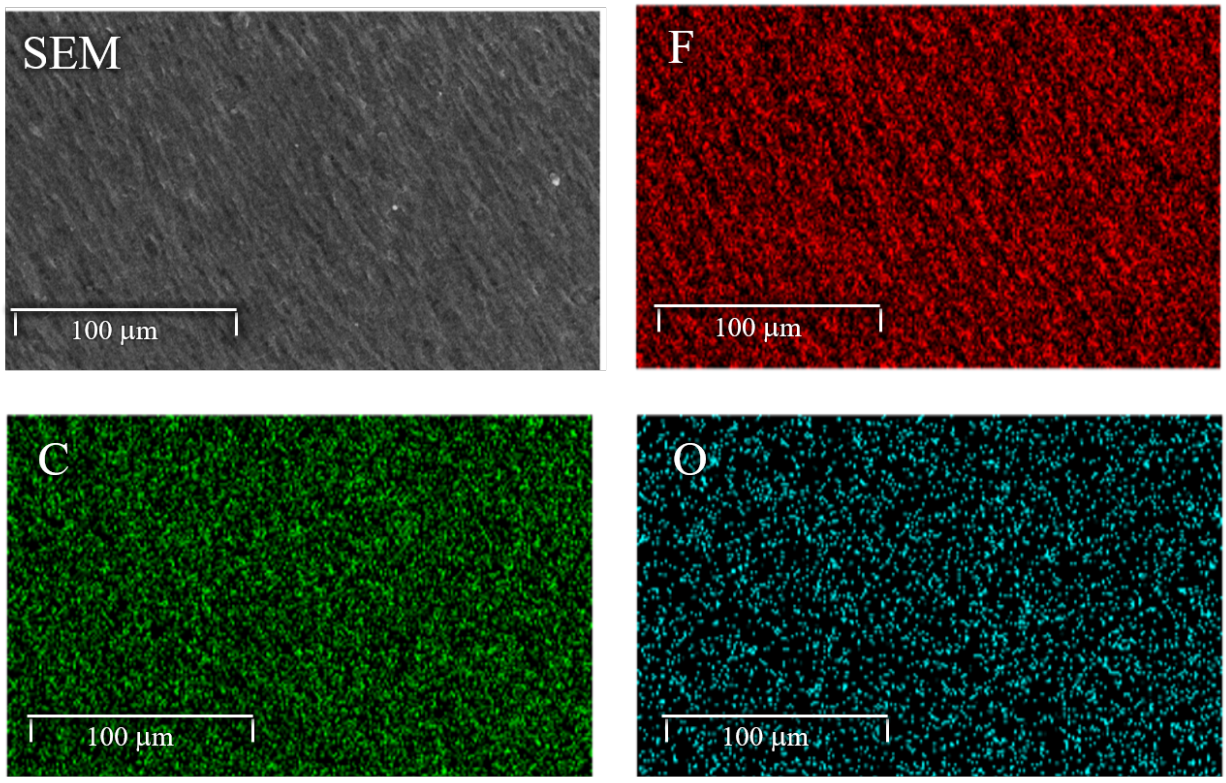

Figure 3.11: SEM and EDX mappings of a new membrane. Key: F (red); C (green); O (blue).

The main elements detected via EDX on cleaned membranes were C, O and F, and they result evenly distributed over the surface due to the homogeneous nature of the ISE membrane (see Fig. 3.11). Fluorine originates from the chemical composition of the PTFE protective membrane layer. Other elements were detected in trace amounts on the cleaned membrane, which were assumed deriving from the accumulation of dust over the membrane. Since there is little F content in wastewater, fluorine is considered as the reference to compare the elemental composition between the new and the fouled membrane. The fouled membrane results (See Table 3.3; Fig. 3.12) indicate a relative decrease in fluorine content (from 45 atomic % to 15 atomic %) while carbon and oxygen have increased dramatically: from 48 to 65 atomic % for C and from 5 to 18 atomic % for O. Other metal elements were detected in smaller quantity in different portions of the fouled membrane's surface, such as Fe, Mn, P, N, Ca, Cl, S, K, Mg, Na, S and Si, in descending order. Furthermore, the composition

Table 3.3: Weight %, statistical error (σ) and Atomic% from Quantitative EDX analysis from the surface of the new membrane and fouled membrane.

	New Membrane			Fouled membrane		
Element	**Wt %**	**Wt % (σ)**	**Atomic %**	**Wt %**	**Wt % (σ)**	**Atomic %**
C	36.78	0.29	47.90	54.55	0.37	65.09
O	5.67	0.17	5.54	20.34	0.26	18.22
F	55.32	0.30	45.54	19.55	0.25	14.75
Fe	0.32	0.09	0.09	1.97	0.10	0.51
P	0.21	0.04	0.11	0.81	0.07	0.37
Ca	0.19	0.04	0.07	0.70	0.04	0.25
Mn	BDL	BDL	BDL	0.69	0.07	0.18
S	0.13	0.03	0.06	0.35	0.03	0.15
K	BDL	BDL	BDL	0.34	0.03	0.12
Si	0.62	0.04	0.34	0.19	0.02	0.10
Cl	0.76	0.04	0.33	0.25	0.03	0.10
Mg	BDL	BDL	BDL	0.15	0.03	0.09
Na	BDL	BDL	BDL	0.12	0.03	0.08

of the sensor fouling was found to be comparable to the typical composition of fouling on filtration membranes found in literature, in particular closely resembling the relative proportion between organic and inorganic content (Al-Halbouni et al, 2008; Zhang et al, 2008; An et al, 2009; Xu et al, 2010). The sensor's membrane fouling was primarily composed of organic pollutants, while the inorganic matter contribution was minor. However, as reported by Wang et al. (2008) and Meng et al. (2007), the inorganic elements such as Mg, Al, Fe, Ca, and Si have significant effects on the formation of the gel layer. Such elements promote the bridging between deposited biopolymers and inorganic compounds, while also enhancing the compactness of the fouling layer. Therefore, although inorganic fouling may account for a relatively small amount of the overall fouling, it does however influence the growth rate and structure of the organic fouling. As expected, due to the practice of adding ferric chloride in the primary clarifiers, iron fouling is consistently mapped by EDX over the entire surface of

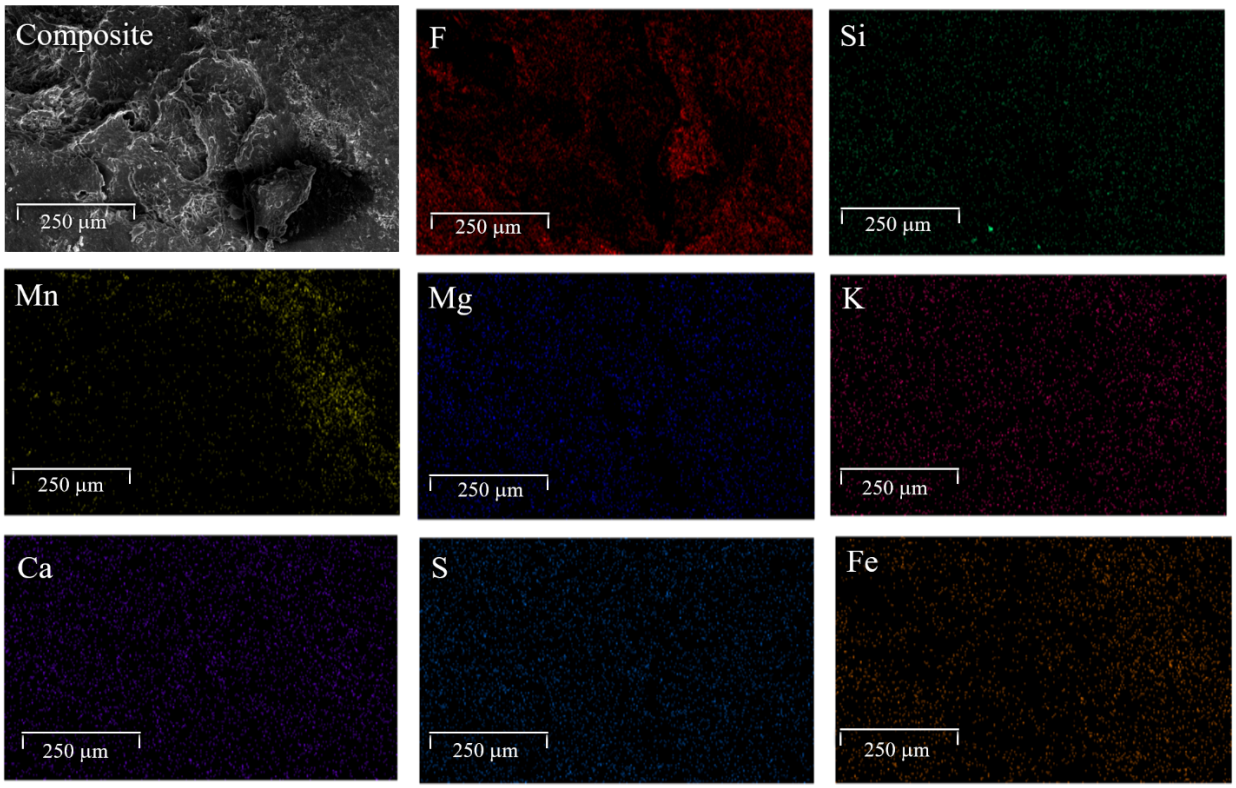

Figure 3.12: SEM and EDX mappings of a fouled membrane. Key: F (red); Si (dark green); Mn (yellow); Mg (blue); K (pink); Ca (purple); S (green water); Fe (orange).

all the fouled membranes examined. In detail, excluding the membrane composition and the organic fouling (C, O and F), iron was found to be the most quantitatively abundant element of the inorganic fouling (26 atomic % of Fe/inorganic fouling). The iron is hypothesized to mainly be present in the form of ferric oxides, as commonly seen in literature (Wang and Waite, 2010; Zhang et al, 2015). Because Fe is detected in high content and is one of the trace inorganic nutrients for bacteria that can enhance the development of biofouling (Rebosura et al, 2018), we can infer it could have also influenced the organic fouling build-up and future studies should address its role. Therefore, iron plays a significant role in the general development of the irreversible fouling of the sensor's membranes, as also was demonstrated in the studies of fouling in filtration membranes (Meng et al, 2007). Most of the elements of the fouling, both organic and inorganic, such as C, O, F, Fe, Mn, and P, are spread out evenly over the membrane surface (see Figure 3.12). However, in some spots of the fouled

membranes some aggregates of K and Cl were observed. Since the mappings of K and Cl agglomerates match perfectly, these are likely deposits of potassium chloride (KCl) (see Fig. 3.13).

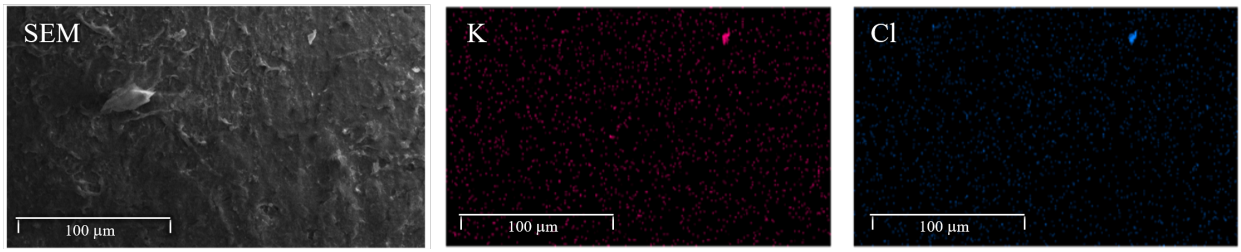

Figure 3.13: SEM and EDX mappings of a KCl precipitate, specifically in pink K and in blue Cl.

Figure 3.14 reports the details of EDX mappings on a crevasse (a) and damages of the membrane surface (b, c). It can be noticed that the crevasse presents a local increase in fluorine concentration (Fig. 3.14a, in red), which could not be accounted by scaling/inorganic fouling considering the typical low content of fluorine in wastewater. The high fluorine content on the membrane, instead, originates from the PTFE coating, emerging from the thick layer of the fouling, showing the detail of a fibrous-like stretched structure. Therefore, the EDX images further confirm the hypothesis of the damaged PTFE, previously described when analyzing the SEM mappings (Figure 3.8). A further level of damage of the membrane was detected in other spots, observing fluorine and chlorine mappings (Fig. 3.14b, c). In more than one spot (see Fig. 3.14b, c) similar patterns were noticed: i) large patches of high concentration of chlorine and ii) uneven and scarce content of fluorine. However, this is in contrast with the typical elemental pattern previously observed within the study, where fluorine is evenly distributed over the surface. In terms of relative atomic proportion percent, the difference between the typical pattern and the damage analysis is the following: the F content decreased from 15% to 9% and the Cl content increased from 5% of the inorganic fouling to 23% of the inorganic fouling. The chlorine spots could hardly derive from a precipitate due to the absence of the counter ion detected, as instead shown in the Fig. 3.13, and

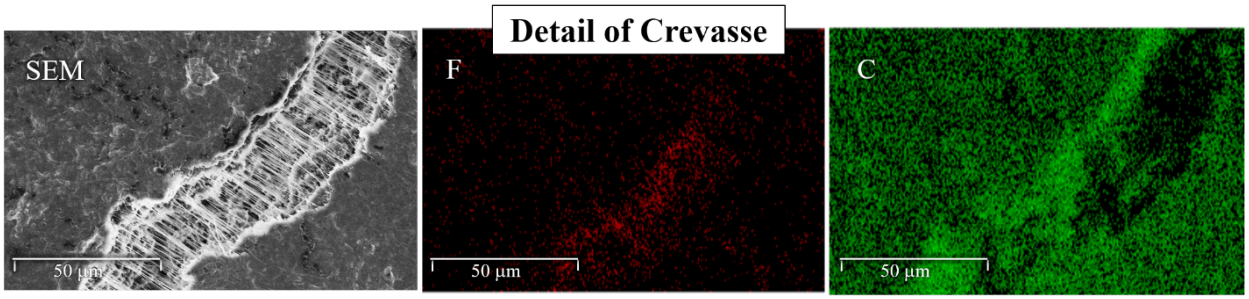

(a)

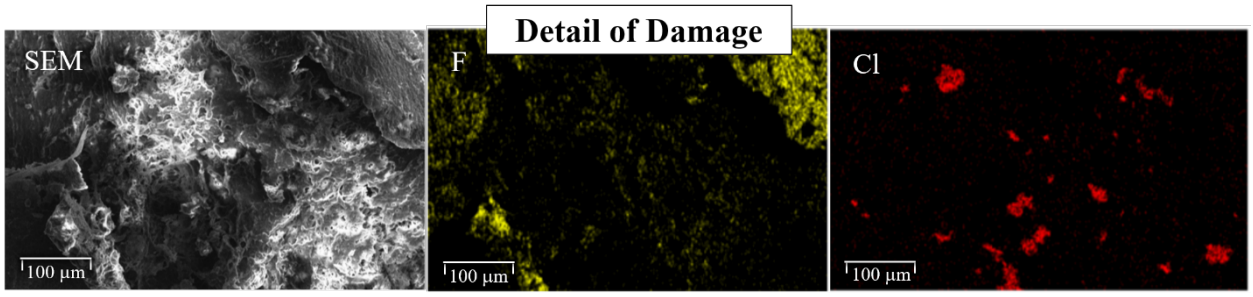

(b)

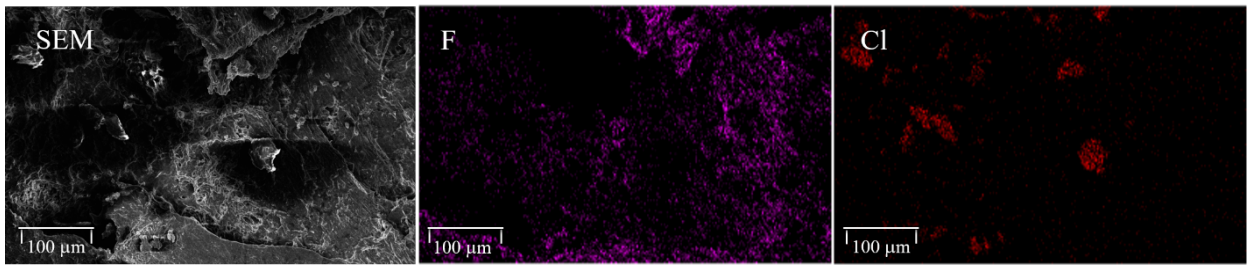

(c)

Figure 3.14: SEM and EDX elemental mappings of a fouled membrane are highlighted in different colours. (a) Detail of higher content of fluorine (red) and carbon (green) in the fouling layer over the crevasse, revealing the Teflon membrane $(C2F4)_n$ below. (b) Detail of crevasse of fouled membrane with Fluorine (purple) and Chlorine (red). (c) Detail of damage images of fluorine (yellow) and chlorine (red) detected on a different spot of the fouled membrane.

the irregular shape. Instead, it can be hypothesized that in some regions of the membrane, the PTFE protective coating has been removed by abrasion, which explains the observed decrease in fluorine content. The abrasion of the PTFE coating leaves the underneath PVC $(C_2H_3Cl)_n$ layer of the membrane exposed, which helps to explain the increase in irregular chlorine patches. Moreover, once the unprotected PVC membrane becomes exposed to the external wastewater environment, it is easily and more rapidly degraded by bacterial activity, thus further escalating the aging process of the electrodes. The damage areas of the PTFE coating were attributed to the recurrent cleaning maintenance procedures performed during the six months of operation. Thus, alternative cleaning methods should be considered in future studies, referring also to the procedures deployed in filtration membrane cleaning, such as sonication and acid and base cleaning.

3.5 Summary and Conclusions

In summary, the major impact of fouling on the sensor's performance is the increase of the response time of the sensor to changes in ammonium concentrations. The effect of the fouling development was found to promote a negative drift (-0.11 mg NH_4^+ $L^{-1}d^{-1}$), which is one order of magnitude higher than the drift of a well-maintained sensor (-0.01 mg NH_4^+ $L^{-1}d^{-1}$), leading to an underestimation of the ammonium content. This characterization of the sensor drift can provide a quantitative reference for future studies on sensor fault detection and impact of sensor performance on control systems. The EDX analysis show that the inorganic fouling is mainly composed of Fe, P, Ca, Mn, S, K and Cl, in decreasing order. The morphology and composition of the sensor's membrane fouling is comparable to literature studies on filtration membrane fouling. Several fibrous cracks of the protective PTFE coating were identified, as well as spots in the membrane where the PVC membrane itself is exposed (patches of high content of chlorine), showing a further stage of damage.

The biomass composition has a high influence in the development and composition of fouling. Therefore, the fouling study conducted can be considered as a reference limited to the site condition (warm climates) and specific wastewater treatment application described. For a more general conclusion and quantification of the effects of fouling over the ISE sensor performance more studies should be conducted in different utilities, applications, and environmental conditions. Also, to further supplement and support the data presented in the current paper, the development of the fouling layer and its effects on the sensor behavior over time should be further investigated by impedance spectroscopy.

Chapter 4

Soft-sensing for on-line fault detection of ammonium sensors in water resource recovery facilities

4.1 Abstract

The increasing demand for online sensors applied to advanced control strategies in water resource recovery facilities has resulted in growing attention on fault detection methods to improve the reliability of sensors installed in such harsh environment. The study herein focuses on the fault detection of ammonium sensors, especially for effluent monitoring, given their potentiality in Ammonium-Based Aeration Control. An Artificial Neural Network model was built to predict the ammonium content in the effluent by utilizing the information from other five sensor installed in the activated sludge tank: NH_4^+; pH; ORP; DO; TSS. The residual between the model prediction and the effluent ammonium sensor signal was utilized for a fault detection mechanism, based on Principal Component Analysis monitoring charts.

Differing from previous research, the present study utilizes sensor faults collected from one year of historic data of the actual sensor setup instead of artificially generating process anomalies using deterministic models. The most common issues identified from the historic data using the proposed fault detection methodology were treatment process anomalies, calibration biases, and fouling drifts. Treatment process anomalies, calibration bias fault, and a fouling drift, were the most common issues identified from the historic data and promptly individuated by the proposed fault detection methodology. Once a fault is detected, the model prediction can be actively used in place of the sensor to control those processes that rely on the said sensor, without affecting the treatment process by utilizing faulty datasets.

4.2 Introduction

4.2.1 Use of sensors in WRRFs

Real-time monitoring is a fundamental aspect in Water Resource Recovery Facilities (WRRFs) for plant safety and control systems implementation (Baggiani and Libelli, 2009; Olsson 2006; Olsson and Jeppsson, 2006). In the last few decades the increasing availability of water quality sensors has facilitated the achievement of better effluent quality and more advanced control systems in order to comply with the stringent standards (Tao et al, 2013; de Canete et al, 2016). Among the variety of water constituents and the corresponding sensor technologies, large attention has been given to ammonium sensors for their potential application in Ammonium-Based Aeration Control (ABAC), and for monitoring the effluent ammonium content to control the formation of chloramines in disinfection.

4.2.2 Reliability of sensors

Sensors accuracy is critical to successfully implement process control and monitoring, especially when processes rely on the information from many sensors. Sensors can display partial failures such as bias, drift or precision degradation, also due to fouling, considering the hostile environment of installation. Also, human errors can deteriorate the sensor performance due to incorrect operation and maintenance procedures (cleaning, calibration, and sample adjustment). When the accuracy and reliability of a sensor decreases, it provides incorrect information for monitoring and control which can result in erroneous control action and false perception performance of the process (Yoo et al, 2008). This potential erratic behavior of sensors has to a common feeling of skepticism on behalf of engineers and plant operators and contributed to a worse reputation than sensors deserve.

4.2.3 Fault detection methods

The identification of a fault, either of the process or of the sensors, can be difficult just by examining the data, because of the large amount of data and the presence of multiple variables which are often highly correlated (Fuente et al, 2012).

In light of the high request of online measurement and the lack of reliability of sensors, fault detection practices, data screening, and information extraction can help improve the reliability of the instrumentation and guarantee data quality. Different types of monitoring charts can be used to detect "out-of-control" situations in a process (Thomann et al, 2002; Rieger et al, 2004). Among the most common are the Shewart charts, mainly used in analytical laboratories for quality control (Montgomery 1996). Fault Detection and Isolation (FDI) methods can usually be distinguished between model-based and data-based approaches, however the latter is preferable due to the complexity of deterministic models of plant-sensor dynamics (Kettunen et al, 2008; Rosen et al, 2008).

Multivariate statistical methods such as principal components analysis (PCA) and partial least squares (PLS) are among the most common data-based fault detection and diagnostics schemes implemented in literature (Tao et al, 2013; Yoo et al, 2008; Baggiani and Libelli, 2009; Garcia-Alvarez et al, 2007). However, these two methods assume linear correlation among variables, which works well in closed-linear processes but degrades the performance in non-linear and dynamic systems (Cheng et al, 2005; Fuente et al, 2012). Literature studies have shown that PCA's minor components can often contain not only noise but significant variance in nonlinear problems (Xu et al, 1992). Also, PCA implicitly assumes that the observations at one instant in time are statistically independent from past observations. This gives problem of autocorrelation of variables in a complex dynamic system.

4.2.4 Artificial Neural Networks

In order to account for the non-linearity of the system, different literature studies have reported new methodologies to extend the applicability of PCA in dynamic non-linear problems, using a model-based PCA approach (Yoo et al, 2003; Kramer et al, 1992; Dong and McAvoy, 1996; Jia et al, 1998; Rosen et al, 2003; Kazor et al, 2016; Lee et al, 2004; Zhao and Yuan, 2011; Xiao et al, 2017). These studies often integrate different machine learning methods to remove the nonlinearity information from the raw data, and then the resulting residuals between model and sensor are analyzed by PCA to generate monitoring charts. Among the most common process models in the model-based PCA approach, different versions of neural networks can be found, showing promising results to calculate a non-linear and dynamic model of the treatment process in nominal operating conditions (Cheng et al, 2005; Fuente et al, 2012).

This study utilizes six online sensors installed in the aeration tank of an activated sludge process. Five of six sensors are used as input of an ANN model to predict the ammonium in

the effluent and compare it to the NH_4^+ effluent sensor signal (sixth sensor). The comparison between model prediction and sensor signal is then further evaluated by PCA monitoring charts and Shewart charts in order to identify process anomalies and partial sensor faults, like biases and drifts. The effluent ammonium sensor is chosen as target sensor for fault detection given the large potential application but higher uncertainty when applied in low range (Cecconi et al 2019). The novelty in the present study is the utilization of sensor faults collected from one year of historic data of the actual sensor setup instead of artificially generate process anomalies by means of deterministic models.

4.3 Materials and Methods

4.3.1 Layout of the WRRF under study

The facility of the present study is located in the Southwestern United States, characterized by an arid to semi-arid climate. The secondary treatment of the plant includes an activated sludge process operating in the Ludzack-Ettinger configuration with an annual average SRT of 5 days. The overall secondary effluent is fed to a subsequent advanced tertiary treatment for water reclamation. The aeration tank has six zones in series with 7in membrane disc diffusers. The process is operated in step-feed mode, with a 60/40 split between the first and third zones, which are operated under anoxic conditions using coarse-bubble diffusers and mechanical mixers, respectively.

4.3.2 Sensors installed

Six online sensors were installed in the aeration zone of the activated sludge tank. In detail, two ammonium sensors (one installed in the fourth aerated zone and one in the effluent),

pH, Dissolved Oxygen (DO), Oxidation-Reduction Potential (ORP), and Mixed Liquor Suspended Solids (MLSS). All the sensors were also equipped with an auto-cleaning system based on ultrasound to delay the growth of fouling and a temperature sensor, to adjust the measurement reading depending on the wastewater temperature. The sensors provided signals with a 2-minute frequency which were recorded with a data logger (Graphtec Mod. GL240). Each sensor was cleaned, throughout the study, on a weekly basis with a cloth damped with water, without chemical cleaning. The electrodes of the ammonium sensors were replaced every six months, following a two-point calibration procedure.

4.3.3 Artificial Neural Network

The neural network implemented in this study is a multi-layer perceptron (MLP), composed of a group of neurons, arranged into hidden layers, interconnected in parallel. Depending on the complexity of the system one or more hidden layers are required, however it is suggested that a network with a single hidden layer with a sufficiently large number of neurons can interpret any input–output model. In wastewater application, neural networks with one hidden layer are the best structure in order to achieve accurate predictions without increasing too much the complexity and the computational costs (Chen et al, 2003; Barron et al, 2009; Khataee et al, 2010a; Aghaeinejad-Meybodi et al, 2015). The number of neurons of the hidden layer is a fundamental parameter which is analyzed to obtain the desired accuracy of the sensors' predictions. To each input is associated a weight or coefficient that determines to which extent the input information is transmitted to its output. Another parameter that determines the topology of the ANN is the activation function, which connects the information from the input to the hidden layer and subsequently from the hidden to the output layer. The most common choice of activation function is the sigmoid transfer function, described by the Eq. 4.2 and represented in Figure 4.1 (Wang et al, 1996). The input for a

node j is given by the following equations (Wang et al, 1996):

$$net_j = \sum_i w_{ij} o_i \tag{4.1}$$

$$output_j = \frac{1}{1 + exp(net_j + \theta_j)} \tag{4.2}$$

Where j is the number of neuron, w_{ij} is the weight between node i and node j and o_i is the output of node i in the preceding layer. θ_j is the bias term, with which the output function can be shifted along the net_j axis.

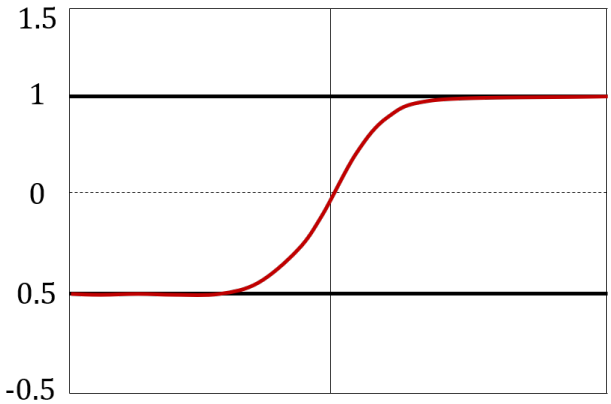

Figure 4.1: Representation of the sigmoid transfer function.

When using the sigmoid function, it is fundamental to previously scale the dataset in the 0.1-0.9 range (Walczak 1996), since the transfer function reports the results within 0 and 1 (Eq. 4.3). This function is non-linear and commonly used because differentiable, which is a

fundamental characteristic during the training of the model.

$$x_i = 0.1 + \frac{0.8(X_i - min(X_i))}{max(X_i) - min(X_i)} \tag{4.3}$$

Where x_i are the normalized values of the real data sets X_i

Once the topology of the neural network is defined, the model needs to be trained in order to minimize the error function by searching for a set of connection weights and biases so that the predicted outputs equals the observed output. Various algorithms are available, but most common training methodology is based on the back-propagation algorithm. Initially the weights are randomly assigned (Bos et al, 1993).

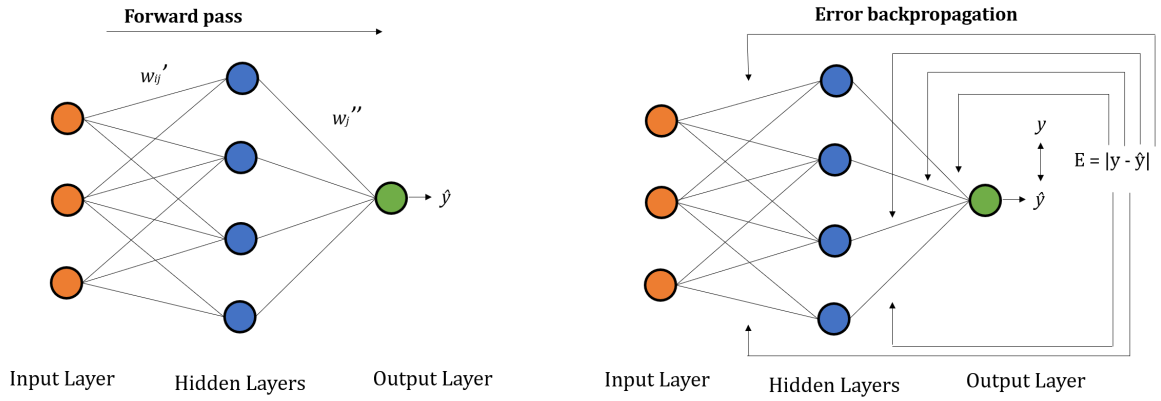

Figure 4.2: a) Representation Forward pass of the training algorithm. b) Second step of the training algorithm represented by the error backpropagation.

During the training there is a first phase of feed-forward mechanism (Fig. 4.2.a), where the external input information signals are transferred forward to calculate the output signals ŷ by performing a weighted summation of all the inputs received from the preceding layer. Then, in the back-propagation phase (Fig. 4.2.b), modifications to the connection weights are made based on the difference, E, calculated between the predicted, ŷ, and observed, y,

output. The training phase is an optimization problem, searching for the minimum on the error surface in a multi-dimensional space. The error surface presents several local minima and probably the searching method will not be able to find the absolute minimum, but a local minimum that is acceptable for the problem considered. Typically, the back propagation is based on a gradient descent algorithm in which the network weights are moved along the negative of the gradient of the performance function. There are a number of variations on the basic algorithm that are based on other standard optimization techniques, such as the scaled conjugate gradient, quasi-Newton, Levenberg-Marquardt algorithms and so on. The mean square error (MSE) and the mean absolute error (MAE) are typically used as error function to measure the performance of the network, according to the following equations (Hassani et al, 2014):

$$MSE = \sum_{t=1}^{N} (Y_{nn} - Y_{exp})^2 / N \tag{4.4}$$

$$MAE = \frac{1}{N} \sum_{t=1}^{N} |Y_{nn} - Y_{exp}| \tag{4.5}$$

Where N, Y_{nn} and Y_{exp} are the number of experimental runs, the neural network predictions and the experimental response, respectively. A fundamental step in the calibration of the model is the splitting of the available dataset into three datasets: a training dataset to estimate the connection weights, a validation dataset to test simultaneously, during the calibration phase, the generalization ability of the model of new samples, and the testing dataset which is utilized to test the general predicting capability of the model once the calibration of the model is finalized. The validation dataset is used during the calibration phase

to stop the training phase and avoid the overtraining which leads to the overfitting of the model. If the model incurs into overfitting during the calibration, it loses its generalization capability showing an increase in the validation error (Fig. 4.3).

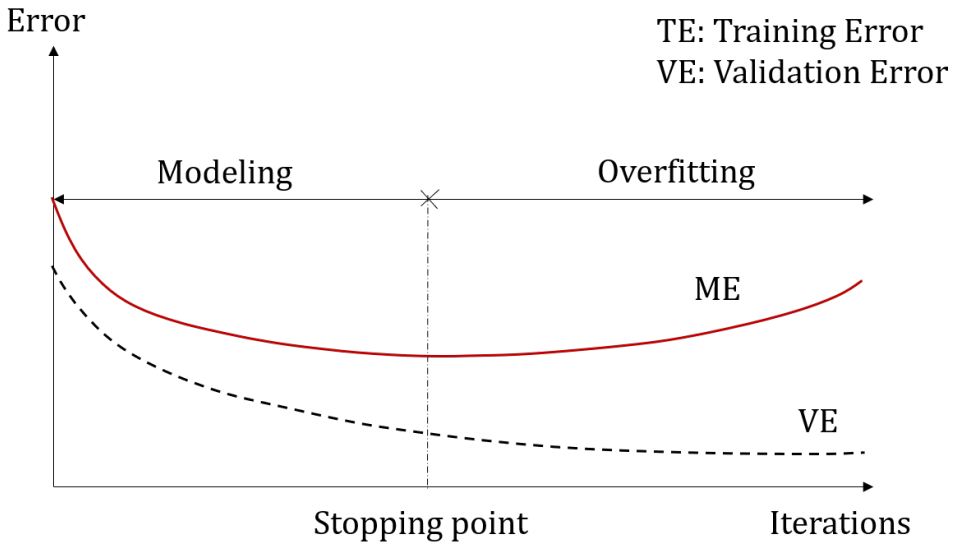

Figure 4.3: Representation of the overfitting problem.

The main neural network developed is utilized to predict the effluent ammonium by exploiting the information from all the other sensors installed. However, diverse networks were also built to be implemented in the fault detection monitoring system, as it will be explained in the following sections. In detail, for each input variable sensor, a neural network was built to predict the targeted variable using the other 4 sensors remaining as input variables. The network structure optimization for every sensor was implemented for a network with one hidden layer of N nodes and one output target variable. To determine the optimal number of nodes N, different networks were tested for each sensor, using from 2 to 20 nodes. The mean square error was calculated for every testing network and the minimum was usually achieved around 10 nodes. The optimum number of nodes was then chosen to be 10, since a larger number of nodes would only increase the complexity and computational time of the model without improving the prediction accuracy.

4.3.4 Sensitivity analysis

A vital question when designing and employing a neural network is the sensitivity of its outputs to input perturbation. The sensitivity can be defined as the mathematical expectation of the output errors of the network due to input alteration in a given continuous interval (Zeng et al, 2001). In order to obtain a reliable and robust neural network it is important to choose correctly the input variables and a consistent dataset. A preliminary sensitivity analysis of the model was performed, to understand which input variables has a higher influence on the output prediction, and to reduce the number of input variables, removing the variables with lower impact on the model output (Zhu et al, 1998). Different approaches can be considered for sensitivity analysis, many of which are based on statistical analysis, by calculating the sensitivity as the ratio of the variance of the output to a given variance of the input error (Choi and Choi 1992). Monte Carlo simulation is frequently used to quantify model uncertainty from model parameters, input data or model structure (De Menezes et al, 2018). The Monte Carlo simulation is performed by running the model N multiple times by random sampling the input data from the distributions of the uncertainty inputs until a statistically significant distribution of the outputs is achieved (Shrestha et al, 2007). The model output uncertainty is then expressed in terms of prediction intervals (or confidence intervals), which are typically related to the quantiles of the model output distribution. In the present research, every input dataset was first de-noised using a cubic spline method:

$$min_p(p\sum_{i=1}^{n}(y(i)-ys(i))^2+(1-p)\int\lambda(t)|\frac{d^2ys(i)}{dt^2}|^2dt) \tag{4.6}$$

With y(i) is the input sensor dataset and ys(i) is the smoothing approximation of the data. P $\in$ (0,1) is a smoothing parameter which was set as 0.05, in order to thoroughly remove the noise but not the daily dynamicity of the dataset. Then, every input smoothed dataset

was normalized at zero mean and 1 variance. In this way the different input datasets were characterized by the same working range. Following, the Monte Carlo simulations were performed by running the prediction model 10000 times and by choosing for each run a random noise from a gaussian distribution with zero mean and 1 variance to apply on one input variable at a time. The model outputs from the N runs were analyzed statistically in order to calculate the 95% confidence interval by dividing the model outputs for each input variable with random noise. Because the input datasets were normalized and the same random noise was applied to them during the sensitivity analysis, receiving the same level of perturbation, it was possible to individuate at which extent the different variables contribute to the model output.

4.3.5 Fault detection methodology

The fault detection methodology utilized consists of two stages (Fig. 4.4): residual generation and residual evaluation. At first the residuals are generated as the difference between the sensor signal and the predicting model output. It is expected that these residuals are approximately zero in nominal conditions, and instead increase when an out-of-control event happens. Then, the residuals are analyzed using two types of monitoring charts: with PCA monitoring techniques and with Shewart charts monitoring, as presented in the following sections.

PCA control charts

The residuals generated between the model output and the corresponding sensor were calculated for every sensor considered in the study. The residuals dataset from the six sensors was used as matrix input to the PCA analysis instead of the actual sensor signals, with the purpose to detect potential process anomalies and sensor faults. Mathematically, PCA evaluates the correlation structure of the process variables. The size of the variance residual

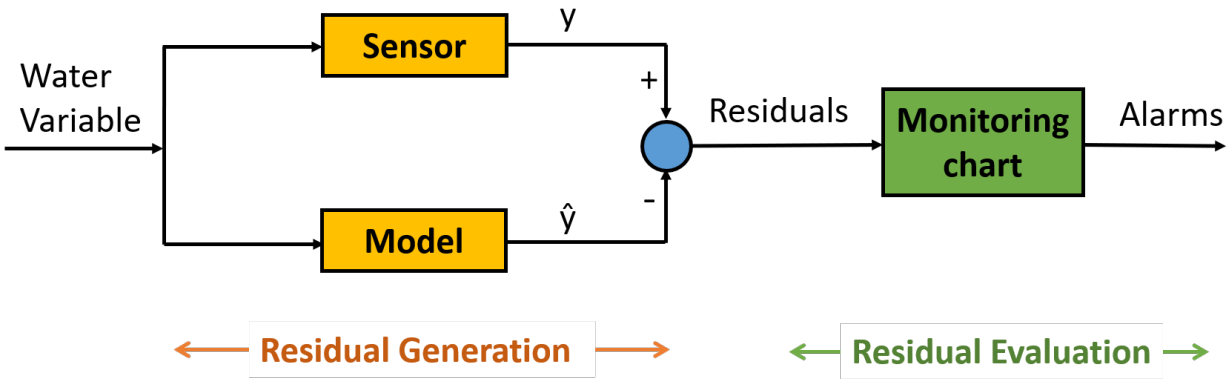

Figure 4.4: Scheme of the two stages fault detection methodology.

indicates the importance of every variable. At first, the residuals from every sensor were normalized for the maximum error obtained during the training of its corresponding neural network. The dataset normalization allowed to compare directly the residuals from different sensors and to remove any influence of the sensor working range. Consider a data matrix X $\in R^{KxJ}$ containing K scaled observations of J process variables. The covariance matrix of X is defined as:

$$S = \frac{1}{K-1} X^T X \tag{4.7}$$

λ_j (j = 1,....J) represent the eigenvalues of the matrix S, disposed in descending order to obtain the principal components, PCs. The transformation matrix $P_{1:A} \in R^{JxA}$ is obtained by choosing A eigenvectors. The prediction of the PCA model for a new observation data x_{new} is the following:

$$\hat{x}_{new} = P_{1:A} t \tag{4.8}$$

Where t = $P_{1:A}^T$ $\hat{x}_{new}$ is the score vector. The resulting residual is determined as:

$$r_{PCA} = x_{new} - \hat{x}_{new} = (I - P_{1:A}P_{1:A}^T)x_{new} \tag{4.9}$$

When PCA is applied for fault detection purposes, two monitoring statistics can be used, usually adopting control charts. The control charts can detect a fault when the statistics values are greater than a certain limit. The Hotelling's T^2 and the square prediction error (SPE or Q) are the most commonly adopted. T^2 can be calculated as follows:

$$T^2(k) = x^T(k)T_k\Lambda_k^{-1}T_k^T x(k) \tag{4.10}$$

Where λ_k is a diagonal matrix made of the first k eigenvalues of S. The process is considered in nominal operating condition for a given significance level α, typically between 90% and 95%, if the statistic value doesn't exceed the threshold calculated:

$$T^2 \leq T_{lim}^2 = \frac{a(p-1)}{p-a}F_{a,p-a,\alpha} \tag{4.11}$$

The Q statistic is calculated as the sum of the squares of the residuals:

$$Q(k) = x^T(k)(I - TT^T)x(k) \tag{4.12}$$

The upper limit of this statistic can be computed as follows:

$$Q(k) \leq Q_{lim} = \Theta_1 \left[\frac{h_0 c_\alpha \sqrt{2\Theta_2}}{\Theta_1} + 1 + \frac{\Theta_2 h_0 (h_0 - 1)}{\Theta_1^2} \right]^{\frac{1}{h_0}} \tag{4.13}$$

With $\Theta_i = \sum_{j=R+1}^{J} \lambda_j^i$ $\qquad\qquad$ $h_0 = 1 - \frac{2\Theta_1 \Theta_3}{3\Theta_2^2}$

Shewart control chart

Shewart charts are widely used in analytical laboratories but not very common in Water Resource Recovery Facilities (Thomann et al 2002). Rieger et al (2004) demonstrated the possibility to apply these control charts to detect sensors anomalies and erratic behavior in wastewater with additional criteria that allows to detect "out-of-control" situations earlier. They demonstrated to be able to detect bias, outliers and drift of the sensor and poor calibration of sensors. In contrast to the typically used Western Electric rules (Montogomery, 1996), the warning phase criteria are more stringent in order to promptly detect anomalies. In detail, the Shewart charts were used by comparing on a weekly basis the residuals between sensor reading and laboratory analysis, used as a reference. If an alarm was generated, further comparison with lab analysis were required in order to check for potential "out-of-control" events, confirm them and request maintenance measures. In our study the control charts were used similarly, in order to detect sensors and process anomalies and erratic behavior. However, in the previous studies the residuals analyzed were dependent on the frequency that the plant performs grab-sampling lab analysis, which is usually on a weekly basis. Instead, in the present research, the residuals are generated by plotting the difference between the model prediction and the sensor signal. A high frequency residuals dataset is generated, with up to 2 minutes frequency sample. Therefore, it was possible to decide how frequently monitoring

the residuals on the control charts and define an averaging window interval of the residuals, in order to avoid outlier's interference or small dynamics discrepancies, related to the level of accuracy of the model prediction. Among the different type of sensors anomalies, drifts are the most difficult to detect given the relatively small visible error but that inevitably increases in time. The Shewart charts in this study were mainly designed to be utilized for sensor's drift detection because of the high relevance and complexity of early stage drift detection. The difference between sensor and model prediction is used as a control variable to detect out-of-control events.

$$R = x_{model} - x_{sensor} \tag{4.14}$$

It is assumed that the control variable is normally distributed with μ =0 and variance σ^2. The monitoring charts are characterized by two different control levels: a warning limit and a control limit (Figure 4.5).

UWL = Upper Warning Limit = + 2 σ_T; UCL = Upper Control Limit = + 3 σ_T

LWL = Lower Warning Limit = - 2 σ_T; LCL = Lower Control Limit = - 3 σ_T

Where σ_T is the standard deviation of the training phase of the model:

$$\sigma_T = \sqrt{\frac{\sum (x_{train} - x_{sensor})^2}{N}} \tag{4.15}$$

With x_{train} is the model prediction obtained during the training phase, x_{sensor} is the corresponding sensor dataset utilized during the training phase and N is the number of samples the training dataset. The rules to produce an alarm for out-of-control detection are the following (See Fig. 4.5):

- 5 values in a row steadily increasing
- 3 values over the Warning Limits consecutively
- 2 values over the Control Limits consecutively

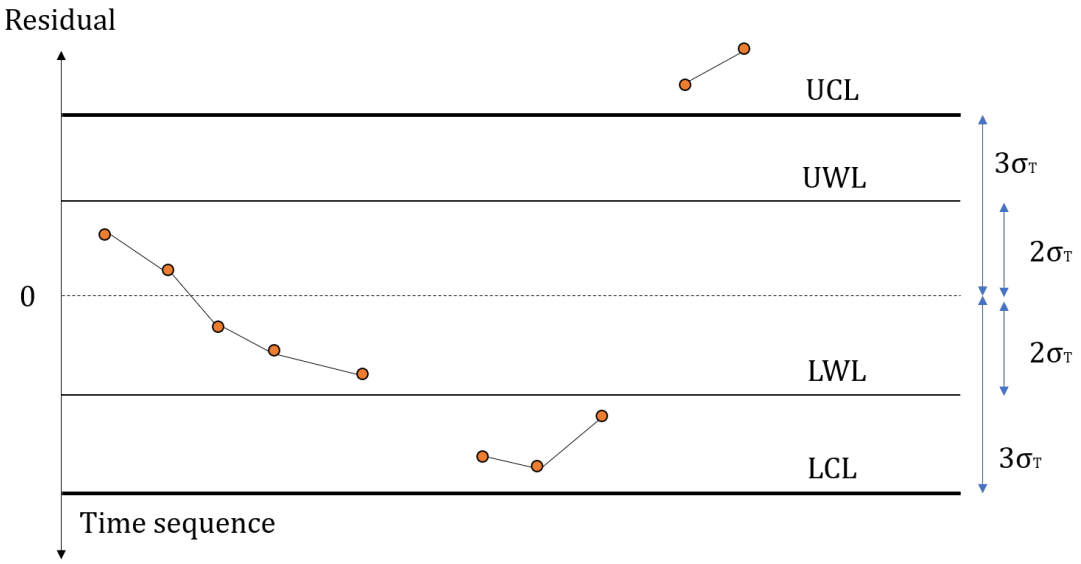

Figure 4.5: Shewart chart scheme. Key: UCL = + 3 σ_T; LCL = - 3 σ_T; UWL = + 2 σ_T; LWL = -2 σ_T, where σ_T is the standard deviation of the training phase of the model.

4.4 Results and Discussion

4.4.1 Preliminary analysis

The quality of the input data in Artificial Neural Networks is of the upmost importance in order to obtain a reliable structure of the model and consequently accurate model outputs. The structure of the model comprises the number of nodes of the hidden layer and their corresponding coefficients (also called weights). High-quality datasets of the input variables

will improve especially the determination of the nodes' coefficients, since they are the base of the correlation between the input and the output variables.

A sensitivity analysis was implemented to individuate which sensors (input variables) have a major influence on the network output (effluent ammonium). The following graphs (Fig 4.6.a to 4.6.f) report the model output range obtained from the perturbation of the input variables. Each graph shows the model outputs as function of one input variable perturbation at a time. Figure 4.6.f represents the composite from all the different input variables. It can be noticed how the ammonium sensor installed in the aeration tank has the highest influence on the model output (Fig. 4.6.a). Also, the input variables' influence on the model output depends on the dynamicity of the actual signal, varying during the day and is different for every input variable. The relative contribution of the different input variables on the model output is reported in Table 4.1. For every input variable it is reported the % of influence on the model compared to the other variables.

The quantification of the uncertainty associated to the results provided by ANN models is essential for their confident and reliable use in practice. The sampling of the parameter space is generally done by Monte Carlo simulations using uniform random sampling across the specified parameter range (Srivastav et al, 2007). Therefore, similarly to the sensitivity analysis, further simulations were also conducted to calculate the uncertainty of the model output using the original sensors noise of every input variable (Fig. 4.7). In detail, the input variables were denoised, but they were not normalized, differently from the sensitivity analysis. Then, Monte Carlo simulations were performed by uniform random sampling across the sensor's noise range (gaussian distribution of the residual between original and denoised dataset). As previously seen, the 95% confidence interval of the model output varies depending on the dynamicity of the input signals and in general the highest output uncertainty is achieved during the maximum daily peak. The maximum uncertainty calculated is around 0.25 ppm, which is comparable to the actual ammonium sensor accuracy achievable

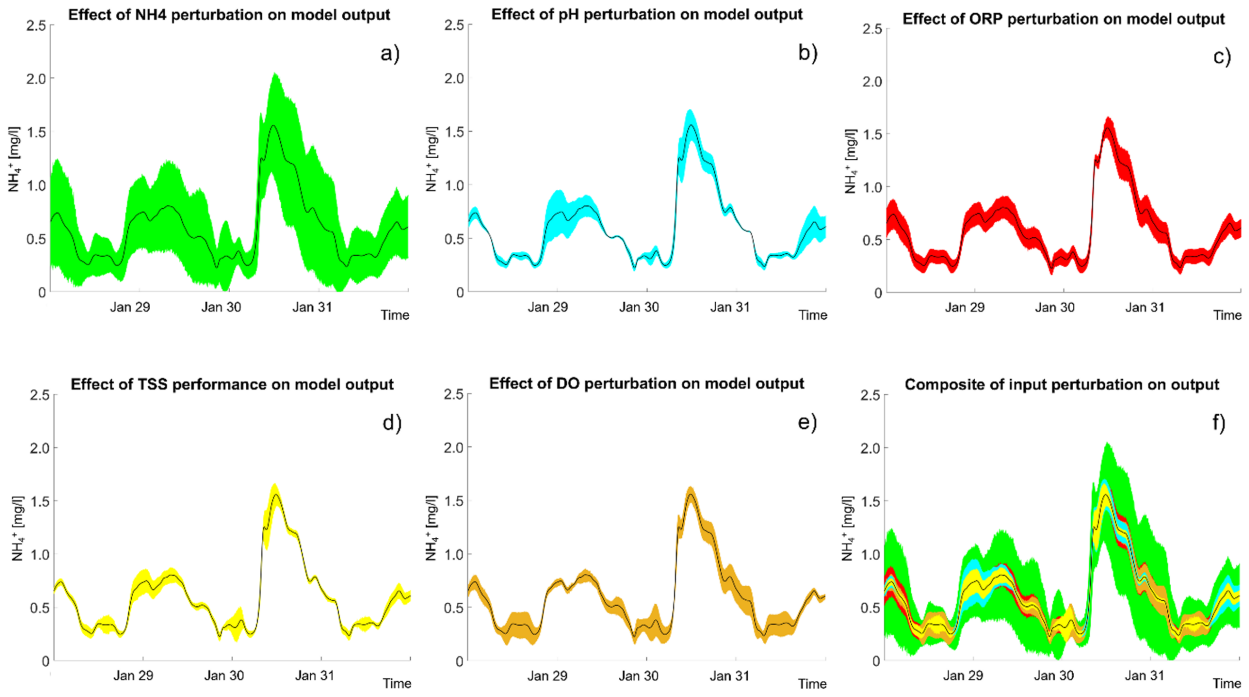

Figure 4.6: Sensitivity analysis of the model output as function of each input variable noise at a time. a) Effect of the variability of ammonium high range input on the model output. b) Effect of the variability of pH input on the model output. c) Effect of the variability of ORP input on the model output. d) Effect of the variability of TSS input on the model output. e) Effect of the variability of DO input on the model output. f) Composite effect of the variability of all the input variables over the model output

in well-maintained conditions. Thus, the model output uncertainty, as a consequence of the input sensors' noise, is acceptable for the ammonium sensor application in the secondary process. The uncertainty of the model as function of the different sensors' noise is reported in Table 4.1.

4.4.2 Model structure

Different model structures can be selected, depending on which variables are chosen as input of the ANN model. We chose 3 different options (Fig. 4.8), according to the sensitivity analysis results: the first model (A in blue) uses all the sensors available for the study; the second model (B in red) excludes from the input variables the ammonium sensor installed

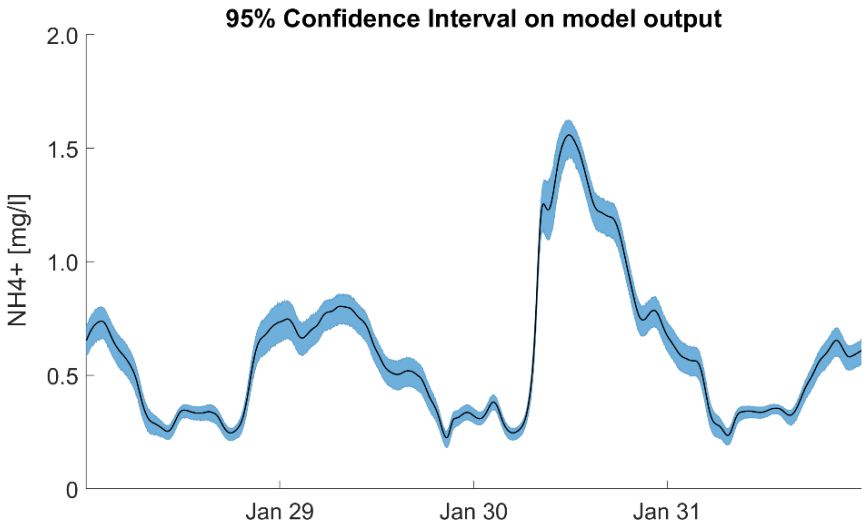

Figure 4.7: 95% Confidence Interval of the model output as function of the input sensors noise.

Table 4.1: Summary of the sensitivity analysis. The contribution of each input variable to the model uncertainty is reported relatively to the remaining input variables. Also, the model uncertainty due to the sensors' noise of the input variables is reported in terms of 95% Confidence Interval.

Input variables	**NH_4^+**	**pH**	**ORP**	**TSS**	**DO**	**Composite**
Input variable contribution (%)	45	25	14	8	8	-
95% CI with original noise [mg/l]	± 0.013	± 0.0004	± 0.0004	± 0.0003	± 0.0001	± 0.19
(min-max) [mg/l]	± 0.20	± 0.07	± 0.03	± 0.05	± 0.09	± 0.25

in the aeration tank and the third model (C in green) utilizes the ammonium high range as the only input variable, since it was demonstrated having the highest influence on the model performance according to the sensitivity analysis.

The prediction accuracy of the different models during the training of the network is reported in Figure 4.9, expressed as Mean Squared Error (MSE) and R^2 as a function of the number of nodes in the hidden layer. In blue is reported model A, in red model B and in green model C, according to the same color arrangement shown in Figure 4.8.

In model A (blue) we use all the sensors as input, which results in a more complex model

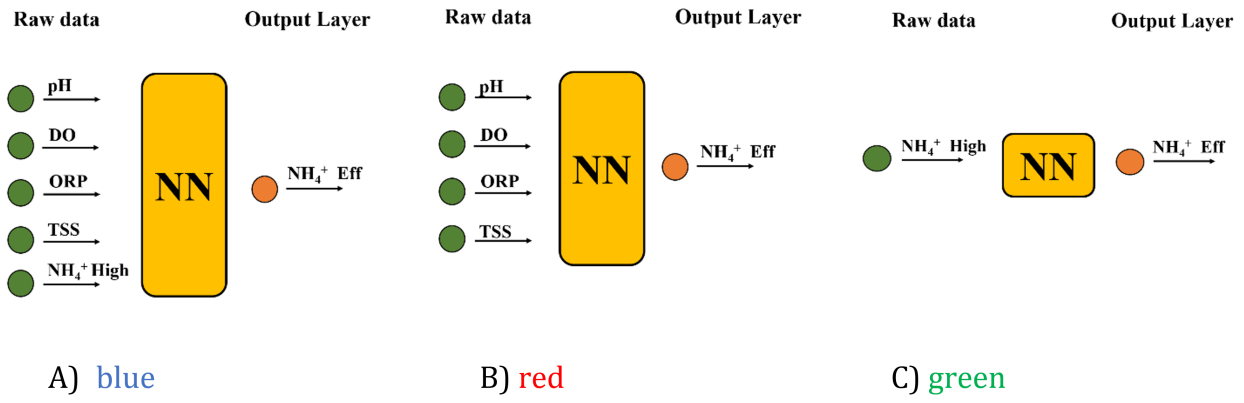

Figure 4.8: Different possible architectures of the neural network depending on the chosen input variables.

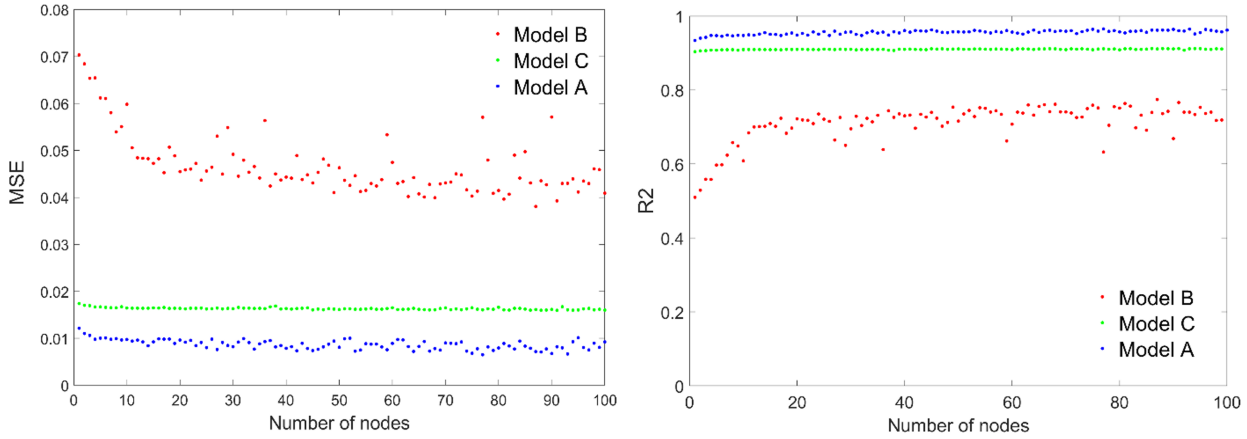

Figure 4.9: MSE (left) and R^2 (right) of the different models during the training phase as a function of the number of nodes in the hidden layer. In blue Model A (all the input variables), in red Model B (all the input variables excluding $NH4_4^+$ high range) and in green Model C (NH_4^+ high range as only input variable).

(more sensors which require thorough maintenance) but also the most accurate (smaller MSE and higher R^2 then the other two options). The accuracy of the prediction is not dependent on the number of nodes of the model. The model A is also the most resilient because the presence of multiple sensors ensures a more robust prediction in the eventuality that a fault of an input sensor occurs. The model B (red) excludes the ammonium high range from the input dataset. For this case, the model prediction is the least accurate (higher MSE and lower R^2), which is in accordance with the sensitivity analysis performed, and it shows the highest dependency on the number of nodes, stabilizing only around 30 nodes (more

complexity and computational time). The model C (green) requires the least computational cost and complexity because it presents only the ammonium high range as input, and the prediction accuracy is high and independent by the number of nodes. However, in the case C, the model resiliency is at its lowest because it relies only on one ammonium sensor, which is also renowned in the literature to be a sensor that requires thorough maintenance and can often incur into faulty behavior (Winkler et al, 2004; Åmand et al, 2013; Papias et al, 2018). On the contrary, model B has a higher resiliency because it utilizes multiple sensors and it excludes the ammonium sensor, which shows erratic behavior regularly. In conclusion, the three possible model structures provide different model prediction accuracy but, at the same time, different model resiliency and complexity.

Figure 4.10 shows the comparison of the three different model predictions with the sensor signal on a new testing dataset. The focus resides in the peaks because the sensor is not reliable below 0.4-0.3 ppm due to the level of interference of the cations present in the wastewater (Cecconi et al 2019). As previously explained, it can be noticed that the model A presents the highest prediction accuracy, especially at the peak of the day, and it shows the least erratic and noisy signal. The model B instead shows a high level of noise, compared to the sensor's signal (in blue), and the least ability to follow the daily dynamicity. This is coherent with the sensitivity analysis results, since the ammonium sensor, which contributes to the 45% of the network prediction, is excluded from the input variables. In detail, on the testing dataset, model A presents a Mean Squared Error of 0.0179, model B of 0.394 and model C of 0.0279.

From the preliminary analysis, it can, therefore, be chosen the preferred model structure depending on the different priorities: model prediction accuracy, complexity, and resiliency. In this study, the model A, which utilizes all sensors available as input variables, is considered as the preferred choice because of the improved prediction accuracy compared to the other cases.

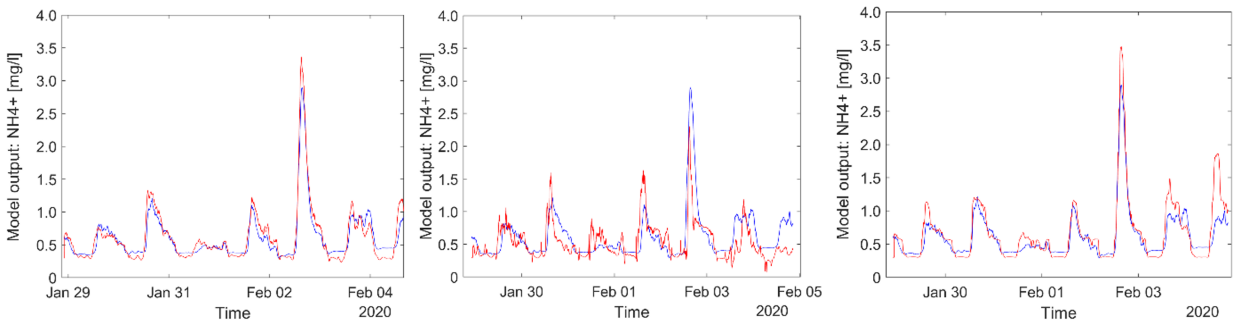

Model A) Model B) Model C)

Figure 4.10: Comparison of the different models' prediction of ammonium in the effluent (in red) with the ammonium sensor signal (in blue).

4.4.3 Fault detection

Once the preferred model structure is decided, the neural network can now be utilized for fault detection purposes. In this study, we consider three possible fault occurrences: i) process anomaly; ii) sensor fault due to wrong calibration procedure; and iii) sensor drift due to fouling development and lack of maintenance. The datasets utilized for the fault detection analysis were directly collected in more than one-year field experience with all the sensors installed. The sensors were thoroughly analyzed in time and different faults and anomalies were individuated, especially associated to the different installations of the ammonium sensors (Cecconi et al., 2019; Cecconi et al., 2020). The use of real and common sensors' faults allows to investigate more representative situations, while many fault detection studies often rely on simulations of the actual fault or large sensors' failures, which can be easily detected with simple data quality control. The fault detection method proposed is based on evaluating via control charts the residual between the model output and the target sensor signal. Two different types of control charts are considered in this study, depending on the type of fault analyzed. Sudden faults like large biases and the effect of a calibration procedure are studied with PCA control charts, since the squared prediction error, Q, will emphasize the amplitude of the sudden increase of the residual. Instead, slow developing

faults like drifts and precision degradation events are better analyzed with Shewart charts, since the residual increase is low, hardly detectable with a normal PCA control chart, but steadily growing in time. Therefore, for drifts events it is important to monitor the sign and the trend of the residual and not only the magnitude. Six different neural network models were built to predict one sensor signal at a time (NH_4^+ high range, Effluent NH_4^+, pH, ORP, TSS, and DO) by using the rest of the variables as inputs accordingly (Fuente et al 2012, Cheng et al 2005). The obtained maximum training error then is used to normalize each model residual, so that the range of the residuals are comparable among the different output variables considered. PCA is applied on the residuals obtained by the 6 models. The square predicting error (Q or SPE) is used to analyze the PCA model. When this exceeds a specific threshold, an alarm is generated. For the Shewart chart monitoring, only one neural network model is built to predict the effluent ammonium using all the other sensors' variables as input. The residual between the model output and the effluent ammonium sensor dataset is then averaged on a six hours basis and is plotted in the monitoring chart to analyze the trend.

(i) Process anomaly

Figure 4.11.a shows the comparison between the effluent ammonium prediction and the sensor signal in absence of fault with corresponding Q Statistics chart (Fig. 4.11.b). No significant alarms are identified (values exceeding the dotted line) for more than a couple of consecutive hours in 3 weeks of data analyzed. Considering the high frequency of the data analyzed, it is decided to ignore residuals that fall outside the limit for less than 3 consecutive hours, in order to avoid false alarms of sensors' faults. The model output (in red) always presents a lower baseline during night-time, compared to the sensor output (in black). Due to the interference of the cations present in wastewater and of the complexity of the water matrix composition, the sensor has a lower accuracy in the lower range of ammonia measurement and it typically overestimates the ammonium content of 0.2-0.3 mg l^{-1}. Therefore, the model prediction during the minimum loads is more accurate than the

actual sensor. It can be noticed than on the sixth day it occurred a considerable peak, almost double than the typical effluent peak that the plant experiences. Because no significant fault alarms can be recognized, it can be inferred that the treatment process incurred into an anomaly and/or presented a higher influent load than usual. On the contrary, during the 16^{th} and 17^{th} day, the daily peak is consistently lower than usual but because no sensor fault is individuated from the control chart it can be inferred it was the actual treatment process experiencing a lower load than usual. Figure 4.11.c shows the contribution plot of the different variables in the Q statistics plot. The six sensors contribute similarly to the statistics, around 15% on average during the 3 weeks considered. Since there is no dominant contribution of one sensor over the others to the squared prediction error, Q, it can be further confirmed that there is no presence of sensors' faults in the dataset analyzed and the plot can be used as a reference when investigating new datasets for sensor faults.

(ii) Sensor calibration fault

Afterwards, the low ammonium sensor dataset was modified after the sixth day by applying the effect of a wrong calibration procedure. By analyzing historical datasets of the same sensor, it was possible to quantify the effect of a calibration performed with a wrong procedure, which can be mainly quantified as a modification of the daily standard deviation. In detail, a calibration event causes a jump in the measurements because it adjusts the offset parameter and the calibration slope. The offset parameter is responsible not only to move the daily average of the measurements, but it also influences the magnitude of the daily dynamics. The fault detection process was performed by using the new faulty dataset as comparison of the neural network prediction of the effluent ammonium. Figure 4.12 shows the comparison between the new faulty sensor dataset and the network prediction (Fig. 4.12.a) and the corresponding Q statistics chart (Fig 4.12.b), reported in logarithmic scale to improve the visibility of the residual spikes. Fig 4.12.c reports the contribution plot of the different variables to the monitoring chart, as average of the days after the calibration (day 6).

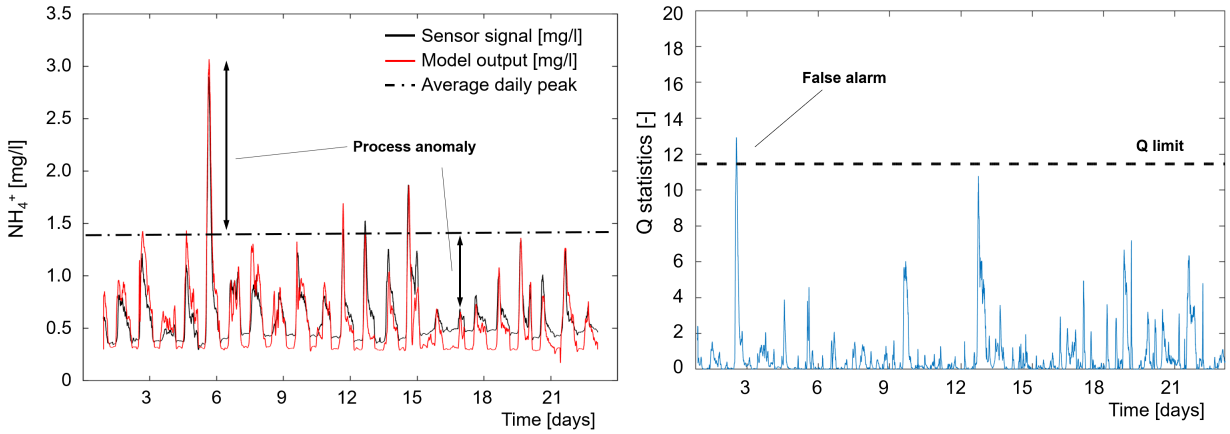

(a)

(b)

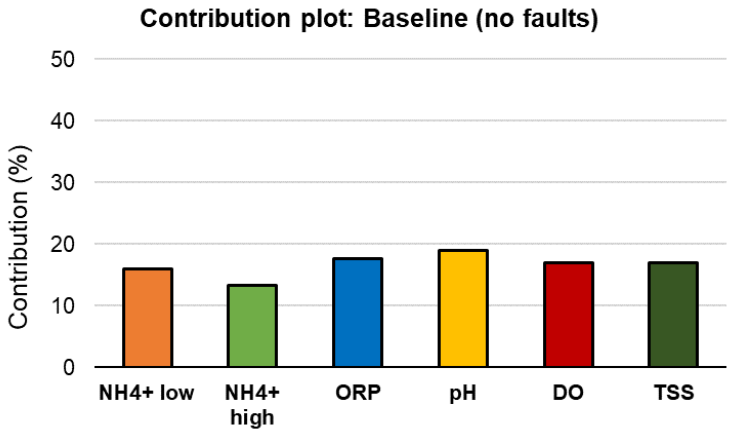

(c)

Figure 4.11: (a) Comparison between the original ammonium dataset from the sensor (blue) and the model predictions (red), applied on a new testing dataset. The dash-dot line shows the position of the maximum daily peak, around 1.4 ppm, on average of the period of data considered. (b) Q statistic chart in absence of any significant fault of all the six sensors analyzed. The dashed line shows the Q limit, which represents the threshold above which the alarm is generated. (c) Contribution plot of the variables in the monitoring chart, as average of the 3 weeks considered.

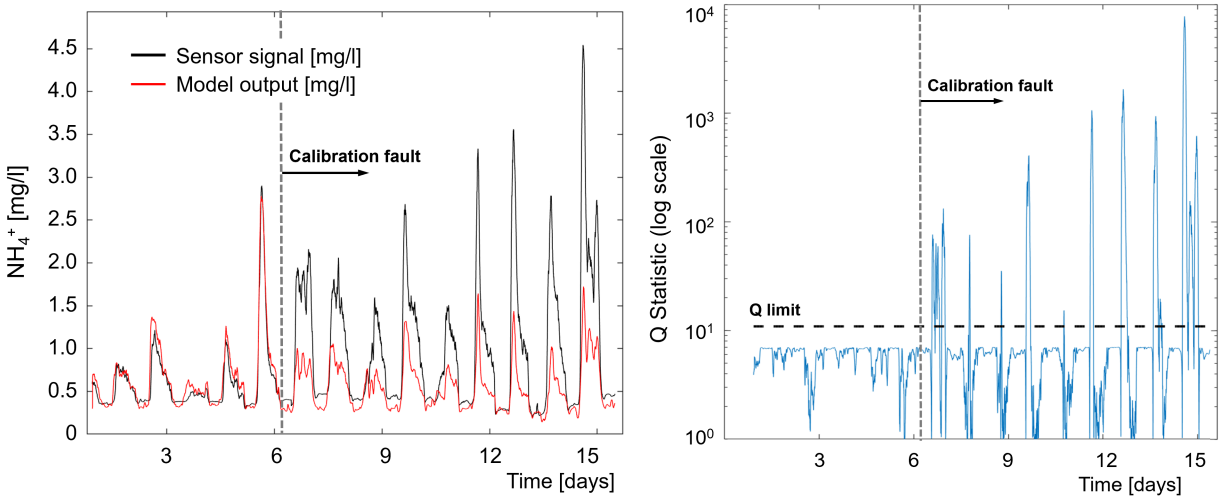

(a)

(b)

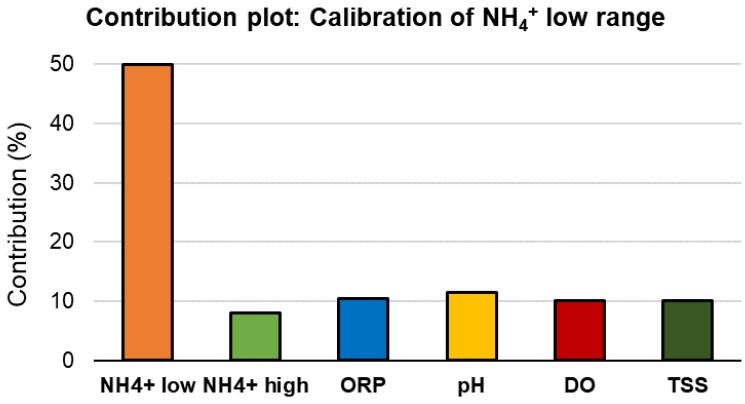

(c)

Figure 4.12: (a) Comparison between the ammonium sensor dataset affected by wrong calibration (black) and the model predictions (red). (b) Q statistic chart reported in logarithmic scale on the y axis, with normalized residuals which were also squared to amplify the larger differences. The dashed line shows the Q limit, which represents the threshold above which the alarm is generated. (c) Contribution plot of the variables in the monitoring chart, as average after the calibration day.

It can be noticed that as soon as the calibration procedure is performed, large daily spikes over the limit can be individuated in the monitoring chart (Fig. 4.12.b). Therefore, the fault can be easily detected within the first day from the wrong maintenance event. An alarm is generated, and it is suggested to perform the according calibration procedures to correct the sensor accuracy by utilizing multiple grab-samples to adjust the calibration slope and offset. The contribution plot (Fig. 4.12.c) shows a large contribution, around 50% on average, of the ammonium low range sensor dataset in the monitoring chart compared to the other five variables which all show a small contribution, around 10% each. The contribution plot helps not only to detect an error, by comparing each new contribution plot to the baseline, but especially to detect which sensor is the one affected by the fault.

(iii) Sensor fouling

The low ammonium sensor dataset was modified after the sixth day by applying the effect of fouling on the sensor performance. As described in Cecconi et al 2020, the effect of fouling on the ammonium sensor performance can be quantified as a linear negative drift, around -0.11 mg NH_4^+ l^{-1} d^{-1}. The fault detection process was performed by comparing the faulty sensor dataset, affected by fouling and the neural network prediction of the effluent ammonium. Figure 4.13.a shows the comparison between the sensor dataset affected by fouling (in black) and the model prediction (in red), and the corresponding monitoring chart in terms of squared prediction error, Q, is reported in Figure 4.13.b. Figure 4.13.c shows the Shewhart monitoring chart, expressed as residual between effluent ammonium sensor and NN model output, plotted on a 6h basis average. Fig 4.13.d reports the contribution plot of the different variables to the monitoring chart during the fouling drift, as average after the sixth day.

It can be noticed that the Q statistics (Fig. 4.13.b) shows an increase in daily peaks after the sixth day. However, compared to the previous fault case of wrong calibration, the peaks are not as consistent, protracted in time and large. Indeed, a fouling drift is characterized

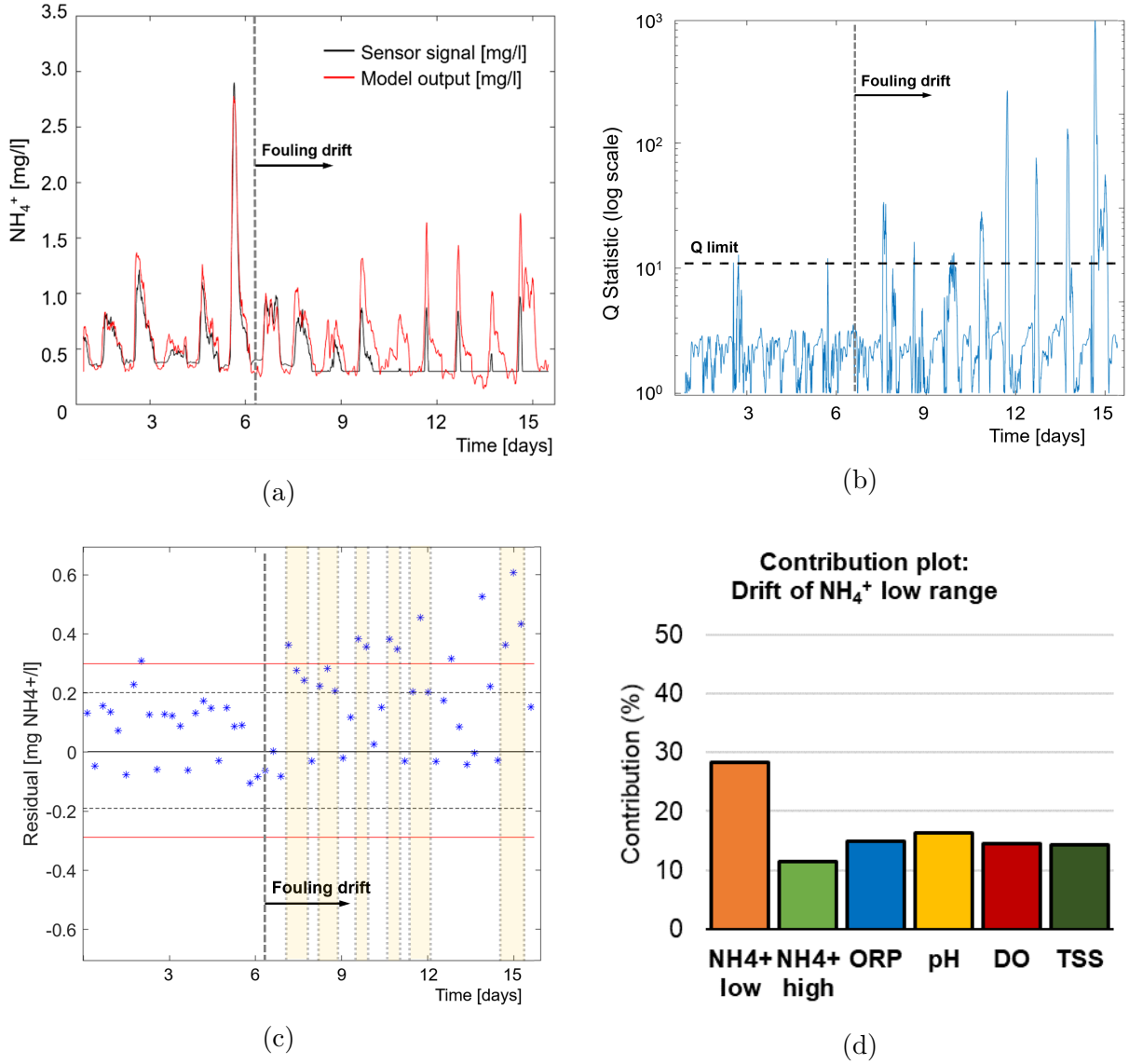

Figure 4.13: (a) Comparison between the ammonium sensor dataset affected by fouling drift (black) and the model predictions (red). (b) Q statistic chart reported in logarithmic scale on the y axis, with normalized residuals which were also squared to amplify the larger differences. (c) Shewhart control charts in the presence of a fouling drift. The residual between effluent ammonium sensor and model output is reported as average on a six hours basis. The black dashed lines report the warning limits and the red lines shows the control limits. The yellow columns highlight when an alarm is detected. (d) Contribution plot of the variables in the monitoring chart as average after the sixth day.

by a slow and consistent increase in the residual in time but not in big differences from the start. Also, with the square prediction error, Q, it is not possible to individuate the sign of the error, whether it is an overestimation or underestimation, and if the error shows a consistent trend in time. Therefore, another way to investigate drift faults was considered by deploying Shewhart control charts on the residuals, averaged on a six-hour basis (Fig. 4.13.c). This averaging time window was found to be the best one to remove outliers and small dynamicity which would not affect a drift, but at the same time frequent enough to get a consistent number of residuals' samples to early detect a drift. Because the drift is a consistent small error that intensifies in time, working with longer averages (6h) improves the response time of the alarm system. Already after one day from the drift beginning, multiple alarms can be individuated (yellow columns, Fig. 4.13.d), while instead no alarm conditions were detected in the first 6 days, in absence of any fouling effect. Also, this methodology simplifies the identification of the type of fault, since the samples falling outside of the limits are consistently in the upper limits and increase in time, denoting a rising underestimation of the sensor measurements, typical of fouling. The contribution plot, Figure 4.13.d, confirms that the error is generated by the ammonium sensor low range, since the influence on the Q error increases from 15% (baseline) to 28%.

(iv) Fault of the input dataset

The proposed fault detection system is based on the quality of the input data of the neural network model, and therefore it can be inferred that if a fault occurs in one of the sensor used as input variable, it will also influence the prediction accuracy and the fault detection efficacy. The following example considers the case study in which the high ammonium sensor, used as input of the network, presents a calibration fault, calculated analogously to the previous case. Because the high ammonium sensor has the highest sensitivity on the model performance, the fault applied will have the largest effect on the model performance, compared to the case in which the fault was to be applied to any of the other input variables. Figure 4.14.a

shows the effect of the wrong calibration procedure on the high range ammonium sensor and Figure 4.14.b shows the effect of this fault on the prediction accuracy of the ammonium low range. As expected, the inaccuracy of the ammonium high range as input variable has a large effect on the prediction of the ammonium low range, with daily peaks doubled than the typical range.

The Q statistics plot (Figure 4.14.c) shows several alarms starting from the sixth day, with large peaks over the limit on a daily basis. The contribution plot, Fig. 4.14.d, shows which variables contributed the most to the fault. It can be noticed that both ammonium high range and low range contributed equally to the statistic increase, around 36% and 34% respectively, and therefore are the main responsible. This system allows to have an internal check control, so that not only it is possible to detect the fault of the sensor of interest, but also to take under control all the other sensors involved in the model. Finally, even if the prediction accuracy of the model is affected, it is possible to promptly individuate the fault in the system and take action on the model structure of the neural network. Once the fault is detected on the high range ammonium sensor, it is discarded by the input variables set and another NN model is built without it: [ORP, pH, TSS and DO] = input; [NH_4^+ effluent] = output. Figure 4.15 shows the performance of the substitute NN model, comparing the ammonium sensor in the effluent (black) and the new model output (red). As expected, the accuracy of the new model is lower (MSE = 0.14), but the model output still follows well the daily peak range. Once the high range ammonium sensor is fixed by an operator, it can be reintegrated in the network to the original model structure. Finally, Table 4.2 summary reports a summary of the contribution of the different variables considered in all the scenarios analyzed.

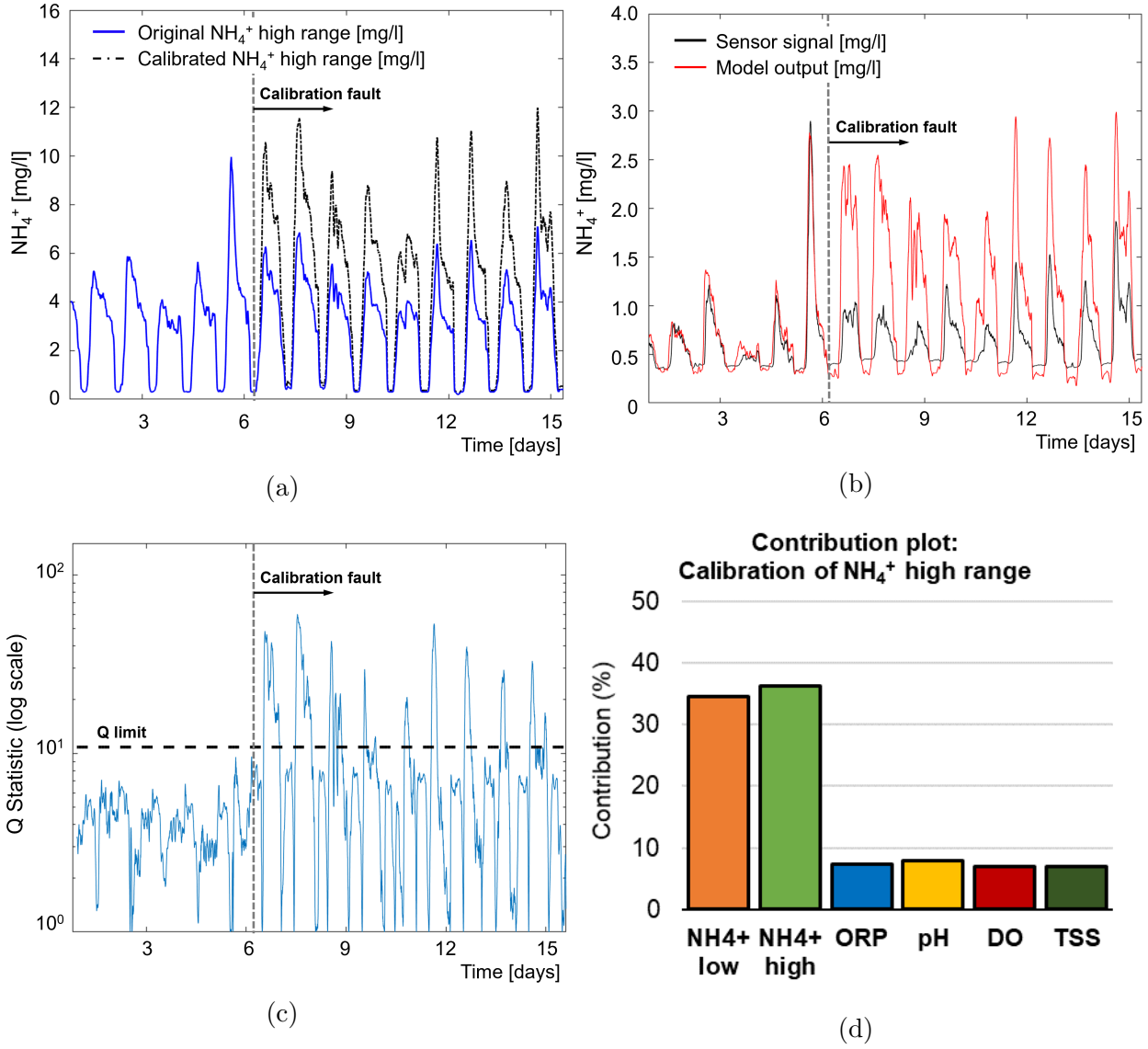

Figure 4.14: (a) Comparison between original high ammonium sensor dataset (in black) and the same dataset affected by a wrong calibration (in blue). (b) Comparison between the effluent ammonium sensor (black) and the model prediction in case of a fault on the ammonium input dataset (red). (c) Q statistic chart reported in logarithmic scale on the y-axis, with normalized residuals which were also squared to amplify the larger differences. (d) Contribution plot of the variables in the monitoring chart, as average after the calibration event (day 6).

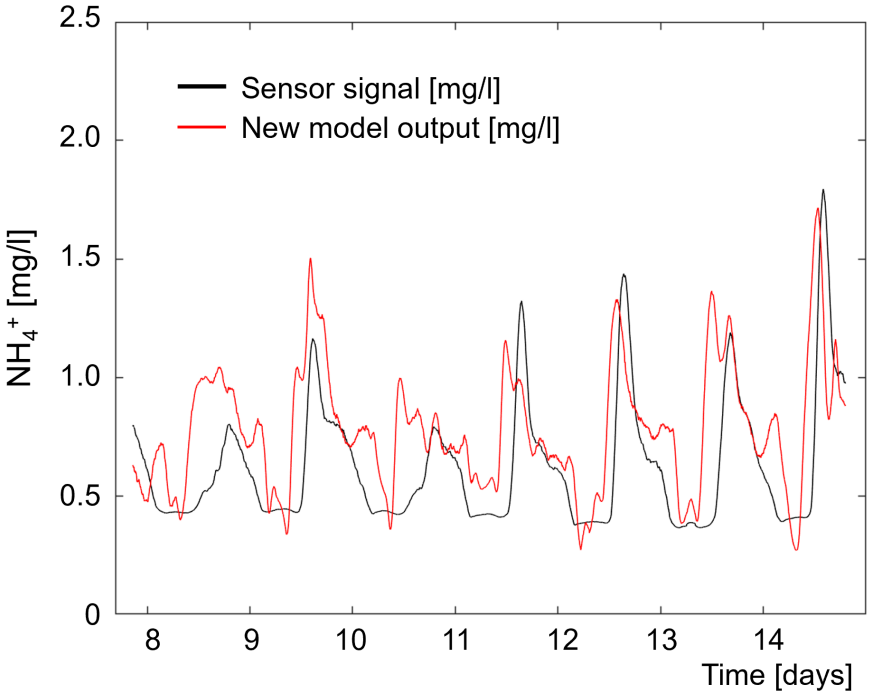

Figure 4.15: Comparison between the effluent ammonium sensor (black) and the model prediction (red) in case of a new model structure that excludes high range ammonium from the input variables.

Table 4.2: Summary of the variables' contribution on the fault detection mechanisms in the different scenarios considered.

Variables	Baseline (no fault)	Calibration on NH_4^+ low range	Calibration on NH_4^+ high range	Fouling drift on NH_4^+ low range
NH_4^+ Low range	16.0%	**50.0%**	**34.6%**	**28.3%**
NH_4^+ High range	13.4.0%	8.0%	**36.3%**	11.5%
ORP	17.6%	10.5%	7.3%	15.0%
pH	19.0%	11.4%	7.9%	16.3%
DO	17.0%	10.1%	7.0%	14.5%
TSS	17.0%	10.0%	6.9%	14.4%

4.5 Conclusions

Soft-sensors accuracy and robustness depends on the correct choice of the input variables and of the quality of the data. It is fundamental to perform preliminary analysis to determine the model structure, especially in terms of the input variables, investigating their sensitivity to the model output accuracy. The variables that contribute the most to the accuracy of the prediction of ammonium in the effluent are ammonium in the high range installation, pH and ORP, in decreasing order. The final structure of the neural network model was composed of a total of five input variables, NH_4^+ high range, pH, ORP, DO and TSS, and shows a good prediction ability, with a mean squared error, MSE, of 0.01 on the training dataset and 0.02 MSE on a testing dataset. Two monitoring methods, Q statistics chart and Shewart chart, were implemented to analyze the residual between model prediction and sensor signal, to detect faults and anomalies of both sensors and the treatment process. They both perform well in absence of sensor faults, not showing any false alarm which is fundamental for the credibility and reliability of the method. The monitoring charts were also used to monitor the actual process and individuate process anomalies, especially larger influent loads. When a wrong calibration procedure is performed on the ammonium effluent sensor, a common operator mistake, the residual between model prediction and the faulty sensor's dataset increases, an alarm is promptly detected in the monitoring chart, and the specific faulty sensor is identified through the contribution plot of the Q statistics. Fouling drifts are better monitored using Shewart charts, displaying multiple alarms already after one day from the beginning of the fouling effect on the sensor's measurement. To summarize, Q statistic charts allow to identify faults and anomalies of all the sensors involved in the network, both input and output variables, thanks to the specific structure of the model, where a neural network is built to predict every variable and the corresponding residuals equally contribute to the chart error. Therefore, it is easier to individuate which sensors are erroneous by looking at the contribution of the different residuals in the Q statistics. Conversely, Shewart charts are

easier to implement because they require only one predictive model and are preferable when analyzing slow and long-term trends, thanks to the preservation of the error sign. However, the monitoring method is not as robust because it cannot indicate which sensor variables are affected by the fault, but it can only generate an alarm.

Chapter 5

Conclusions and Future Directions

Real-time measurements of water quality variables are fundamental for modern water treatment and reuse applications. With the progress of more advanced and complex technologies has increased the necessity to closely monitor the water composition before, during and after the different processes. To improve at once the quality of water bodies and minimize the treatment energy and chemicals consumption, different control strategies have been developed, which rely directly on the signals of multiple online instrumentation. However, the implementation of new strategies in large scale can be hindered by the lack of reliability of the sensors required, with many water professionals not feeling sufficiently confident to entirely depend on them (Harremoës et al., 1993). Measurements inaccuracy and erroneous behavior are typical for any type of on-line sensor used in the WRRFs due to severe environmental conditions, anomalies in the electrical system, inadequate maintenance or other external factors. The wastewater matrix composition is often the major detrimental factor for the correct performance of instrumentation and depending on the technology behind the sensor and/or the type of water quality measured, different type of faults can occur: interference of other ionic species in the direct measurement of the sensor, typical issue of Ion Selective Technology; air bubbles and solids disturbance of light scattering for optical and

fluorescence-based sensors; grease and biofouling coating of the sensing surface, creating a fictitious environment, not representative of the bulk matrix. While the general issues concerning field application of online sensors are commonly known in practice by operators and wastewater technicians, scientific research has been rarely involved in the thorough investigation of the interaction between the complex wastewater matrix and sensors' technology. In this dissertation, an effort is made to present a framework by which online sensors, with specific detail on ammonium Ion Selective Electrode sensors, can be reliably used for both monitoring and control purposes in treatment processes of water resource recovery facilities, WRRFs. The main focus of this dissertation is to analyze the interactions between wastewater and sensor's technology, in order to: (1) identify factors that can influence and interfere with the sensors performance in field applications and the operating conditions ranges that are the most critical to the technology; subsequently (2) develop a model structure based on machine learning to improve the reliability of the sensor in the specific conditions and settings that are most critical.

In general, the methodologies and approaches utilized in this dissertation resulted in significant increase in reliability and accuracy of ammonium sensors. Coupling the prediction model with the appropriate fault detection monitoring chart allowed to promptly detect diverse faults that commonly occur with ammonium sensors operations. The methodology developed can find significant use in diverse applications. The neural network model predictions can be used in parallel with the hardware sensors as a diagnosis tool to recognize faster when a sensor faults occurs, and to distinguish between fault in the sensor's reading from a fault in the actual process operations. Also, the predictions of the model can then guarantee dataset continuity during outages of the sensor apparatus. This will be especially significant for less reliable water quality sensorial technologies such as for ion-selective ammonium sensors applied in advanced aeration control systems. Therefore, control systems can rely as a backup on the predictive ability of the soft-sensing network, thus improving the overall treatment efficiency, and ultimately minimizing the undesirable upsets in the

treatment performance. Finally, the model can be used to determine on real-time when any sensor requires maintenance, monetizing the difference in adopting an adaptive against a fixed maintenance schedule. Figure 5.1 shows a schematic representation of the different applications of the neural network model for process monitoring and control. Finally, the soft-sensor is not meant to be used as a replacement of any hardware sensor since it requires to be recalibrated often, but is a tool to improve the reliability of hardware sensors.

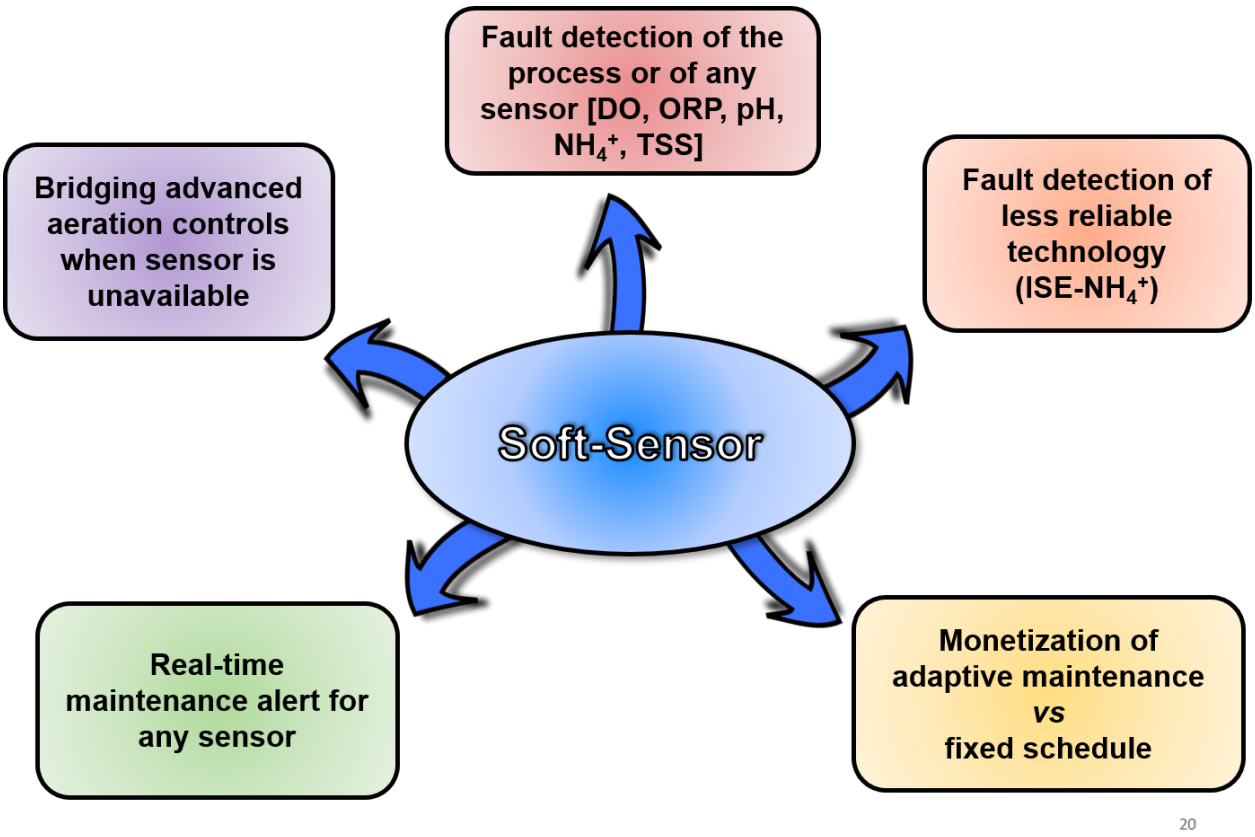

Figure 5.1: Scheme of the possible applications of the neural network model.

There are multiple directions for future investigation in order to directly test the framework proposed:

- The fault detection mechanism could be implemented real-time in an ammonium-based aeration control system, ABAC, in order to quantify the acquired improvement of the control system thanks to the increased accuracy of the sensors involved. In detail, the

application of the monitoring charts to detect an anomaly could be analyzed using a simulation environment. Figure 5.2.a shows the scheme of a PID control loop typically used for ABAC control systems, while Figure 5.2.b shows the integration of the fault detection mechanism in the PID control loop. First, the biological process of the treatment plant considered should be calibrated and validated, utilizing real, high-frequency data from the plant. Then, the ABAC control loop would be implemented in the simulation platform, studying the process performance. Using the diverse sensors' faults presented in this dissertation, a comparison could be analyzed between the consequences of an ammonium sensor's fault on the conventional control system and on the control with the fault detection integration.

- The soft-sensor could be implemented not only passively, to detect sensors' faults but also actively to determine the correct maintenance schedule of a sensor, by monitoring the residual between model prediction and sensor's signal. Future studies should analyze the possible advantages, both economically and in terms of process stability, on employing adaptive/active maintenance schedules, compared to the fixed schedules typically applied.

- Eventually, the soft-sensor model could be directly implemented in large scale plants and integrated to the existing control systems.

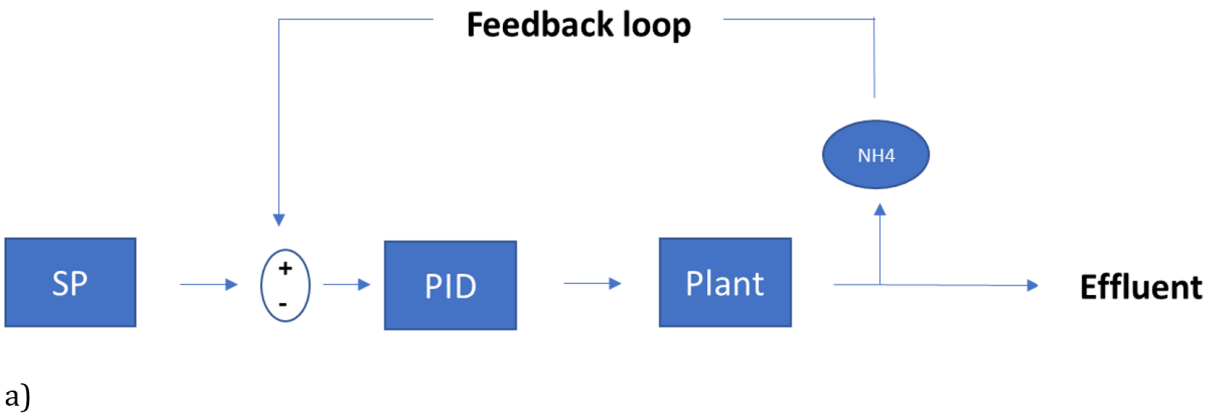

a)

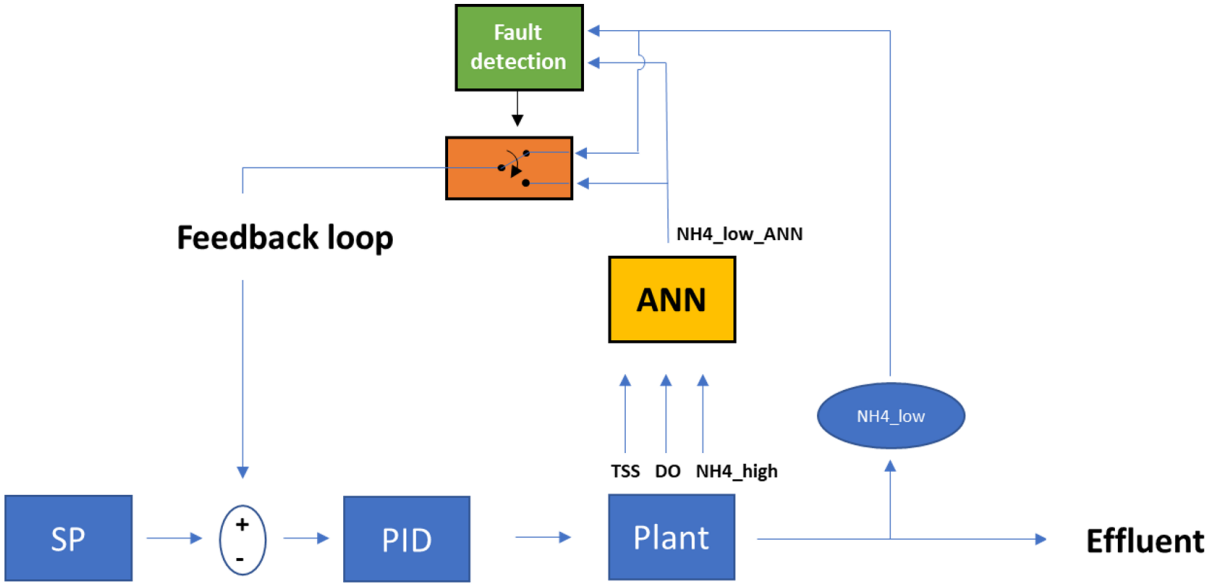

b)

Figure 5.2: a) Control loop scheme of Ammonium-Based Aeration Control. b) ABAC control scheme with fault detection mechanism integration.

Bibliography

Adu-Manu, K. S., Tapparello, C., Heinzelman, W., Katsriku, F. A., Abdulai, J-D. (2017) Water quality monitoring using wireless sensor networks: current trends and future research directions, ACM Transaction on Sensor Networks, 13, 1-41.

Aghaeinejad-Meybodi, A., Ebadi, A., Shafiei, S., Khataee, A. R., Rostampour, M. (2015). Modeling and optimization of antidepressant drug fluoxetine removal in aqueous media by ozone/H2O2 process: comparison of central composite design and artificial neural network approaches. J Taiwan Inst Chem Eng, 48(0), 40–48.

Aguado, D. and Rosen, C. 2008. Multivariate statistical monitoring of continuous wastewater treatment plants. Engineering Applications of Artificial Intelligence, 21, 1080–1091.

Alferes, J., Tik, S., Copp, J., Vanrolleghem, P.A. (2013) Advanced Monitoring of Water Systems Using In Situ Measurement Stations: Data Validation and Fault Detection. Water Sci. Technol. 68 (5), 1022-1030.

Al-halbouni, D., Traber, J., Lyko, S., Wintgens, T., Melin, T., Tacke, D., Hollender, J. (2008). Correlation of EPS content in activated sludge at different sludge retention times with membrane fouling phenomena, 42, 1475–1488.

Åmand, L., Olsson, G., Carlsson, B. (2013) Aeration control – a review, Water Science Technology, 67(11), 2374-2398.

Amy, G. (2008). Fundamental understanding of organic matter fouling of membranes. Desalination, 231(1–3), 44–51.

An, Y., Wang, Z., Wu, Z., Yang, D., Zhou, Q. (2009). Characterization of membrane foulants in an anaerobic non-woven fabric membrane bioreactor for municipal wastewater treatment, 155, 709–715.

Anderson, E. L. and Buhlmann, P. (2016) Electrochemical Impedance Spectroscopy of Ion-Selective Membranes: Artifacts in Two-, Three-, and Four-Electrode Measurements, Anal. Chem., 88, 9738-9745.

APHA (1998). Standard Methods for the Examination of Water and Wastewater, 20th ed. American Public Health Association, Washington, DC.

APHA. 2005. Standard methods for the examination of water and wastewater, 21st edn. American Public Health Association, Washington, DC.

Armstrong, R. D., Covington, A. K., Evans, G. P. (1983) Mechanistic studies of the valinomycin-based potassium-selective electrode using AC impedance methods, Electroanal. Chem., 159, 33-40.

Aslam, M., Charfi, A., Lesage, G.,Heran, M., Kim, J. (2017) Membrane bioreactors for wastewater treatment: A review of mechanical cleaning by scouring agents to control membrane fouling, Chemical Engineering Journal, 307, 897-913.

Baggiani, F. Marsili-Libelli, S. (2009) Real-time fault detection and isolation in biological wastewater treatment plants. Water Science and Technology 60 (11), 2949–2961.

Barron L, Havel J, Purcell M, Szpak M, Kelleher B, et al. (2009) Predicting sorption of pharmaceuticals and personal care products onto soil and digested sludge using artificial neural networks. Analyst 134: 663–670.

Bilad, M.R., Declerck, P., Piasecka, A., Vanysacker, L., Yan, X.,Vankelecom, I.F.J., 2011b. Treatment of molasses wastewaterin a membrane bioreactor: influence of membrane pore size. Separation and Purification Technology 78 (2), 105e112.

Bonastre, A., Ors, R., Capella, J. V., Fabra, M. J. Peris, M. 2005 In-line chemical analysis of wastewater: present and future trends. TrAC Trends Anal. Chem. 24(2), 128–137.

Bongards, M. (2001) Improving the efficiency of a wastewater treatment plant by fuzzy control and neural networks, Water Science and Technology, vol.43, no.11, pp.189-196.

Bouhabila, E., Aim, R. B. and Buisson, H. (2001). Fouling characterization in membrane bioreactors. Separation and Purification Technology. 22-23, 123-132.

Bourgeois, W., Burgess, J. E., Stuetz, R. M. (2001). On-line monitoring of wastewater quality: A review. Journal of Chemical Technology and Biotechnology, 76(4), 337–348.

Bourgeois, W., Gardey, G., Servieres, M., Stuetz, R. M. (2003). A chemical sensor array based system for protecting wastewater treatment plants. Sensors and Actuators, B: Chemical, 91(1–3), 109–116.

Bos, M., Bos, A., van der Linden, E. (1993) Data processing by Neural Networks in quantitative chemical analysis, Analyst, 118, 323-328.

Buck, R.P. and Lindner, E. (1994). "Recommendations for nomenclature of ion-selective electrodes" (PDF). Pure Appl. Chem. 66 (12): 2527–2536.

Cammann, K., Schroeder, A. 1979. Working with ion-selective-electrodes. ISBN 0387-09320-6. Springer Verlag, New York, USA.

Campisano, A., J. Cabot Ple, D. Muschalla, M. Pleau, and P. A. Vanrolleghem (2013). Potential and limitations of modern equipment for real time control of urban wastewater systems, Urban Water Journal, 10(5), 300-311.

Cao, C., Jiang, J., Sun, H., Huang, Y., Tao, F., Lian, B. (2016). Carbonate Mineral Formation under the Influence of Actinobacteria: Morphology and Polymorphism, 7(March), 1–11.

Caravelli, A. H., Contreras, E. M., Zaritzky, N. E. (2010). Phosphorous removal in batch systems using ferric chloride in the presence of activated sludges. Journal of Hazardous Materials, 177(1–3), 199–208.

Cecconi, F., Reifsnyder, S., Ito. Y., Jimenez, M., Sobhani, R., Rosso, D. (2019) ISE-ammonium sensors in WRRFs: field assessment of their influencing factors. Environmental Science: Water Research Technology, 5(4), 737-746.

Cecconi, F., Reifsnyder, S., Sobhani, R., Cisquella-Serra, A., Madou, M.J., Rosso, D. (2020) Functional behavior and microscopic analysis of ammonium sensors subject to fouling in activated sludge processes, Environmental Science: Water Research Technology, DOI: 10.1039/D0EW00359J.

Chang, I-S., Le Clech, P., Jefferson, B. and Judd, S. (2002). Membrane fouling in membrane bioreactors in wastewater treatment. Journal of Environmental Engineering. 128(11), 1018-1029.

Chen, J. C., Chang, N. B., Shieh, W. K. (2003). Assessing wastewater reclamation potential by neural network model, Eng Appl Artif Intell, 16, 149–157.

Cheng, C., Chiu, M-S, (2005) Nonlinear process monitoring using JTIL-PCA, Chemometrics and intelligent laboratory systems, 76, 1-13.

Choi D. J., Park H., (2001) A hybrid artificial neural network as a software sensor for optimal control of a wastewater treatment process. Water Res, 35, 3959–3967.

Choi, J.Y., Choi, C-H. (1992) Sensitivity analysis of multilayer perceptron with differentiable activation functions, IEEE Transactions on Neural Networks, 3, 101-107.

Cote, M., B. P. A. Grandjean, P. Lessard, and J. Thibault, (1995) Dynamic modelling of the activated sludge process: Improving prediction using neural networks, Water Res., 29, 995-1004.

De Canete, J. F.; del Saz-Orozco, P.; Baratti, R.; Mulas, M.; Ruano, A.; Garcia-Cerezo, (2016) A. Soft-sensing estimation of plant effluent concentrations in a biological wastewater treatment plant using an optimal neural network. Expert Systems with Applications 2016, 63, 8 19.

De Menezes, F.C., Fontes, R.M., Oliveira-Esquerre, K.P., Kalid, R. (2018), Application of uncertainty analysis of artificial neural networks for predicting coagulant and alkalizer dosages in a wastewater treatment process, Brazilian Journal of Chemical Engineering, 35(4), 1369-1381.

Despagne, F.; Massart, D. L. (1998) Neural Networks in multivariate calibration, Chemom. Intell. Lab. Syst, 40, 145- 163.

Devisscher, M., Bogaert, H., Bixio, D., Van de Velde, J. and Thoeye, C. (2002). Feasibility of automatic chemicals dosage control a full-scale evaluation. Wat. Sci. Tech. 45(4–5), 445–452.

Dong, D., McAvoy, T.J. (1996), Nonlinear principal component analysis-based on principal curves and neural networks, Computers and Chemical Engineering, 20, 65– 78.

Durrenmatt, D., Gujer, W. (2012). Data-driven modeling approaches to support wastewater treatment plant operation. Environmental Modelling Software, 30, 47–56.

Ekman, M., Bjorlenius, B., Andersson, M., 2006. Control of the aeration volume in an activated sludge process using supervisory control strategies. Water Res. 40, 1668-1676.

Fettweis, M., Riethmuller, R., Verney, R., Becker, M., Backers, J. et al., (2019) Uncertainties associated with in-situ high-frequency long-term observations of suspended particulate matter concentration using optical and acoustic sensors, Progress in Oceanography, 178, 102162.

Frankær, C. G., Hussain, K. J. , Rosenberg, M., Jensen, A., Laursen, B. W., Sørensen, T. J. (2019) Investigating the time response of an optical pH sensor based on a polysiloxane-polyethylene glycol composite material impregnated with pH-responsive triangulenium dye, ACS Sens., 4, 8381-8389.

Fu, C. and Poch, M. (1996). System identification and real-time pattern recognition by neural networks for an activated sludge process. Environ. Internat., 21(1), 57–69.

Fuente, M.J., Garcia-Alvarez, D., Sainz-Palmero, G.I., Vega, P. (2012) Fault detection in a wastewater treatment plant based on neural networks and PCA, in Proc. 20th Mediterranean Conf. Control Autom., Jul. 2012, pp. 758–763.

Garcia-Alvarez, D., Fuente, M.J., Vega, P., Sainza, G. (2007) Fault detection and diagnosis using multivariate statistical techniques in a wastewater treatment plant, IFAC Proceedings Volumes, 42(11), 952-957.

Gerrity, D., Pecson, B., Trussel, R.S., Trussel, R.R. (2013). Potable reuse treatment trains throughout the world. Journal of Water Supply: Research Technology. 62(6), 321-328.

Ghernaout, D., Aichouni, M., Alghamdi, A. (2018) Applying big data in water treatment industry: A new era of advance, Int. Journal of Advanced and Applied Sciences, 5(3), 89-97.

Gross, E. M, Kelly, R. S., Cannon, D. M. (2008). Analytical Electrochemistry: Potentiometry. Journal of the Analytical Sciences Digital Library.

Guo, X., Liu, L., Wang, W., Zhang, J., Wang, Y., Yu, S.-H. (2011) Controlled crystallization of hierarchical and porous calcium carbonate crystals using polypeptide type block copolymer as crystal growth modifier in a mixed solution. CrystEngComm, 13, 2054–2061.

Guo, W., Ngo, H-H. and Li, J. (2012). A mini-review on membrane fouling. Bioresource Technology. 122, 27-34.

Haimi, H., Mulas, M., Corona, F., Vahala, R. (2013). Data-derived soft-sensors for biological wastewater treatment plants: An overview. Environmental Modelling Software, 47, 88–107.

Hamed, M. M.; Khalafallah, M. G.; Hassanien, E. A. (2004) Prediction of wastewater treatment plant performance using artificial neural networks. Environ. Model. Software, 19, 919–928.

Harremoes, P., A. G. Capodaglio, B. G. Hellstrom, M. Henze, K. N. Jensen, A. Lynggaardensen, R. Otterpohl, and H. Soeberg (1993). Waste-water treatment plants under transient loading – performance, modeling and control. Water Science and Technology 27 (12), 71–115.

Hassani, A., Vafaei, F., Karaca, S., Khataee, A.R. (2014) Adsorption of a cationic dye from aqueous solution using Turkish lignite: kinetic, isotherm, thermodynamic studies and neural network modeling. J. Ind. Eng. Chem. 20(4), 2615–2624.

Hauser, Peter C. (2016). "Chapter 2. Determination of Alkali Ions in Biological and Environmental Samples". In Astrid, Sigel; Helmut, Sigel; Roland K.O., Sigel (eds.). The Alkali Metal Ions: Their Role in Life. Metal Ions in Life Sciences. 16. Springer. pp. 11–25.

Hering, J. G., Waite, T. D., Luthy, R. G., Drewes, J. E., Sedlack, D. L. (2013) A changing framework for urban water systems. Environ. Sci. Technol., 47 (19), 10721-10726.

Hochstrat. R., Wintgens, T., Kazner, C., Melin, T., Gebel, J. (2010) Options for water scarcity and drought management-the role of desalination. Desal. Water Treat., 18(1-3), 96-102.

Holenda, B., Domokos, E., Redey, A., Fazakas, J. (2008) Dissolved oxygen control of activated sludge wastewater treatment process using model predictive control, Computers Chemical Engineering, 32, 1270-1278.

Ingildsen, P. Olsson, G. 2002 Exploiting online in-situ ammonium, nitrate and phosphate sensors in full-scale wastewater plant operation. Water Sci. Technol. 46(4–5), 139 – 147.

Ingildsen, P. Wendelboe, H. 2003 Improved nutrient removal using in situ continuous on-line sensors with short response time. Water Sci. Technol. 48(1), 95–102.

ISO 15839 (2003). Water quality – On-line sensors/ Analysing equipment for water – Specifications and performance tests, ISO 15839, ISO, Geneva, Switzerland.

Jarusutthirak, C., Amy, G. L. (2002). Influence of wastewater secondary effluent on NF and UF membrane filtration. Desalination, 145, 247–255.

Jeppsson, U., Alex, J., Pons, M.N., Spanjers, H. and Vanrolleghem, P.A. (2002). Status and future trends of ICA in wastewater treatment – a European perspective. Wat. Sci. Tech., 45(4–5), 485–494.

Jia, F., Martin, E.B., Morris, A.J. (1998), Non-linear principal component analysis for process fault detection, Computers Chemical Engineering, 22, 851-854.

Jiang, S., Li, Y., Ladewig, B. P. (2018). A review of reverse osmosis membrane fouling and control strategies. Science of the Total Environment, 595(October 2017), 567–583.

Joss, A., Salzgeber, D., Eugster, J., Konig, R., Rottermann, K., Burger, S., Fabijan, P., Leumann, S., Mohn, J., Siegrist, H. (2009). Full-scale nitrogen removal from digester liquid with partial nitritation and anammox in one SBR. Environmental Science Technology, 43(14), 5301–5306.

Kadlec, P., Gabrys, B., Strandt, S., (2009) Data-driven soft sensors in the process industry.

Comput. Chem. Eng. 33, 795–814.

Kaelin, D., Rieger, L., Eugster, J., Rottermann, K., Banninger, C. Siegrist, H. (2008) Potential of in-situ sensors with ion-selective electrodes for aeration control at wastewater treatment plants. Water Science and Technology. 58 (3), 629–637.

Kazadi Mbamba, C., Lindblom, E., Flores-Alsina, X.,. Tait, S., Anderson, S., Saagi, R., Batstone, D. J., Gernaey, K. V., Jeppsson, U. (2019) Plant-wide model-based analysis of iron dosage strategies for chemical phosphorous removal in wastewater treatment systems, Water Research, 155, 12-25.

Kazor, K., Holloway, E.W., Cath, T.Y., Hering, A.S. (2016) Comparison of linear and nonlinear dimension reduction techniques for automated process monitoring of a decentralized wastewater treatment facility, Stoch Environ. Res. Risk Assess, 30, 1527-1544.

Kettunen, M., Zhang, P. Jamsa-Jounela, S. L. 2008 An embedded fault detection, isolation and accommodation predictive controller for an industrial benchmark process. Comput. Chem. Eng. 32, 2966.

Khataee AR, Mirzajani O. UV/peroxydisulfate oxidation of CI basic blue 3: modeling of key factors by artificial neural network. (2010a) Desalination;251: 64–9.

Kim, M.H., Al-Ghusain, I.A., Hao, O.J., Lim, B.S. (1994) Modeling of nitrate disappearance and sludge rising in a settling column system. Water Research. 28(9), 1861-1872.

Kim, J., Deng, Q., Benjamin, M. M. (2008). Simultaneous removal of phosphorus and foulants in a hybrid coagulation/membrane filtration system. Water Research, 42(8–9), 2017–2024.

Kramer, M.A. (1992) Autoassociative neural networks, Computers and Chemical Engi-

neering, 16(4), 313-328.

Le-Clech, P., Chen, V., Fane, T. A. G. (2006). Fouling in membrane bioreactors used in wastewater treatment. Journal of Membrane Science, 284(1–2), 17–53.

Lee, J-M., Yoo, C, Choi, S.W., Vanrollenghem, P.A., Lee, I-B, (2004) Nonlinear process monitoring using kernel principal component analysis, Chemical Engineering Science, 59, 223-234.

Leverenz, H. L., Tchobanoglous, G., Asano, T. (2011) Direct potable reuse: a future imperative. J. Water Reuse Desalin., 1(1), 2.

Lewis, S. B., Buck, R. P. (1976) Optimizing permselectivity for neutral carrier membrane electrodes, Analytical Letters, 9(5), 439-449.

Lewis, W. K., Whitman, W. G. (1924) Principles of gas absorption. Ind. Eng. Chem, 16, 1215-1220.

Li, K., Zhang, Y., Xu, L., Zeng, F., Hou, D., Wang, J. (2017). Optimizing stretching conditions in fabrication of PTFE hollow fiber membrane for performance improvement in membrane distillation. Journal of Membrane Science, 550(December), 126–135.

Li, X., Liu, Y., Liu, F., Liu, A., Feng, Q. (2017) Comparison of ferric chloride and aluminum sulfate on phosphorous removal and membrane fouling in MBR treating BAF effluent of municipal wastewater, Journal of Water Reuse and Desalination, 7(4), 442-448.

Lim, A. L., Bai, R. (2003). Membrane fouling and cleaning in microfiltration of activated sludge wastewater. Journal of Membrane Science, 216(1–2), 279–290.

Liu, G., Gao, C., Li, X., Guo, C., Chen, Y., Lv, J. (2015). Preparation and properties of porous polytetrafluoroethylene hollow fiber membrane through mechanical operations, 42696, 1–10.

Liu, J., Jang, S., Wong, D. S. (2016). Developing a Soft Sensor with Online Variable Selection for Industrial Multi-mode Processes. 26th European Symposium on Computer Aided Process Engineering (Vol. 38). Elsevier Masson SAS.

Longo, S., d'Antoni, B.M., Bongards, M., Chaparro, A., Cronrath, A., Fatone, F., Lema, J.M., Mauricio-Iglesias, M., Soares, A., Hospido, A., (2016). Monitoring and diagnosis of energy consumption in wastewater treatment plants. A state of the art and proposals for improvement. Appl. Energy, 179, 1251-1268.

Lynggaard-Jensen, A. (1999). Trends in monitoring of waste water systems. Talanta 50(4), 707–716.

Mahdavi, M., Amin, M. M., Hajizadeh, Y., Farrokhzadeh, H., Ebrahimi, A. (2017) Removal of different NOM fractions from spent filter backwash water by polyaluminum ferric chloride and ferric chloride, Arab. J. Sci. Eng., 42, 1497-1504.

Meng, F.G., Zhang, H.M., Yang, F.L., Liu, L.F. (2007). Characterization of cake layer in submerged membrane bioreactor, Environ. Sci. Technol. 41, 4065-4070.

Metcalf Eddy, Inc. Water Reuse: Issues, Technologies, and Applications (by Takashi Asano et al. – 1st ed.), ISBN 0071459278,

McGraw-Hill, New York, NY. 2007.

Mikhelson, K. N. (2006) AC-Impedance studies of ion transfer across ionophore-based ion-selective membranes. Chem. Anal., 51, 853-867.

Mjalli, F. S., Al-Asheh, S., Alfadala, H. E. (2007) Use of Artificial Neural Network Black-Box Modeling for the Prediction of Wastewater Treatment Plants Performance, J. Environ. Manage, 83, 329.

Montgomery, D.C. (1996). Introduction to Statistical Quality Control. 3rd edition, Wiley, New York, USA.

Morel, F.M.M., Hering, J.G. (1993). Principles and Applications of Aquatic Chemistry. Wiley, New York, USA.

Morf, W. E., Lindner, E, Simon, W. (1975) Theoretical treatment of the dynamic response of ion-selective membrane electrodes, Anal. Chem., 47(9), 1596-1601.

Ohmura, K., Thurlimann, C.M., Kipf, M., Carbajal, J.P., Villez, K., (2018). Characterizing long-term wear and tear of ion-selective pH sensors. Water Science Technology. 80(3), 541-550.

Olsson, G., and Newell, B. (1999). Wastewater Treatment System: Modelling, Diagnosis and Control. IWA Publishing: London, UK.

Olsson, G., Newell, B., Rosen, C., Ingildsen, P. (2003). Application of information techology to decision support in treatment plant operation, Water Science Technology, 47(12), 35-42.

Olsson, G. 2006 Instrumentation, control and automation in the water industry—state-of-the-art and new challenges. Water Sci. Technol. 53(4–5), 1.

Olsson, G. Jeppsson, U. 2006 Plant-wide control: dream, necessity or reality? Water Sci. Technol. 53(3), 121.

Olsson, G., 2015. Water and Energy: Threats and Opportunities, second ed. Water Intell.

Okun, D. A., (1996) Water reclamation and nonpotable reuse: an option for meeting urban water supply needs. Desalination, 106 (1-3), 205-212.

Oneby, M.A., Bromley, C.O., Borchardt, J.H., Harrison, D.S. (2010). Ozone treatment of secondary effluent at U.S. municipal wastewater treatment plants. Ozone: Science Engineering. 32, 43-55.

Papias, S., Masson, M., Pelletant, S., Prost-Boucle, S., Boutin, C. (2018) In situ continuous monitoring of nitrogen with ion-selective electrodes in a constructed wetland

receiving treated wastewater: an operating protocol to obtain reliable data, Water Science Technology, 77(6), 1706-1713.

Park, C., Muller, C. D., Abu-Orf, M. M., Novak, J. T. (2006). The Effect of Wastewater Cations on Activated Sludge Characteristics: Effects of Aluminum and Iron in Floc. Water Environment Research, 78(1), 31–40.

Peng, Y. Z., Gao, J. F., Wang, S. Y., Sui, M. H. (2002). Use pH and ORP as fuzzy control parameters of denitrification in SBR process. Water Science Technology, 46(4-5), 131–137.

Racar, M., Dolar, D., Spehar, A., Kras, A., Kosutic, K. (2017) Optimization of coagulation with ferric chloride as a pretreatment for fouling reduction using nanofiltration of rendering plant secondary effluent, Chemosphere, 181, 485-491.

Radu, A., Anastasova-Ivanova, S., Paczosa-Bator, B., Danielewski, M., Bobacka, J., Lewenstam, A., Diamond, D. (2010) Diagnostic of functionality of polymer membrane-based ion selective electrodes by impedance spectroscopy. Anal. Methods, 2, 1490-1498.

Reardon, D.J., 1995. Turning down the power. Civ. Eng. New York 65, 54. Rebosura, M. Jr., Salehin, S., Pikaar, I., Sun, X., Keller, J., Sharma, K., Yuan, Z. (2018) A comprehensive laboratory assessment of the effects of sewer-dosed iron salts on wastewater treatment processes, Water Research, 146, 109-117.

Regan, F., Lawlor, A., Flynn, B. O., Torres, J., Martinez-Catala, R., O'Mathuna, C., Wallace, J. (2009). A demonstration of wireless sensing for long term monitoring of water quality. Proceedings – Conference on Local Computer Networks, LCN, (October), 819–825.

Regmi, P., Miller, M.W., Holgate, B., Bunce, R., Park, H., Chandran, K., Wett, B., Murthy, S., Bott, C.B. (2014). Control of aeration, aerobic SRT and COD input for

mainstream nitritation/denitrification. Water Research, 57, 162-171.

Rieger, L., Siegrist, H., Winkler, S., Saracevic, E., Votava, R. Nadler, J. (2002) In-situ measurement of ammonium and nitrate in the activated sludge process. Water Science and Technology. 45(4–5), 93 – 100.

Rieger, L., Alex, J., Winkler, S., Boehler, M., Thomann, M., Siegrist, H. (2003) Progress in sensor technology—progress in process control? Part I: Sensor property investigation and classification. Water Sci. Technol. 47 (2), 103–112.

Rieger, L., Thomann, M., Joss, A., Gujer, W., Siegrist, H. (2004) Computer-aided monitoring and operation of continuous measuring devices, Water Science Technology, 50(11), 31-39.

Rieger, L., Thomann, M., Gujer, W. Siegrist, H. (2005) Quantifying the uncertainty of on-line sensors at WWTPs during field operation. Water Research. 39 (20), 5162–5174.

Rieger, L.; Takács, I.; Siegrist, H. (2012a) Improving Nutrient Removal While Reducing Energy Use at Three Swiss WWTPs Using Advanced Control. Water Environ. Res., 84 (2), 171–189.

Rieger, L., Jones, R.M., Dold, P.L., Bott, C.B. (2014) Ammonia-based feedforward and feedback aeration control in activated sludge processes. Water Environ. Res. 86 (1), 63e73.

Rosen, C., Rottorp, J., Jeppsson, U. (2003) Multivariate on-line monitoring: challenges and solutions for modern wastewater treatment operation, Water Science technology, 47(2), 171-179.

Rosen, C., Rieger, L., Jeppsson, U. Vanrolleghem, P. A. (2008) Adding realism to simulated sensors and actuators. Water Sci. Technol. 57(3), 337.

Rosso, D., Larson, L.E., Stenstrom, M.K., (2008). Aeration of large-scale municipal

wastewater treatment plants: state of the art. Water Sci. Technol. 57, 973-978.

Rosso, D. Aeration, Mixing, and Energy: Bubbles and Sparks, ed. D. Rosso, IWA Publishing, Irvine, California, 2018, p. 300.

Rosso, D. and Al-Omari, A. (2019) Carbon Capture and Management Strategies for Energy Harvest from Wastewater, Project U3R14/4879 Report, The Water Research Foundation, Alexandria, VA.

Rygaard, M., Binning, P. J., Albrechtsen, H. J. (2011) Increasing urban water self-sufficiency: New era, new challenges. J. Environ. Manage., 92 (1), 185-194.

Samuelsson, O., Zambrano, J., Bjork, A., Carlsson B. (2019) Automated active fault detection in fouled dissolved oxygen sensors, Water Research, 166, 115029.

Santos, J.C.B., Le Pera, E., Souza Junior, V.S., Oliveira, C.S., Juilleret, J., Correa, M.M., Azevedo, A.C. (2018). Porosity and genesis of clay in gneiss saprolites: the relevance of saprolithology to whole regolith pedology. Geoderma 319, 1-13.

Sawyer C. N. and Bradney L. (1945) Rising of activated sludge in final settling tanks. Swg. Wks J. 17, 1191-1209.

Schneider. M.Y., Carbajal J.P., Furrer, V., Sterkele, B., Maurer, M., Villez, K. (2019) Beyond signal quality: The value of unmaintained pH, dissolved oxygen, and oxidation-reduction potential sensors for remote performance monitoring of on-site sequencing batch reactors, Water Research, 161, 639-651.

Schraa, O., Tole, B., Copp, J.B. (2006) Fault detection for control of wastewater treatment plants, Water Science Technology, 53(4), 375-382.

Sedlak, R.I. (1991). Phosphorous and Nitrogen Removal From Municipal Wastewater: Principles and Practice. Lewis Publishers, Florida, USA.

Shrestha, D.L., Kayastha, N., Solomatine, D.P. (2009), A novel approach to parameter

uncertainty analysis of hydrological models using neural networks, Hydrol. Earth Syst. Sci, 13, 1235-1248.

Shuck, W. W., Presseley, T. A., Dolloff, F. B. (1973) Automatic control system for the safe and economical removal of NH3 by breakpoint chlorination, U. S. Patent 3,760,829.

Srivastav, R.K., Sudheer, K.P., Chaubey, I. (2007) A simplified approach to quantifying predictive and parametric uncertainty in artificial neural networks hydrologic models, Water Resources Research, 43,W10407.

Stumm, W., Morgan, J.J. (1996). Aquatic Chemistry: Chemical Equilibria and Rates in Natural Waters. Third ed. Wiley, New York, USA.

Suzuki, K., Siswanta, D,. Otsuka, T., Amano, T., Ikeda, T., Hisamoto, H., Yoshihara, R,. Ohba, S. (2000) Design and synthesis of a more highly selective ammonium ionophore than nonactin and its application as an ion-sensing component for an ion-selective electrode. Anal. Chem., 72, 2200-2205.

Tao, E.P., Shen, W.H., Liu, T.L., Chen, X.Q. (2013) Fault diagnosis based on PCA for sensors of laboratorial wastewater treatment process. Chemometrics and Intelligent Laboratory Systems, 128, 49-55.

Thomann, M., Rieger, L., Frommhold, S., Siegrist, H. Gujer, W. 2002 An efficient monitoring concept with control charts for on-line sensors. Water Science and Technology. 46(4–5), 107–116.

Thomann, M. (2008) Quality Evaluation Methods for Wastewater Treatment Plant Data. Water Sci. Technol., 57 (10), 1601–1609.

Thürlimann, C. M., Dürrenmatt, D. J., Villez, K. (2018). Control Engineering Practice Soft-sensing with qualitative trend analysis for wastewater treatment plant control. Control Engineering Practice, 70(March 2017), 121–133.

Uprety, K., Kennedy, A., Balzer, W., Baumler, R., Duke, R., Bott, C., 2016. Implementation of ammonia-based aeration control (ABAC) at full-scale wastewater treatment plants. Proc. Water Environ. Fed 2015, 1-10.

Villez, K., Ruiz, M., Sin, G., Colomer, J., Rosen, C., Vanrollenghem, P.A. (2008) Combining multiway principal component analysis (MPCA) and clustering for efficient data mining of historical data sets of SBR processes, Water Science Technology, 57(10), 1659-1666.

Wade Miller, G. (2006) Integrated concepts in water reuse: Managing global water needs. Desalination, 187 (1-3), 65-75.

Waite, T. D. (2002). Challenges and opportunities in the use of iron in water and wastewater treatment. Reviews in Environmental Science and Biotechnology, 1(1), 9–15.

Walczak, B. (1996). Neural Networks with robust backpropagation learning algorithm, Anal. Chim. Acta 322, 21.

Waltrip, G.D., Snyder, E.G. (1985). Elimination of odor at six major wastewater treatment plants. J. Wat. Pollut. Control Fed. 57, 1027-1032.

Wan, J., Gu, J., Zhao, Q., Liu, Y. (2016) COD capture: a feasible option towards energy self-sufficient domestic wastewater treatment, Sci Rep, 6, 25054.

Wang, J.H.; Jiang, J.H.; Yu, R.Q. Robust back propagation algorithm as a chemometric tool to prevent the overfitting to outliers. Chemom. Intell. Lab. Syst. 1996, 34, 109-115.

Wang, X. M., Waite, T. D. (2010). Iron speciation and iron species transformation in activated sludge membrane bioreactors. Water Research, 44(11), 3511–3521.

Wang, Z., Wu, Z., Yin, X., Tian, L. (2008) Membrane fouling in a submerged membrane bioreactor (MBR) under sub-critical flux operation: Membrane foulant and gel layer

characterization. Journal of Membrane Science, 325, 238-244.

WEF, 2009. Energy Conservation in Water and Wastewater Treatment Facilities, WEF Manual of Practice. McGraw-Hill, Inc., New York, NY [WWW Document]. WEF Man. Pract.

Whelan, A., Regan, F. (2006). Antifouling strategies for marine and riverine sensors. Journal of Environmental Monitoring, 8(9), 880–886.

Winkler, S., Rieger, L., Saracevic, E., Pressi, A., Gruber, G (2004) Application of ion-selective sensors in water quality monitoring, Water Science Technology, 50(11), 105-114.

Wu, J., Le-Clech, P., Stuetz, R. M., Fane, A. G., Chen, V. (2008). Effects of relaxation and backwashing conditions on fouling in membrane bioreactor. Journal of Membrane Science, 324(1–2), 26–32.

Xiao, H., Huang, D., Pan, Y., Liu, Y., Song, K. (2017) Fault diagnosis and prognosis of wastewater processes with incomplete data by the auto-associative neural networks and ARMA model, Chemometrics and Intelligent Laboratory Systems, 161, 96-107.

Xu, L., Oja, E., Suen, C.Y. (1992) Modified Hebbian learning for curve and surface fitting, Neural Networks, 5(3), 441-457.

Xu, P., Bellona, C., Drewes, J. E. (2010). Fouling of nanofiltration and reverse osmosis membranes during municipal wastewater reclamation: Membrane autopsy results from pilot-scale investigations. Journal of Membrane Science, 353(1–2), 111–121.

Xue, C-H., Jia, S-T., Zhang, J-Z., Ma (2010) Large-area fabrication of superhydrophobic surfaces for practical applications: an overview. Scinece and Technology of Advanced Materials, 11, 033002.

Yang, T., Xiong, H., Liu, F., Yang, Q., Xu, B., Zhan, C., (2019) Effect of UV/TiO2

pretreatment on fouling alleviation and mechanisms of fouling development in a cross-flow filtration process using ceramic UF membrane, Chemical Engineering Journal, 358, 1583-1593.

Yim, H.S.; Kibbey, C.E.; Ma, S.C.; Kliza, D.M.; Liu, D.; Park, S.B.; Torre, C.E.; Meyerhoff, M.E. (1993). Polymer membrane-based ion-, gas-, and bio-selective potentiometric sensors. Biosens. Bioelectron, 8, 1–38.

Yoo, C.K., Vanrollenghem, P.A., Lee, I-B. (2003), Nonlinear modeling and adaptive monitoring with fuzzy and multivariate statistical methods in biological wastewater treatment plants, Journal of Biotechnology, 105, 135-163.

Yoo, C. K., Villez, K., Van Hullw, S. W.H., Vanrollenghem, P.A. (2008), Enhanced process monitoring for wastewater treatment systems. Environmetrics, 19, 602-617.

Yu, W., Graham, N. J. D., Fowler, G. D. (2016) Coagulation and oxidation for controlling ultrafiltration membrane fouling in drinking water treatment: Application of ozone at low dose in submerged membrane tank, Water Research, 95, 1-10.

Zanetti, L., Frison, N., Nota, E., Tomizioli, M., Bolzonella, D., Fatone, F. (2012). Progress in real-time control applied to biological nitrogen removal from wastewater. A short- review. Desalination, 286, 1–7.

Zeng, X., Yeung, D.S. (2001) Sensitivity Analysis of multilayer perceptron to input and weight perturbation, IEEE Transactions of Neural Networks, 12(6), 1358-1366.

Zhang, B., Sun, B., Jin, M., Gong, T., Gao, Z. (2008). Extraction and analysis of extracellular polymeric substances in membrane fouling in submerged MBR. Desalination 227 (1-3), 286-294.

Zhang, X., Shi, F., Niu, J., Jiang, Z., Wang (2008). Superhydrophobic surfaces: from structural control to functional application, Journal of Materials Chemistry, 18, 621-

633.

Zhang, Z., Bligh, M. W., Wang, Y., Leslie, G. L., Bustamante, H., Waite, T. D. (2015). Cleaning strategies for iron-fouled membranes from submerged membrane bioreactor treatment of wastewaters. Journal of Membrane Science, 475, 9–21.

Zhao, L., Yuan, D. (2011) Nonlinear robust PLS modeling of wastewater effluent quality indices, Journal of Software, 6(6), 1067-1074.

Zhu, J., Zurcher, J., Rao, M., Meng, M.Q-H. (1998) An on-line wastewater quality predication system based on a time-delay neural network, Engineering Applications of Artificial Intelligence, 11, 747-758.

Appendix A

Oxygen transfer investigations in an aerobic granular sludge reactor

A version of this appendix is published in Environmental Science: Water Research Technology, 2020,6, 679-690.

A.1 Abstract

The aerobic granular sludge process is an alternative to the conventional activated sludge process adopted in water resource recovery facilities. This study presents the first independent assessment of aerobic granular sludge technology in terms of oxygen transfer efficiency and nutrient removal performance. Using off-gas testing, a full-depth pilot reactor with granular biomass was compared to an identical reactor with floccular biomass. The granular process presented lower oxygen transfer efficiency than the floccular sludge (2.3 $\%/m$ vs. 3.2 $\%/m$, respectively). The granular sludge was also tested at different operating conditions in order to address potential retrofitting for existing aeration basins. With regard to oxygen trans-

fer efficiency, the experiments show a marginal improvement at lower MLSS ($\sim 0.2\%/m$) and at medium side-water-depth ($\sim 0.3\%/m$). Satisfactory effluent water quality levels, in terms of nitrogen and phosphorous removal, were obtained for the granular sludge except for decreased MLSS conditions during which the nitrification/denitrification process was highly penalized.

A.2 Introduction

Activated sludge (AS) treatment is the most common technology adopted in water resource recovery facilities (WRRFs) for biological nutrient removal (Metcal and Eddy, 2014; Barnard and Stensel, 2014). After increased urbanization and industrialization taxed sanitation efforts, AS significantly improved worldwide water sanitation partially due its robustness and reliability (Sheik et al, 2014). However, despite its widespread implementation, AS treatment presents various drawbacks, such as high energy-intensity and pumping requirements especially for the removal of nutrients (i.e., P and N), large physical footprint, high sludge production, and the associated settling problems (Bozkurt et al, 2016; Giesen et al, 2013; deBruin et al, 2004;). In recent years, aerobic granular sludge technology has been widely studied as a promising alternative that might overcome some of the limitations associated with conventional biological treatment (Liu and Tay, 2004; Weissbrodt et al, 2014; Majone et al, 1999; McSwain et al, 2004; Tay et al, 2001). Thanks to its dense microbial structure, aerobic granular sludge aggregates can be formed in sequencing batch reactors (SBRs) with short fill periods and various substrates (McSwain et al, 2004; Morgenroth et al, 1997; McSwain et al, 2005). As opposed to flocs, granules are denser thus resulting in lower sludge volumes, and they have significantly higher settling velocities such that secondary clarifiers are not required, thus reducing the technology's footprint and capital investment (Tay et al, 2001; Beunn et al, 1999; Beun et al, 2000; Etterer et al, 2001). The absence of secondary clarifiers

prevents the occurrence of common problems and instabilities such as bulking and the rising of the biomass (Martins et al, 2004). In addition, the combination of the absence of secondary clarifiers, with its operation as a sequential batch reactor (SBR), enables the operation of the AGS process at high biomass concentrations which increases its resilience to high organic and toxic shocks (deBruin et al, 2004; Adav et al, 2008; Beun et al, 2002). Furthermore, the AGS technology is characterized by simultaneous nitrification/denitrification which removes the need for the recirculation pumping system of conventional nitrogen treatment and the associated costs. Despite the various advantages of AGS technology in comparison to the AS, the technology adoption at full-scale remains hindered by questions regarding its complexity, its time-consuming start-up periods, and the instability caused by filamentous growth (Pijuan et al, 2011; Liu et al, 2006). The AGS is composed of millions of biomass cells, which are aggregated in dense, spherical structures. Because of the large variety of microorganisms and type of environments present in granules, the aerobic granular sludge technology is characterized by its capacity to simultaneously remove COD, nitrogen (through nitrification and denitrification), and phosphate in one reactor (Fig. A.1). Stressing operational conditions (shear, high biomass selectivity, etc.) trigger the bacterial production of specific types of extracellular polymeric substances (EPS), which in turn facilitates the formation of dense and robust granules. While EPS encapsulation provides advantages that enhance the settling properties of the system, this more compact configuration may not be so advantageous in terms of oxygen transfer efficiency, because gas diffusion through the compacted granule could be hindered and the bioadsorption of oxygen transfer inhibitors could be lower compared to activated sludge systems (Rosso and Stenstrom, 2006).

Also, granular encapsulation enables the system to operate at high biomass concentrations, which has been identified as a factor affecting oxygen transfer in floccular systems (Cornel and Krause, 2006; Cornel et al, 2003). A significant decrease in aeration efficiency for systems operating on real wastewater at MLSS concentrations higher than 6 g L^{-1} (like membrane bioreactor or aerobic digesters) was observed by Baquero et al. (2018).The evident structural

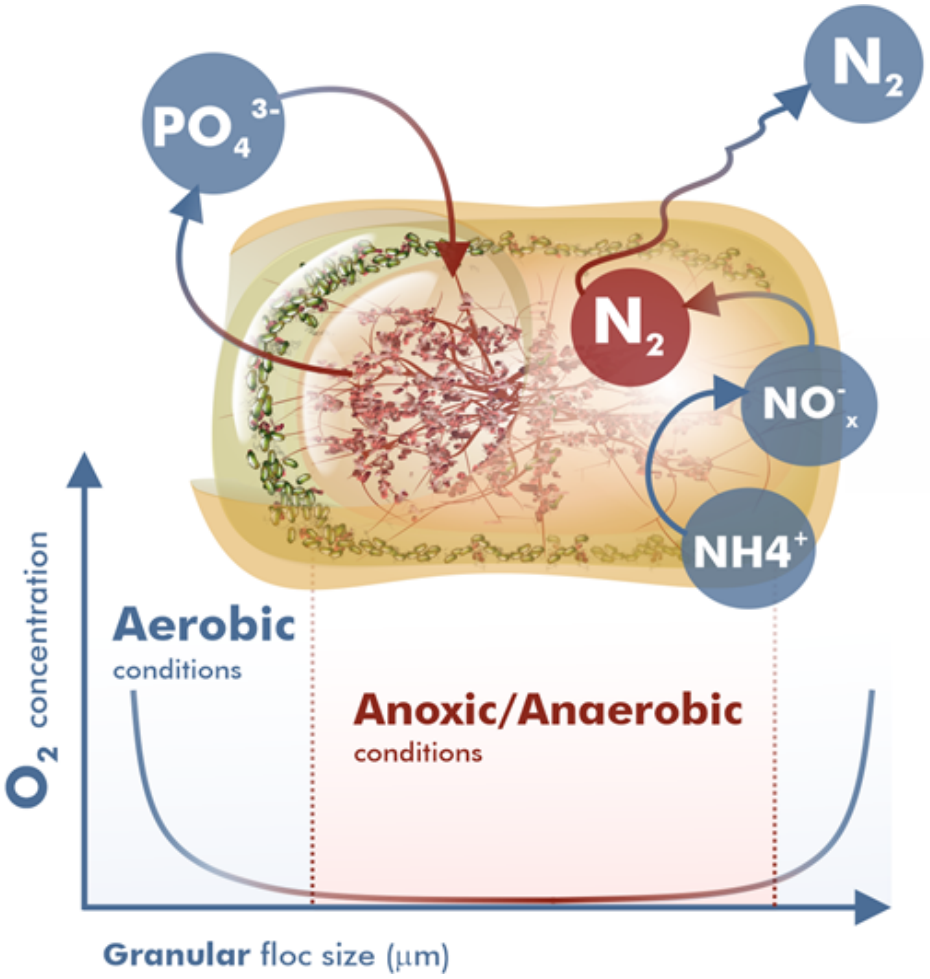

Figure A.1: Conceptual illustration of the structure of an aerobic granule.

differences between floccular and granular biomass prevent the extrapolation of the observed decrease in AGS systems, therefore leaving the correlation between oxygen transfer and solids concentration in AGS to be elucidated. The standard oxygen transfer efficiency in process conditions (αSOTE) for granular systems has yet to be evaluated independently. Oxygen transfer efficiency during biological oxidation is crucial for both granular and AS processes, as it is necessary for process design and ultimately governs operating costs (Metcal and Eddy, 2014; Rosso et al, 2005; Rosso and Shaw, 2015; WEF, 2009). Therefore, gaining insight into oxygen transfer efficiency is necessary for a thorough technical assessment of AGS processes. The goal of this study is to present for the first time the evaluation of the oxygen transfer efficiency of aerobic granular sludge technology. To provide a better understanding

of the fundamental mechanisms affecting aeration efficiency for both floccular and granular systems, two parallel full depth pilot-scale reactors were tested with the two types of biomass at different operating conditions and with different cleaning regimes. The performance of each configuration, in terms of COD and nutrient removal, was documented. Our findings are expected to help the full-scale design of AGS processes.

A.3 Materials and Methods

A.3.1 Pilot description

Two pilot reactors provided by Aqua-Aerobics were set up at the Fairfield-Suisun Sewer District (FSSD) in Fairfield, California (Fig. A.2a). Each column was 600mm in diameter and approximately 6.5m tall. The side water depth (SWD) was varied from approximately 5m to 6m, depending on the testing run. The reactors were independently operated as automated sequencing batch reactors and were equipped with heating jackets for temperature control. The reactors were filled with influent from the bottom, while the effluent was discharged from the top. A blower fed the 9in EPDM membrane disc diffusers (Environmental Dynamics International; Columbia, MO); there was one in each column, placed approximately 300mm (1ft) from the floor. A side-stream of primary effluent from the main treatment plant was collected in a buffer tank which was continuously mixed and maintained in constant volume in order to feed a controlled volume to the pilots. The influent quality data are reported in Table A.1, and it was based on the laboratory analysis of 24-hour composite samples and collected three times a week.

Online analyzers were placed in the pilot influent tank, in the reactors, and in the effluent boxes, as reported in Fig. A.2b. Ammonia (HACH Amtax) and phosphate (HACH Phosphax) analyzers were reagent-based and required sample filtration (HACH Filtrax), while pH (HACH pHD), NOx (HACH Nitratax eco), TSS (HACH Solitax), ORP (HACH pHD-S),

(a)

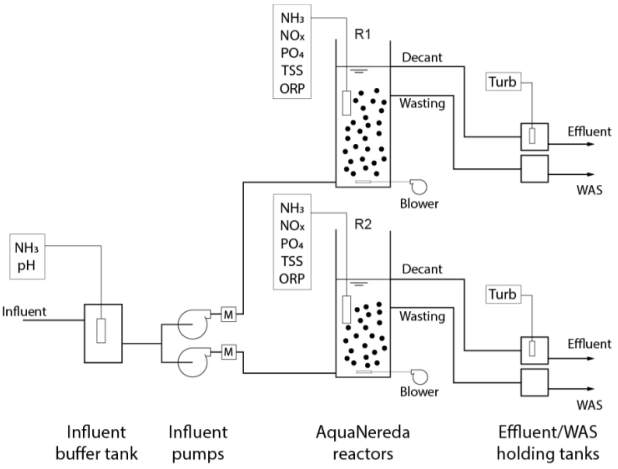

(b)

Figure A.2: Photograph of the two pilot-scale reactors (a). Process flow diagram with real-time monitoring analyzer locations (b).

and turbidity (HACH Solitax t-line) were in situ sensors placed directly in the monitoring locations.

Composite and grab samples were collected for laboratory analysis of COD (total and soluble), total nitrogen, total Kjeldahl nitrogen, nitrate, nitrite, ammonia, dissolved reactive phosphorus, total phosphorus, and alkalinity (HACH TNT test kits).

Table A.1: Water quality characteristics of the influent during the days of testing.

Time	**$CBOD_5$** [mg l^{-1}]	**tCOD** [mg l^{-1}]	**sCOD** [mg l^{-1}]	**TN** [mg-N l^{-1}]	**NOx** [mg-N l^{-1}]	**TKN** [mg-N l^{-1}]	**NH_4^+** [mg-N l^{-1}]	**TP** [mg-P l^{-1}]	**Alkalinity** [mg_{CaCO_3} l^{-1}]
Day 1	135	357	148	45.5	0.37	45.1	34.2	6.08	424
Day 2	-	337	155	39.4	0.42	39.0	29.8	5.44	462
Day 3	128	386	175	43.0	0.20	42.8	32.8	5.90	450
Average	132	360	159	42.6	0.33	42.3	32.3	5.81	445

A.3.2 Experiment Setup

Initially, both reactors started up with granular sludge seed, operated at the typical default conditions of AGS systems as instructed by the technology provider, at a SWD of approximately 6 m (19 ft). Once both reactors were acclimated after about one month, one of the

two reactors (R2) was modified, during the testing period, to lower the SWD to approximately 4.6 m (15 ft) based on typical SWD for activated sludge reactors in the United States. The first reactor (R1) was maintained as a reference, maintaining the design flow rate and default conditions throughout the pilot testing period with aerobic granular biomass at full side-water-depth (6 m) and high biomass concentration (10 g L^{-1} MLSS). The second parallel reactor (R2) was tested with different side-water-depths and biomass concentrations. Every operating condition was evaluated both at high (2 mg L^{-1}) and low (1 mg L^{-1}) DO setpoints, therefore the results are always reported in a set of four experiments: two from the default reactor, run at high and low DO setpoint, and two from the second reactor, run at both DO setpoints. After the experiments on the aerobic granular sludge were terminated, the reactor R2 was emptied and the conventional activated sludge from the treatment plant was tested to evaluate the oxygen transfer efficiency of the AS system for direct comparison with the AGS results. The AS system was operated at 5.5 m (18 ft) SWD, at high (3 g L^{-1}) and low (1.7 g L^{-1}) MLSS, and at both high (2 mg L^{-1}) and low (1 mg L^{-1}) DO setpoint. The comparison between AGS and AS in terms of oxygen transfer efficiency was conducted at different ranges of biomass content because the scope of the study was to compare the two technologies within their typical range of application in order to provide reference data for full-scale design of an AGS process. Therefore, the granular system was tested at higher biomass concentration (around 10 g L^{-1} MLSS), the floccular system was tested at a lower biomass content (around 3 g L^{-1}), and both were in line with the default conditions of the two technologies. Table A.2 reports the summary of all the experiments and the different operating conditions tested on both the activated sludge and the aerobic granular sludge.

The AquaNereda® process (Royal HaskoningDHV; Amersfoort, Netherlands) is a sequencing batch process and the reaction cycle was set at 4.5 hours for both reactors, per manufacturer specifications. The pilot testing after acclimation period lasted approximately 6 weeks. The off-gas testing was conducted in the third week of the testing period and different comparisons and operating conditions were tested: floccular and granular biomass; different

Table A.2: Summary of the different experiments and operating conditions tested for the floccular and granular biomass.

Experiment	Reactor	Biomass type	MLSS	SWD	DO setpoint
1	1	AGS	High	Full	High
2	1	AGS	High	Full	Low
3	2	AGS	High	Mid	High
4	2	AGS	High	Mid	Low
5	2	AGS	Low	Mid	High
6	2	AGS	Low	Mid	Low
7	2	AS	High	Full	High
8	2	AS	High	Full	Low
9	2	AS	Low	Full	High
10	2	AS	Low	Full	Low

MLSS:		Depth:		DO stp:	
High AGS	10.0 g L^{-1}	Full AGS	6.0 m (19 ft)	High	2.0 mg L^{-1}
Low AGS	6.0 g L^{-1}	Low AGS	4.6 m (16 ft)	Low	1.0 mg L^{-1}
High AS	3.0 g L^{-1}	Full AS	5.5 m (18 ft)		
Low AS	1.7 g L^{-1}				

DO set points; different biomass concentration; and different SWD.

A.3.3 Off-gas analysis

Oxygen transfer in process conditions was measured using the off-gas method following the ASCE testing protocol (ASCE, 1997) with an instrument as in Leu et al (2009). Off-gas analysis relies on a mass balance on the water column where the air flow is transiting, measuring both the oxygen partial pressure (pO2, Pa or atm) and the air flux (Redmon et al., 1983; Schuchardt et al., 2007). These two parameters, together with DO, salinity, total atmospheric pressure P, and temperature T, are used for the calculation of the standard

oxygen transfer efficiency at field conditions (αSOTE, %) and of the standard oxygen transfer rate at field conditions (αSOTR, kg_{O2} h^{-1}) and of their respective airflow-weighted averages. The equations to calculate OTE, OTR, αSOTE and αSOTR are reported below:

$$OTE = \frac{O_{2,in} - O_{2,out}}{O_{2,in}} \tag{A.1}$$

$$OTR = k_L a(C^*_\infty - DO) * V \tag{A.2}$$

$$\alpha SOTE = \frac{OTE * C^*_{\infty,20}}{(\Omega\beta C^*_\infty - DO)\theta^{T-20}} \tag{A.3}$$

$$\alpha SOTR = \frac{OTR * C^*_{\infty,20}}{(\Omega\beta C^*_\infty - DO)\theta^{T-20}} \tag{A.4}$$

where: $O_{2,in}$ and $O_{2,out}$ = mole ratios (-)

$k_L a$ = liquid-side volumetric oxygen transfer coefficient (t^{-1})

C^*_∞= oxygen saturation concentration at temperature T (mg L^{-1})

DO = dissolved oxygen concentration in the mixed liquor (mg L^{-1})

V = water volume (m^3)

$C^*_{\infty,20}$= oxygen saturation concentration at 20 °C (mg L^{-1})

Ω = barometric pressure correction factor (-)

β = salinity correction factor (-)

θ = temperature correction factor (= 1.024 for the ASCE Standard, 1984)

T = temperature, (°C)

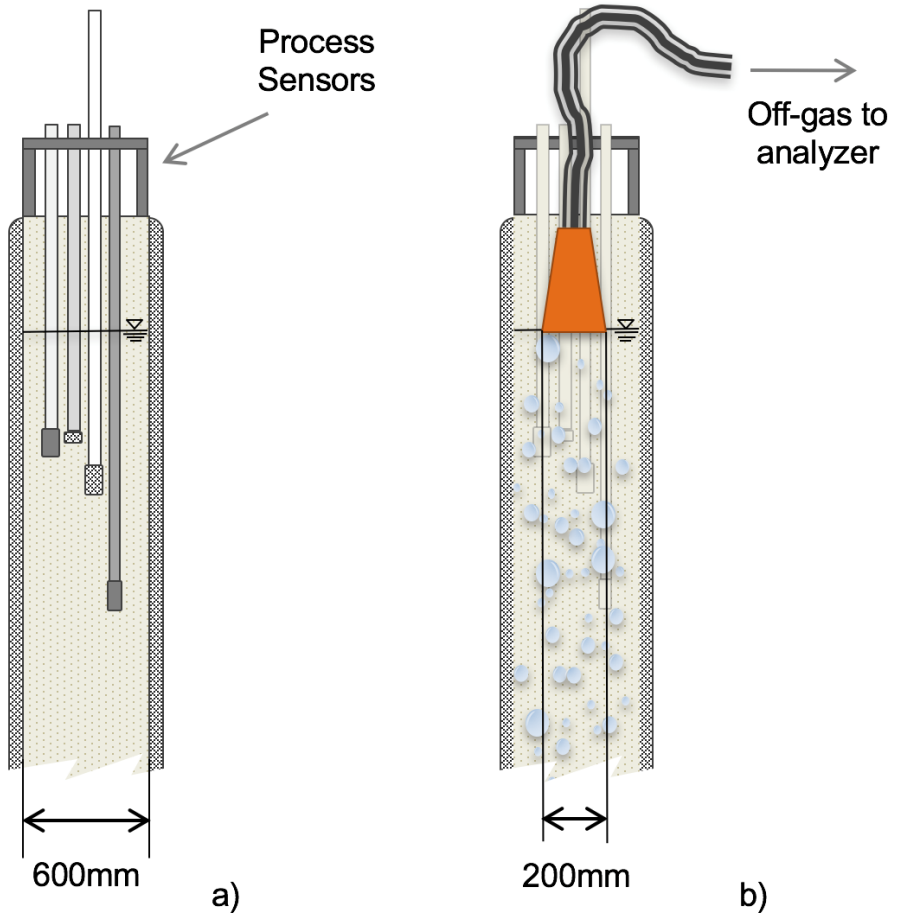

Figure A.3: Drawing of the conical off-gas collection apparatus floating in the reactor and of the process sensors installation.

The dissolved oxygen in both the reactors was measured continuously (YSI models 58 and 52; Yellow Springs Instruments, Yellow Springs, OH). During the tests, a gas sample exiting the reactor surface was captured (Figure A.3) and the oxygen content and off-gas flow were measured in order to calculate the oxygen transfer efficiency. Also, carbon dioxide and water

vapor content were removed with pellets of NaOH (CAS No. 1310-73-2) and CaSO4 (CAS No. 7778-18-9), respectively.

A.4 Results and Discussion

A.4.1 Floccular vs granular sludge

Oxygen mass transfer efficiency at different operating conditions in terms of DO setpoint, biomass concentration, and side-water-depth was assessed for the two types of biomass. Figure A.4 shows the comparison results between floccular and granular biomass, with both run at high (nominal 2 mg L^{-1}) and low (nominal 1 mg L^{-1}) DO set points. While the activated sludge reactor was operated at 3 g L^{-1} MLSS and 5.5 m (18 ft) SWD, the granular reactor was operated at 10 g L^{-1} MLSS and 5.8 m (19 ft) SWD. Figure A.4 (bottom) shows the main aeration performance indicators, in terms of αSOTE/Z (in red), DO measured (in orange), and airflow rate (in yellow) expressed as an average of the aeration cycle. Figure 4b reports nutrient removal performance in terms of effluent levels of ammonia (in orange), NOx (in blue), and orthophosphate (in green). The dashed lines show the design treatment goals for ammonia (in orange, 2 mg L^{-1}) and for phosphate (in green, 0.5 mg L^{-1}).

AS (floccular biomass) resulted in higher oxygen transfer efficiency in comparison to AGS (granular biomass). The results were consistent for both of the studied DO setpoints (3.2 %/m compared to 2.3%/m, on average as SOTE/z). It was observed that, operating under identical setpoints, granular biomass tests were consistently associated with higher airflow rate (1.22 compared to 1.02 SCFM, on average) and lower (and limiting) dissolved oxygen content (0.5 against 1.3 mg L^{-1}, on average) compared to the floccular biomass. While the AS process presented no evident phosphorous removal (as expected) with a reduced nitrification/denitrification performance at the low DO setpoint, the granular reactor consistently presented an excellent removal of nitrogen and phosphorous with effluent levels lower than

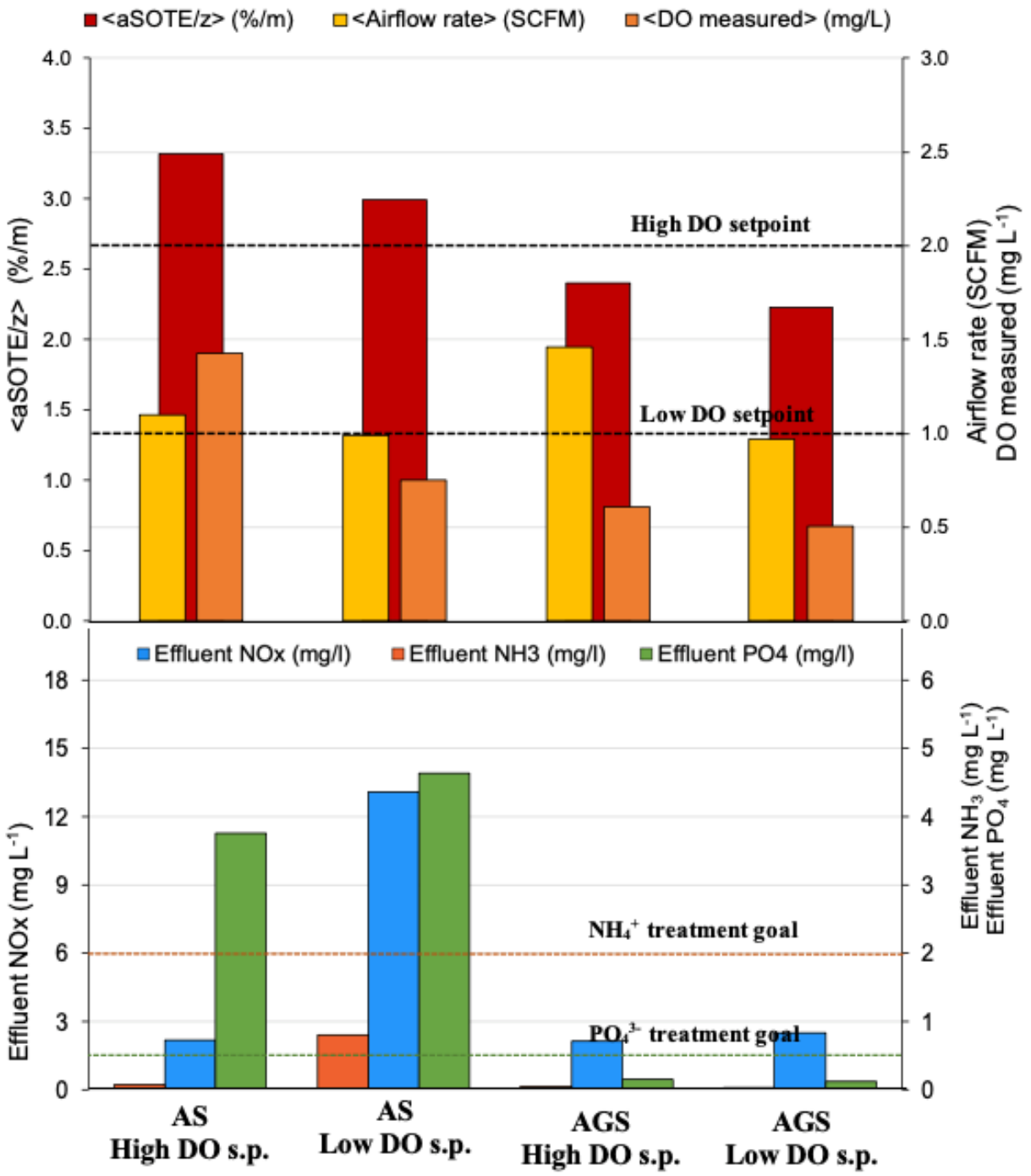

Figure A.4: Comparison between activated sludge (AS) and aerobic granular sludge (AGS), both at high (2 mg l-1) and low (1 mg l-1) DO setpoint, in terms of (a) aeration performance and (b) nutrients removal.

the design treatment goals (despite the low levels of dissolved oxygen achieved during the aeration cycle).

The observed differences between floccular and granular biomass in aeration performance were further scrutinized by compiling all conducted (floccular and granular) experiments. Figure A.4 includes all the experiments conducted, both for floccular and granular biomass, and demonstrates the expected oxygen transfer efficiency (*i.e.*, αSOTE/Z) improvement along the aeration cycle. While efficiency indicators are expected to increase as the effect of compounds (i.e., surfactants, colloids) inhibiting oxygen mass transfer diminishes during the oxidation process (Rosso et al ,2008), the observed steeper increase in the floccular system pinpoints significant differences between both systems. Such differences were further analyzed in Fig. A.6 where the aeration capacity of the system was taken into consideration. Figure A.6 shows the obtained levels of DO during the aeration cycle for those tests operated at high DO setpoint (2 mg L^{-1}). Similarly, floccular and granular sludge presented highly differentiated results.

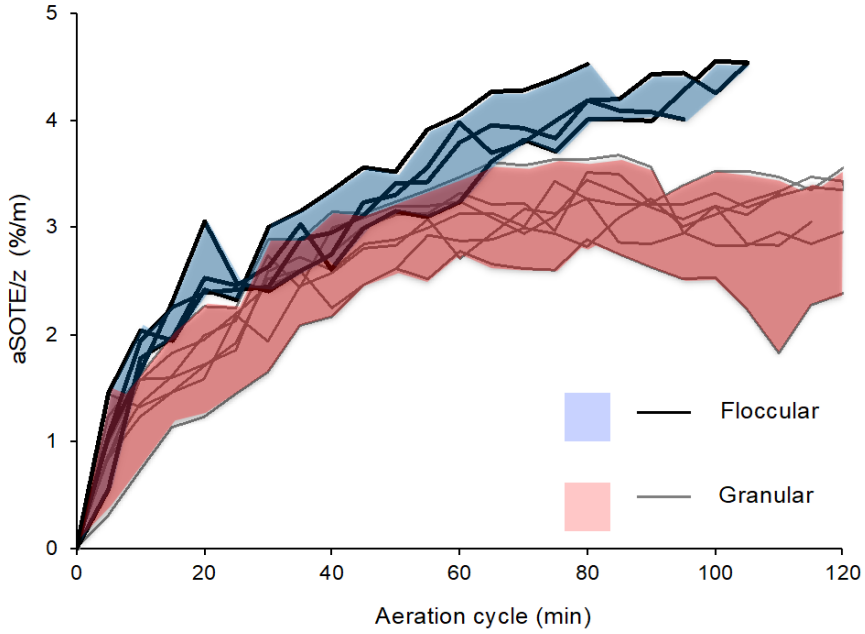

Figure A.5: Oxygen transfer efficiency during the aeration cycle. All the experiments are shown, distinguishing between floccular biomass (green shade) and granular biomass (orange shade).

Figure A.5 shows how granular sludge experiments consistently exhibited lower oxygen transfer efficiency (avg. 28±5%) during the aeration cycle compared to floccular biomass for all

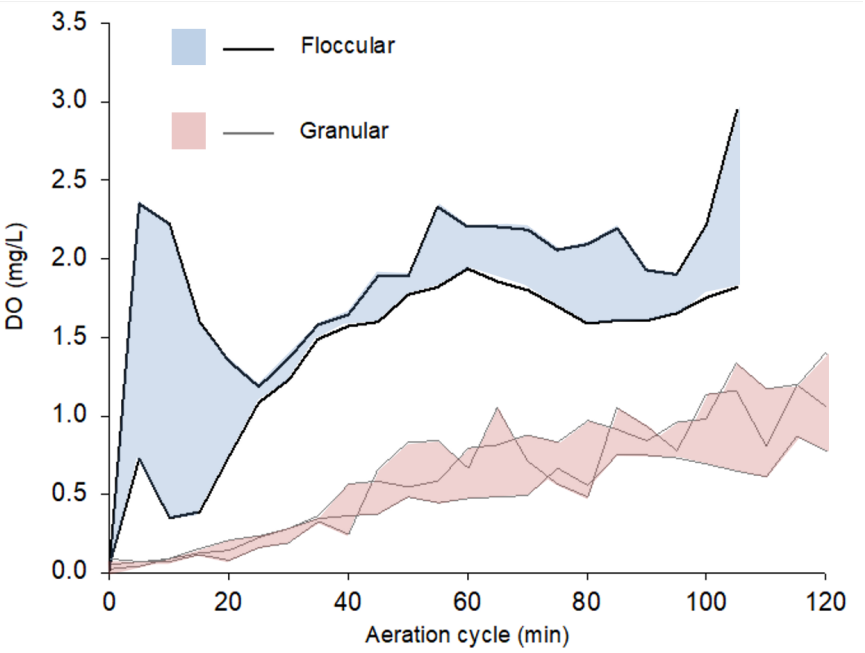

Figure A.6: Dissolved oxygen during the aeration cycle. All the experiments at high DO setpoint (2 mg L^{-1}) are shown, distinguishing between floccular biomass (blue shade) and granular biomass (pink shade). The black dashed line highlights the DO setpoint imposed in the tests analyzed.

of the different operational conditions tested. The observed differences in aeration efficiency between floccular and granular sludge could be attributed to different factors. Other studies have shown the effect of mixed liquor concentrations on aeration efficiency for AS systems, especially loaded systems (Krause et al, 2003; Cornel and Krause, 2006; Baquero et al., 2018; Jiang et al., 2017; Rosso et al., 2018; Amaral et al 2019). In these studies, it was shown that when MLSS exceeds 8 g L^{-1}, the sludge exhibits a distinct non-Newtonian nature (shear-thinning), and its shear-thinning nature forces bubble coalescence to increase the interfacial velocity between the bubble and the liquid, which decreases in turn the local viscosity. The coalescence results in larger bubbles which decreases specific area, interfacial viscosity, and hydrodynamic resistance. Therefore, according to these studies, if we translate those results for the granular system, the MLSS ($\sim$10g L^{-1}), which is higher than the 8g L^{-1} threshold, should behave as non-Newtonian fluid while the floccular system operated at 3g L^{-1} should maintain its Newtonian characteristics and the aeration efficiency will be highly impacted by

the wastewater characteristics (i.e., surfactants, COD fractions). This supports the difference in shape of the curves (Fig. A.5): oxygen transfer efficiency for AGS does not improve as much during the aeration cycle, because it is mainly affected by the viscous nature of the mixed liquor, due to the high content of biomass. Instead, for the activated sludge, the oxygen transfer improves significantly during the aeration cycle because it is more significantly influenced by the concurrent decrease in COD fractions and surfactants due to the bacterial activity. Therefore, it could be inferred that the large difference in OTE between granular and floccular systems is the difference in MLSS operating range expected for the two type of biomass. Because of the dense structure, granular systems have the advantage to be operated at high MLSS, which increases treatment capacity. However, this operational condition could lead to drawbacks when considering the oxygen transfer efficiency of the system, and therefore it can impact the energy balance of the process. The observed lower oxygen transfer efficiency in the AGS might have resulted from the combination of other factors. As mentioned, the AGS system presented a different trend during the aeration cycle regarding dissolved oxygen (Fig. A.6). AGS experiments at high DO setpoint (2 mg L^{-1}) showed that the dissolved oxygen never actually reached the setpoint during the entire cycle, regardless of the other operating conditions. The floccular system, in contrast, presented higher levels of dissolved oxygen, reaching the setpoint faster with an airflow rate comparable or lower than in the granular experiments. Therefore, from the high airflow rate delivered and the low DO measured, it can be inferred that the granular sludge experiments not only presented a lower oxygen transfer efficiency, but were also subject to air limitation likely due to limited diffuser capacity or the geometry of the pilot reactor itself. The different EPS organization and composition between floccular and granular biomass may have also impacted the adsorption capacity of oxygen transfer inhibitors, which can concurrently reduce the gas-liquid interfacial area, $K_L a$ (Germain et al, 2007). It has been shown that in floccular systems the changes in EPS composition can lead to improved bio-adsorption properties, especially if the protein versus polysaccharides content increasesincreases (Rahman et al., 2017, 2016; Winckel et al.,

2016). This results in an improvement of the removal of those compounds actively hindering oxygen mass transfer (*i.e.*, surfactants, colloids, etc.) which improves the overall efficiency indicators (Garrido-Baserba et al., 2015; Rosso and Stenstrom, 2007). However, because the EPS composition of the AGS system is significantly adapted to facilitate the development of dense and large granules (McSwain et al., 2004; Zheng et al., 2005, Zhu et al., 2015), it might not be maximized for the adsorption capacity which could have contributed to the observed lower aeration efficiency.

A.4.2 Transitioning from floccular to granular: Retrofit considerations

The experiments have shown satisfactory nutrient removal performance but lower aeration efficiency for the granular sludge compared to the floccular biomass. This would result in an increase in costs for the aeration system per unit of volume. Because AGS systems allow to work for smaller tank volumes, thanks to the high MLSS, the overall increase/decrease in energy use of the air supply system is uncertain. Therefore, when retrofitting AS existing full-scale plants to AGS systems, a thorough evaluation of the costs should be performed, including the potential increase of costs associated with aeration. Overall, even if the floccular technology presents a higher oxygen transfer efficiency, it can be inferred that the energy and maintenance requirements for clarifiers and recirculation pumping would offset or exceed the increase in aeration costs for AGS technology. Despite the low levels of dissolved oxygen reached in the granular experiments, which might be attributed to air limitations influenced by the specific geometry of the pilots (full depth but small diameter), the nutrient removal performance remained consistent. Future studies should focus on the aeration specifications of the full-scale design and retrofit with AGS processes to accurately quantify the optimal air requirements and diffuser layout for such full-scale facilities. In the following sections, we present the results from tests performed on the granular biomass for different MLSS and side-water-depth to address the optimal settings for oxygen transfer and to evaluate the

potential retrofitting of existing basins.

A.4.3 AGS optimization

Two pilot reactors were operated with granular sludge, with the first reactor kept at default conditions, at full side-water-depth (6 m), and high biomass concentration (10 g L^{-1} MLSS), while the second reactor was tested at different biomass concentrations, side-water-depths, and cleaning regimes. The findings from this study are a fundamental step toward evaluating the potential retrofitting of AGS technology in existing basins and at different operating conditions.

A.4.4 AGS: high and low biomass concentration

The effect of biomass concentrations on oxygen transfer efficiency and nutrients removal performance was investigated for aerobic granular sludge. To address this, different experiments were performed on the pilot reactors, testing the granular system at the default conditions (10 g L^{-1} MLSS) and at lower biomass concentration (6 g L^{-1}). Figure A.7 shows the data from experiments on the granular system tested at high and low biomass concentration at 5 m SWD, distinguishing between the experiments run at high (2 mg L^{-1}) and low (1 mg L^{-1}) DO set points. The results are reported following the same format of the previous comparison.

For the lower biomass concentration at both high and low DO setpoints, the oxygen transfer efficiency was marginally higher (avg. 74%) (i.e., 2.6%/m compared to 2.8%/m in average as SOTE/Z). Surprisingly, the variations in biomass concentration had little effect on the aeration efficiency of the AGS system, in contrast to the significant effect on nutrient removal performance. Indeed, according to the predictions based on floccular systems (i.e., AS and MBR from Baquero et al., 2018), a decrease in OTE of no less than 30% would have been expected when increasing the MLSS concentration from 6 g L^{-1} to 10 g L^{-1} instead

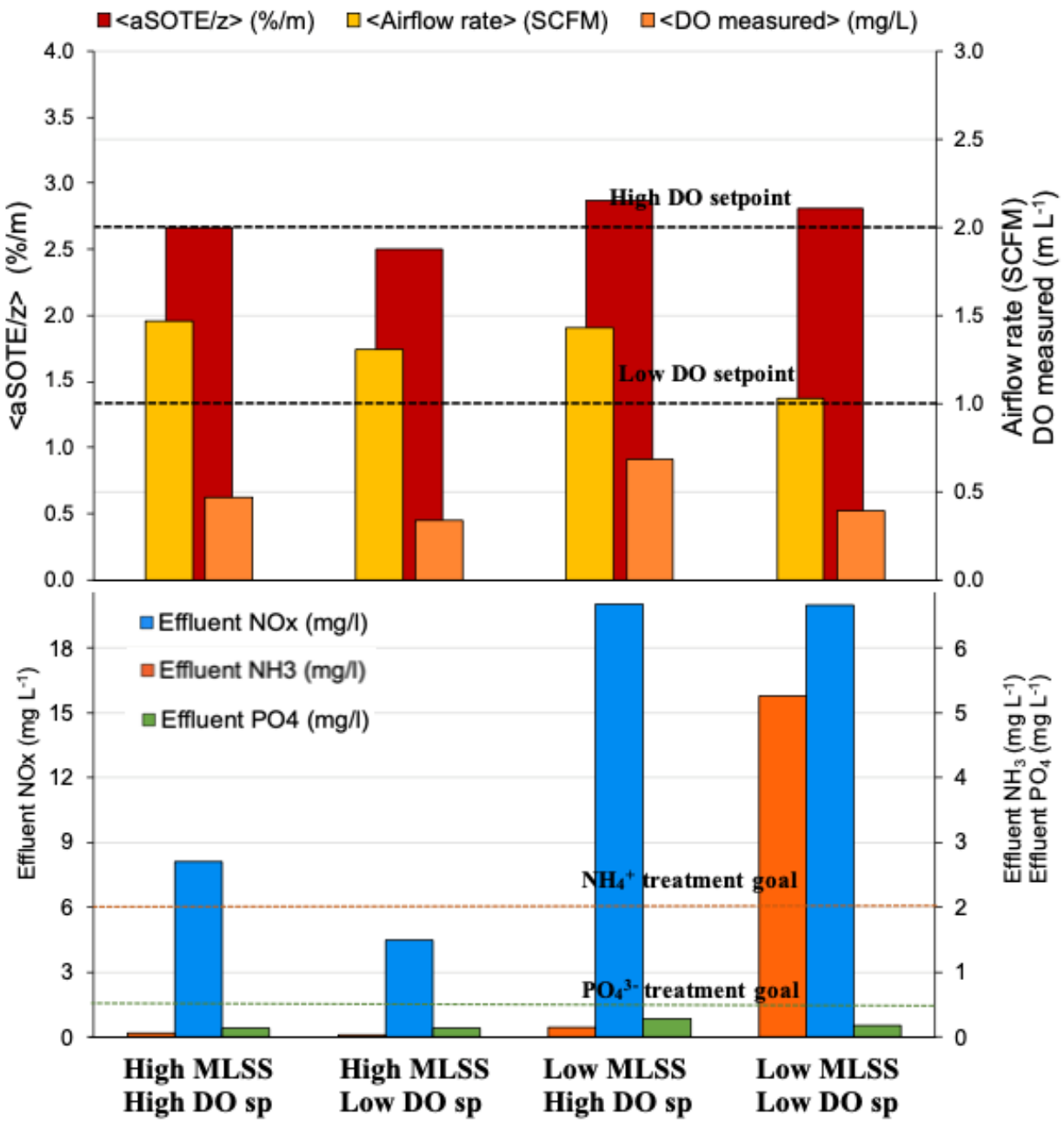

Figure A.7: Aerobic granular sludge system tested at high (10 g L^{-1}) and low (6 g L^{-1}) MLSS, both at high (2 mg L^{-1}) and low (1 mg L^{-1}) DO setpoint, in terms of (a) aeration performance and (b) nutrients removal.

of the observed 7% for AGS. Therefore, the behavior of granular biomass has yet to be fully studied given its different morphology compared to floccular biomass, supporting the need to further investigate the relationship between oxygen transfer and biomass content for

granular systems. While little effect was found in terms of aeration efficiency when biomass concentration was decreased to 6 g L^{-1}, the nutrient removal performance was significantly affected. The denitrification performance was penalized, as NOx levels at the end of the reaction cycle more than doubled, and the nitrification process was highly affected at low DO setpoint with ammonium effluent levels exceeding the treatment goals. Orthophosphate removal in contrast was consistent and unaffected by the different DO setpoints and biomass concentrations. The difference in DO patterns between high and low AGS biomass is reported in Fig. A.8. DO at low biomass conditions was higher after the first 40 minutes of the aeration phase. The observed difference between the two setups confirmed that at low biomass conditions, oxygen transfer was enhanced. As previously discussed, a limitation on the setup may have influenced the consistently lower DO than the imposed setpoint, limiting the metabolism of biomass and the concurrent nutrients removal performance. Given the almost negligible benefits on oxygen transfer efficiency in comparison to the significant deterioration of the nitrification/denitrification process, decreasing biomass concentration from the default conditions (10 g L^{-1}) was not an ideal process configuration.

A.4.5 AGS: shallow water depth

One of the differences between the original AGS design and most facilities in North America is the side-water-depth (SWD). Especially in North America, aeration basins are shallow, often not deeper than 5m, while the original design depth for AGS technology is 6 m or more. The depth of the reactor is an important parameter for granular technology. It is thought that the amount of freeboard is important during the feeding phase from the bottom to help the larger granules to be retained in the sludge bed; and the depth of the reactor is fundamental during the sedimentation phase, as deeper reactors result in the improved selection of larger and denser granules. Also, given that the saturation of gases is proportional to depth, upwards discharge in deeper tanks would reduce gas exertion and solids flotation if not performed carefully. The pilot reactors were tested with aerobic granular sludge at

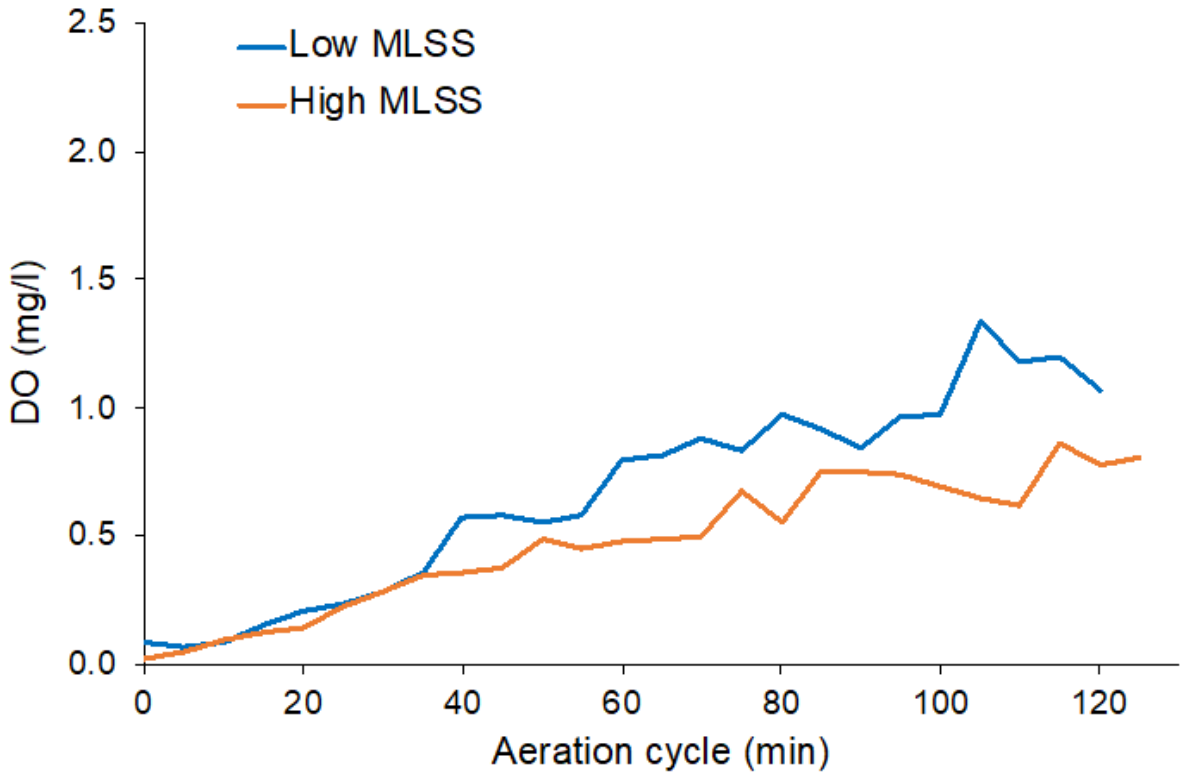

Figure A.8: Dissolved oxygen during the aeration cycles for aerobic granular sludge at high (10 g L^{-1}; in orange) and low (6 g L^{-1}; in blue) MLSS concentrations. Both experiments were conducted with a DO set point of 2 mg L^{-1}, indicated by the black dashed line.

full water depth (5.8 m or 19ft, AquaNereda's default depth) and at medium water depth (4.9 m or 16ft). Figure A.9 shows the data obtained from the experiments of the granular system tested at full and medium side-water-depth, at 10 g L^{-1} MLSS, and distinguishing between the experiments run at high (2 mg L^{-1}) and low (1 mg L^{-1}) DO setpoints. The results reported are consistent with other comparisons.

An increase in oxygen transfer efficiency is expected at higher depth, due to the longer bubble residence time (US EPA, 1989). OTE, on average, was lower for medium SWD (12.4%) in comparison to full SWD (13.0%), which in terms of standard conditions per unit of depth, corresponds to an average αSOTE/Z of 2.6%/m for medium depth and 2.3%/m for full depth. The transfer efficiency per unit of depth was marginally higher (0.09x) for medium depth, both for high and low DO setpoints, which could fall into the uncertainty range of

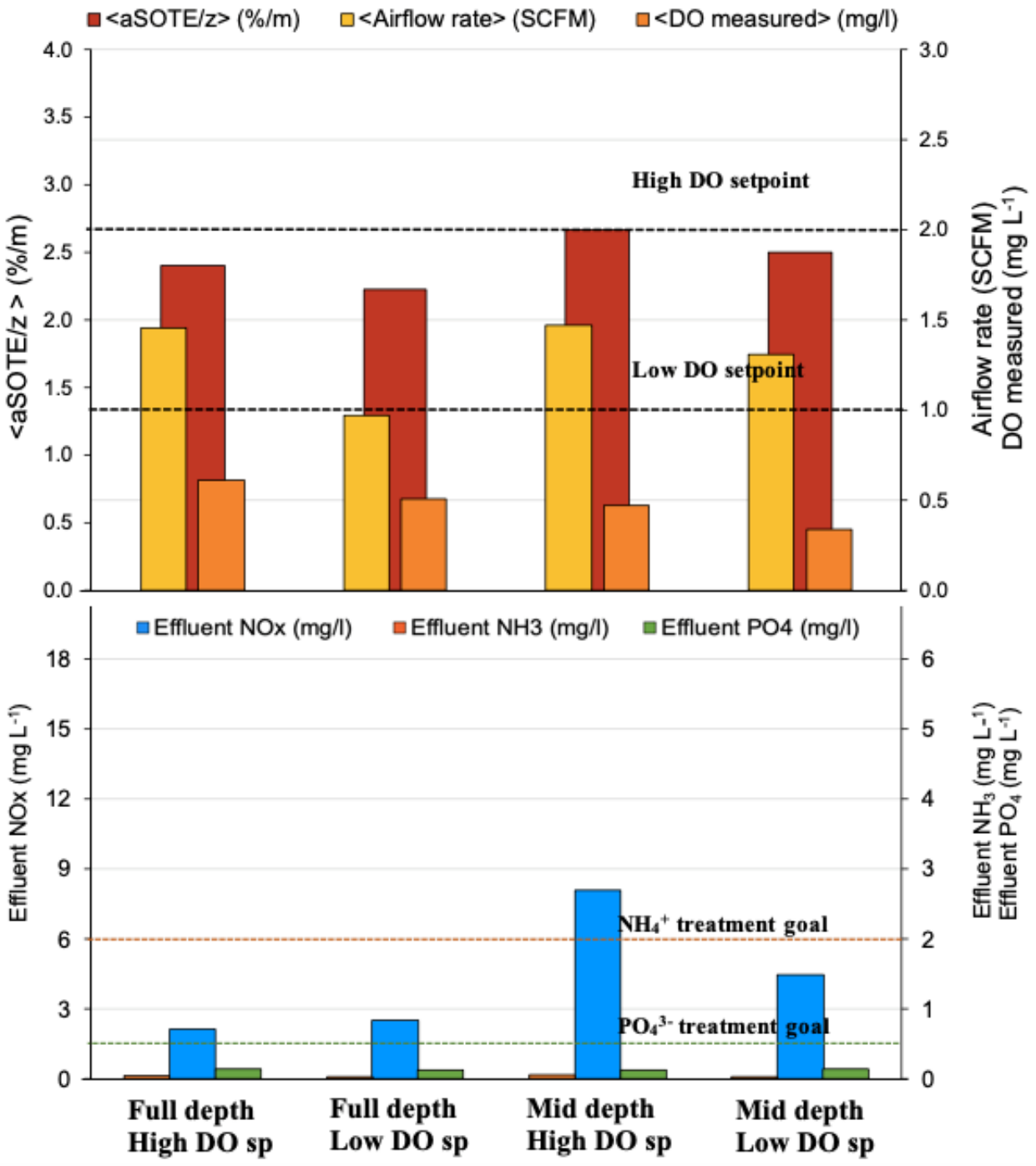

Figure A.9: Aerobic granular sludge system tested at full (5.8 m) and medium (4.9 m) SWD, both at high (2 mg L^{-1}) and low (1 mg L^{-1}) DO setpoint, in terms of (a) aeration performance and (b) nutrients removal.

the experimental setup, but would be expected due to less bubble coalescence. Phosphorus removal and nitrification were unaffected by the different side-water-depths and DO set

points. Nonetheless, denitrification performance at middle side-water-depth, especially at high DO setpoint, was impacted with a NOx effluent level which doubled compared to full depth. However, nitrate effluent levels met the required discharge limits, and denitrification performed better than previous experiments at low biomass content.

A.4.6 AGS: clean and fouled diffusers

Since the 1970's, fine-pore diffusers have been the most common technology employed for biological processes in aeration systems (Aberley et al., 1974; US EPA, 1989). Fine-pore diffusers are associated with higher aeration efficiency (AE, kgO2 kWh1) compared to other aeration technologies (US EPA, 1989; Rosso, 2019) , but they are subject to fouling and aging over time (Gillot et al., 2005; USEPA, 1989; Wagner and Pöpel, 1998; Rosso and Shaw, 2014). The resulting increase in the energy required for supplying the same amount of oxygen to the biological process over time eventually reduces its original efficiency to half or less than the initial values (Garrido-Baserba et al., 2018, 2017; Rosso and Stenstrom, 2006). Diffuser cleaning, thus, has become a necessary procedure to curb the aeration efficiency decline and maintain the long-term benefits of using fine-pore diffusers (Rieth et al., 1990, Rosso and Stenstrom, 2006). Among the different methods to clean fine-pore diffusers, two are the most used and complementary: dewatering the aeration basin is used to wash the diffusers from the top which is effective in biofouling accumulation, and acid cleaning (low-strength hydrochloric acid at 10 to 15% wt) is used to remove inorganic scaling.

A set of experiments were designed to evaluate granular sludge by comparing the aeration efficiency between a reactor with a fouled diffuser and one with a cleaned diffuser. While the diffuser of one reactor had been fouled for six months, the diffuser of the second reactor was cleaned via tank-top hosing, although the effectiveness of the cleaning procedure could not be verified due to the pilot geometry and limited accessibility of the column bottom. In order to analyze the effect of diffuser fouling on oxygen transfer for AGS systems, it is fundamental

to maintain the other key variables and operational conditions that could interfere/influence the mass transfer. Therefore, biomass concentration, DO setpoint and side-water-depth were kept unvaried before and after cleaning the diffuser to improve the reliability of the comparison. In detail, the comparison was conducted at medium side-water-depth (4.9 m, or 16 ft), at high biomass concentration (10 g L^{-1} MLSS) and at 1.5 mg L^{-1} of DO setpoint. Figure A.10 reports the outcome of the experiments in terms of αSOTE/Z, airflow rate, and DO measured.

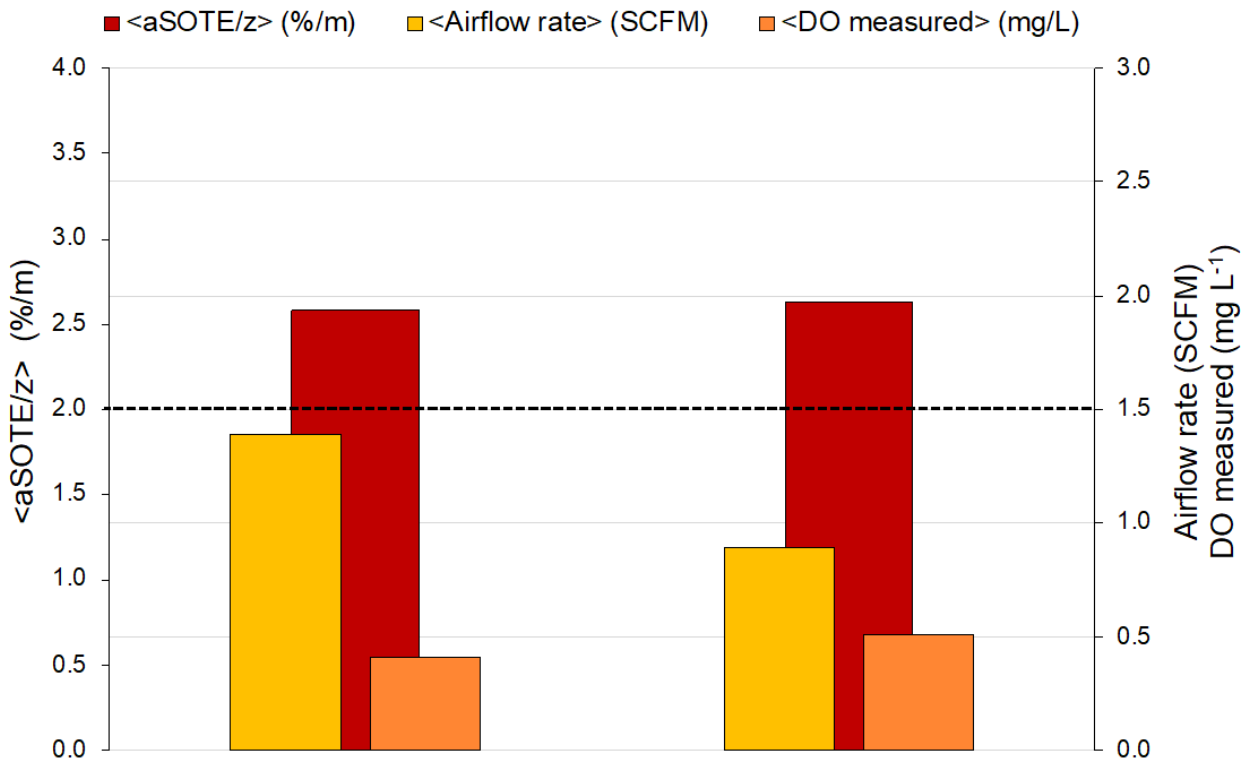

Figure A.10: Aeration performance comparison of granular sludge with cleaned and fouled diffuser, at mid depth (4.9 m), at 10 g L^{-1} MLSS, and at 1.5 mg L^{-1} DO setpoint. The graph reports in red the αSOTE/Z calculation, in yellow the airflow rate and in orange the DO measured, expressed as cycle average. The dashed line shows the DO setpoint.

Comparing the experiments between the cleaned and the fouled diffuser, no significant differences in terms of αSOTE/Z were recorded, (2.7%/m and 2.6%/m in average, respectively).

While the two experiments showed similar dissolved oxygen concentrations, the airflow rate for the reactor with the cleaned diffuser was significantly higher (36% in average), which was unexpected since the other parameters, αSOTE/Z and DO, were comparable. In consideration of the practical issues encountered in the field during the cleaning procedure and the inconclusive results in terms of aeration efficiency obtained, future studies should better address the effect of the diffuser cleaning for aerobic granular sludge systems.

As a summary of all the experiments and analysis conducted, Table A.3 reports the results of the off-gas test and of the nutrients removal performance.

Table A.3: Summary of the results of the off-gas analysis and nutrients removal performance at the different operational conditions tested.

Biomass type	**MLSS** [g L^{-1}]	**SWD** [m (ft)]	**DO stp.** [mg L^{-1}]	**αSOTE/Z** [%/m]	**AFR** [SCFM]	**DO** [mg L^{-1}]	**OUR** [mg $L^{-1}h^{-1}$]	**NH_4^+ Eff** [mg L^{-1}]	**NOx Eff** [mg L^{-1}]	**PO_4 Eff** [mg L^{-1}]
AGS	10.0	5.8 (19)	2.0	2.4	1.46	0.61	53.6	0.04	2.10	0.10
AGS	10.0	5.8 (19)	1.0	2.2	0.97	0.51	33.1	0.03	2.50	0.12
AGS	10.0	4.9 (16)	2.0	2.7	1.47	0.47	59.8	0.05	8.10	0.13
AGS	10.0	4.9 (16)	1.0	2.5	1.31	0.34	51.0	0.03	4.46	0.14
AGS	6.0	4.9 (16)	2.0	2.9	1.03	0.39	44.5	0.14	19.99	0.27
AGS	6.0	4.9 (16)	1.0	2.8	1.43	0.68	60.9	5.26	19.99	0.17
AS	2.9	5.5 (18)	2.0	3.3	1.10	1.43	52.8	0.08	2.16	3.75
AS	2.9	5.5 (18)	1.0	3.0	0.99	0.75	46.7	0.80	13.06	4.63
AS	1.7	5.5 (18)	2.0	3.0	-	2.04	41.3	0.01	5.22	3.99
AS	1.7	5.5 (18)	1.0	2.9	0.98	1.16	40.1	0.03	10.15	4.30

A.5 Conclusions

This paper reports the first independent assessment of aerobic granular sludge technology in terms of oxygen transfer efficiency and nutrient removal performance. Using off-gas testing, aerobic granular sludge was compared to the activated sludge process, using two full depth pilot-scale reactors. The granular process consistently presented lower oxygen transfer efficiency than the floccular sludge, 2.3%/m and 3.2%/m, respectively. Biomass concentration

(*i.e.*, MLSS) was identified as the main parameter influencing the observed differences in OTE. While the results were in agreement with high MLSS systems (*e.g.*, MBRs and aerobic digesters), the specific characteristics of the AGS system (*i.e.*, higher biomass due EPS granular encapsulation) suggest different behavior and dynamics than expected for floccular systems, indicating that further studies may reveal the exact relationship between MLSS and OTE. On the other hand, air limitation in the pilot setup may have impacted the lower OTE of the AGS when compared to floccular sludge. Nevertheless, despite the air limitation issues described for the granular sludge, nutrient removal was not affected by low levels of dissolved oxygen in the water. The exact influence of encapsulated EPS could not be quantified, and future studies should include the bioadsorption capacity of surfactants and their influence on the OTE of AGS. A set of experiments solely focused on granular biomass were performed to gain insight into the most influential operational conditions that enhance aeration efficiency in AGS systems. The experiments with medium SWD (∼5 m, typical SWD of the aeration basins in the North America) showed lower OTE (∼5%) compared to the full water depth (∼6 m, the default AGS design value), as expected, and satisfactory nutrient removal performance, except for denitrification at the high DO set point. Future studies should address the different operating conditions at larger scale. Also, a systematic study on diffuser fouling should be planned as part of longer-term evaluations.

A.6 References

Aberley, R.C., Rattray, G.B. and Dougas, P.P. (1974) Air Diffusion Unit. Journal WPCF. 46(5): 895-910.

Adav, S. S., Lee, D., Show, K., Tay, J. (2008). Aerobic granular sludge: Recent advances, i, 411–423.

Amaral, A., Gillot, S., Garrido-Baserba, M., Filali, A. et al., (2019) Modelling gas – liquid

mass transfer in wastewater treatment: when current knowledge needs to encounter engineering practice and vice versa, Water Sci. Technology, 80(4), 607–619.

American Society of Civil Engineers—ASCE 1984, 1991, 2007 Measurement of Oxygen Transfer in Clean Water.

American Society of Civil Engineers, New York,1 1996 ASCE 2-91.

American Society of Civil Engineers—ASCE 1997 Standard Guidelines for In-Process Oxygen Transfer Testing, ASCE 18-96, 3 45 E. 47th St, New York, NY.

Baquero-Rodriguez, G. A., Lara-Borrero, J. A., Nolasco, D., Rosso, D. (2018). A Critical Review of the Factors Affecting Modeling Oxygen Transfer by Fine-Pore Diffusers in Activated Sludge. Water Environment Research 90 431-441.

Barnard, J. L. , Stensel, H. D. (2014) The activated sludge process in service of humanity, DSD International Conference, Hong Kong, November, 1214.

Beun J. J., Hendriks A, van Loosdrecht MCM, Morgenroth M, Wilderer PA, Heijnen JJ. (1999). Aerobic granulation in a sequencing batch reactor. Wat. Res. 33(10):2283–2290.

Beun, J. J., van Loosdrecht, M. C., Heijnen, J. J. (2000). Aerobic granulation. Water Science and Technology, 41(4–5), 41–48.

Beun, J. J., Hendriks, A., Loosdrecht, M. C. M. V. A. N., Morgenroth, E., Wilderer, P. A., Heijnen, J. J. (2001). Aerobic Granulation in a Sequencing Batch, 33(10), 702–712.

Bozkurt, H., van Loosdrecht, M. C. M., Gernaey, K. V., Sin, G. (2016). Optimal WWTP process selection for treatment of domestic wastewater - A realistic full-scale retrofitting study. Chemical Engineering Journal, 286, 447–458.

Cornel P. and Krause, S. (2006) Membrane bioreactors in industrial wastewater treatment – European experiences, examples and trends, Water Science Technology, 53(3),

37–44.

Cornel, P., Wagner, M., Krause, S. (2003) Investigation of oxygen transfer rates in full scale membrane bioreactors, Water Science Techonology, 47(11), 313–319.

De Bruin LMM, De Kreuk MK, van der Roest HFR, Van Loosdrecht MCM, Uijterlinde C. (2004). Aerobic granular sludge technology, alternative for activated sludge technology? Wat Sci Technol 49(11–12):1–9.

Etterer, T., Wilderer, P. A. (2001). Generation and properties of aerobic granular sludge. Water Science and Technology, 43(3), 19–26.

Garrido-Baserba, M., Asvapathanagul, P., McCarthy, G. W, Gocke, T. E., Olson, B. H., Park, H-D. et al. (2016) Linking biofilm growth to fouling and aeration performance of fine-pore diffuser in activated sludge, Water Research, 90, 317–328.

Garrido-Baserba, M.; Sobhani, R.; Asvapathanagul, P.; McCarthy, G. W.; Olson, B. H.; Odize, V.; Al-Omari, A.; et al. (2017) Modelling the link amongst fine-pore diffuser fouling, oxygen transfer efficiency, and aeration energy intensity. Water Res., 111, 127–139; Elsevier Ltd.

Germain, E., Nelles, F., Drews, A., Pearce, P., Kraume, M., Reid, E. et al. (2007) Biomass effects on oxygen transfer in membrane bioreactors, Water Research, 41, 1038–1044.

Giesen, A., de Bruin, L. M. M., Niermans, R. P., van der Roest, H. F. (2013). Advancements in the application of aerobic granular biomass technology for sustainable treatment of wastewater. Water Practice and Technology, 8(1), 47–54

Gillot, S., Capela-Marsal, S., Roustan, M., Héduit, A. (2005) Predicting oxygen transfer of fine bubble diffused aeration systems - Model issued from dimensional analysis, Water Research, 39(7), 1379–1387.

Henze, M., van Loosdrecht, M.C., Ekama, G.A., Brdjanovic, D., 2008. Biological Wastew-

ater Treatment: Principles, Modelling and Design. IWA Publishing.

Hertle, A., 2015. Fine Bubble Diffused Air Aeration Systems (Water Encycl.). IWA, 2008. Biological Wastewater Treatment - Principles. Modelling and Design, United Kingdom. Jenkins, T. E.; Vanysek, P.; Us, I. L.; Ricco, H. S. (2008) (12) United States Patent, 2 (12).

Jiang, L., Garrido-baserba, M., Nolasco, D., Al-omari, A., Declippeleir, H., Murthy, S. (2017) Modelling oxygen transfer using dynamic alpha factors. Water Research, 124, 139–48.

Kaliman, A., Rosso, D., Leu, S.-Y. Stenstrom, M. K. 2008 Fine- pore aeration diffusers: accelerated membrane ageing studies. Wat Res 42, 467–475.

Krause, S., Cornel, P., Wagner, M. (2003) Comparison of different oxygen transfer testing procedures in full-scale membrane bioreactors. Water Sci. Technol, 47 (12), 169–176.

Leu, S.-Y., Rosso, D., Larson, L. E., Stenstrom, M. K. (2009) Real- Time aeration efficiency monitoring in the activated sludge process and methods to reduce energy consumption and operating costs, Water Environ. Res, 81, 2471–2481.

Liu, Y., Tay, J-H. (2004) State of the art of biogranulation technology for wastewater treatment, Biotechnology Advances, 22(7), 533–563.

Liu, Y., Liu, Q. (2006) Causes and control of filamentous growth in aerobic granular sludge sequencing batch reactors, Biotechnology Advantages, 2006, 24, 115–127.

Majone, M., Dircks, K., Beun, J. (1999) Aerobic storage under dynamic conditions in activated sludge processes. The state of the art, Water Science and Technology, 39(1), 61–73.

Martins AMP, Pagilla K, Heijnen JJ, van Loosdrecht MCM. 2004. Filamentous bulking sludge—A critical review. Wat Res 38(4):793–817.

McSwain, B. S., Irvine, R. L., Wilderer, P. A. (2004) The influence of settling time on the formation of aerobic granules, Water Science and Technology, 50(10), 195–202. McSwain, B. S., Irvine, R. L., Hausner, M., Wilderer, P. A. (2005) Composition and distribution of extracellular polymeric substances in aerobic flocs and granular sludge, Applied and environmental microbiology, 71(2), 1051–1057.

Metcalf Eddy (2014) Wastewater Engineering: Treatment and Resource Recovery. 5th editio. McGraw-Hill Education.

Morgenroth, E., Sherden, T., Van Loosdrecht, M. C. M., Heijnen, J. J., Wilderer, P. A. (1997) Aerobic granular sludge in a sequencing batch reactor, Water Research, 31(12), 3191–3194.

Pijuan, M., Werner, U., Yuan, Z. (2011) Reducing the startup time of aerobic granular sludge reactors through seeding floccular sludge with crushed aerobic granules, Water Research, 45(16), 5075–5083.

Rahman, A., Meerburg, F. A., Ravadagundhi, S., Wett, B., Jimenez, J. A., Bott, C., et al., (2016) Biofl occulation management through high-rate contact-stabilization: A promising technology to recover organic carbon from low-strength wastewater, Water Research, 104, 485–496.

Rahman, A., Mosquera, M., Thomas, W., Jimenez, J. A., Bott, C., Wett, B. et al., (2017) Impact of aerobic famine and feast condition on extracellular polymeric substance production in high-rate contact stabilization systems, Chemical Engineering Journal, 328, 74–86.

Reardon, D. J. (1995) Turning down the power. Civ. Eng. 65(8), 54–56.

Redmon, D. T., Boyle, W. C. Ewing, L. 1983 Oxygen transfer efficiency measurements in mixed liquor using off-gas techniques. J. Water Pollut. Control Fed. 55, 1338–1347.

Rieth, M., Boyle, W., Ewing, L. (1990) Effects of selected design parameters on the fouling characteristics of ceramic diffusers, Journal of the water pollution control federation, 62, 877–886.

Rosso, D. (2018) Aeration, Mixing, and Energy: Bubbles and Sparks — IWA Publishing. Rosso D, editor. Irvine, California: IWA publishing; 300 p.

Rosso, D., Iranpour, R. Stenstrom, M. K. 2005 Fifteen years of off-gas transfer efficiency measurements on fine-pore aerators: key role of sludge age and normalized air flux. Water Environ. Res. 77(3), 266–273.

Rosso D. and Stenstrom, M. (2006) Economic implications of fine-pore diffuser aging. Water environment research: a research publication of the Water Environment Federation., 78(8), 810–815.

Rosso, D. Stenstrom, M. K. 2006a Surfactant effects on a-factors in aeration systems. Water Res. 40, 1397–1404.

Rosso, D.; Stenstrom, M. K.; Larson, L. E. (2008). Aeration of Large-Scale Municipal Wastewater Treatment Plants: State of The Art. Water Sci. Technol., 57 (7), 973–978.

Schuchardt, A., Libra, J.A., Sahlmann, C., Wiesmann, U., Gnirss, R. (2007) Evaluation of oxygen transfer efficiency under process conditions using the dynamic off-gas method, Environ. Technol., 28, 479-489.

Sheik, A. R., Muller, E. E. L., Wilmes, P.(2014) A hundred years of activated sludge: time for a rethink. Front. Microbiol., 5, 47.

Stenstrom, M. K., Vazirinejad, H. O. Ng, A. 1984 Economic evaluation of upgrading aeration systems. J. Water Pollut. Control Fed. 56(1), 20–26.

Tay, J. H., Liu, Q. S., Liu, Y. (2001). The effects of shear force on the formation, struc-

ture and metabolism of aerobic granules. Applied Microbiology and Biotechnology, 57(1–2), 227–233.

Trillo, I., Jenkins, T.E., Redmon, D., Hilgart, T., Trillo, J. (2004) Implementatino of Feedforward Aeration Control Using On-Line Off-gas Analysis, The Grafton WWTP Experience. Proceedings of the Water Environment Federation, WEFTEC 2004 91-95 27-45.

Wagner, M. R., Pöpel, H. J. (1998) Oxygen transfer and aeration efficiency - Influence of diffuser submergence, diffuser density, and blower type, Water Science and Technology, 38(3), 1–6.

WEF, 2009. Energy conservation in water and wastewater treatment facilities, WEF Manual of Practice [WWW Document]. WEF Man. Pract.McGraw-Hill, Inc., New York, NY

Weissbrodt, D. G., Shani, N., Holliger, C. (2014) Linking bacterial population dynamics and nutrient removal in the granular sludge biofilm ecosystem engineered for wastewater treatment, FEMS Microbiology Ecology, 88(3), 579–595.

Van Winckel, T., De Clippeleir, H., Mancell-egala, A. et al., (2016) Balancing flocs and granules by external selectors to increase capacity in high-rate activated sludge systems, In: Proceedings of WEFTEC 2016, Water Environment Federation, New Orleans, Louisiana, USA, pp. 5628-5633.

U.S. Environmental Protection Agency – USEPA 1989 Fine Pore (Fine Bubble) Aeration Systems, EPA/625/1-89/023; U.S. Environmental Protection Agency: Cincinnati, Ohio.

Zheng, Y., Yu, H., Sheng, G. (2005) Physical and chemical characteristics of granular activated sludge from a sequencing batch airlift reactor, Process Biochemistry, 40, 645–650.

Zhu, L., Zhou, J., Lv, M., Yu, H., Zhao, H., Xu, X. (2015) Chemosphere Specific component comparison of extracellular polymeric substances (EPS) in flocs and granular sludge using EEM and SDS-PAGE,Chemosphere, 121, 26–32.